Dipl.-Ing. Roland Hohl

Process Analytical Technology for Monitoring of Pharmaceutical Processes

DISSERTATION

zur Erlangung des akademischen Grades
Doktor der technischen Wissenschaften
eingereicht an der

Technischen Universität Graz

Betreuer

Univ.-Prof. Dr. Johannes G. Khinast

Institute of Process and Particle Engineering
Research Center Pharmaceutical Engineering GmbH Graz,

Graz, Juli 2017

EIDESSTATTLICHE ERKLÄRUNG

Ich erkläre an Eides statt, dass ich die vorliegende Arbeit selbstständig verfasst, andere als die angegebenen Quellen/Hilfsmittel nicht benutzt, und die den benutzten Quellen wörtlich und inhaltlich entnommenen Stellen als solche kenntlich gemacht habe. Das in TUGRAZonline hochgeladene Textdokument ist mit der vorliegenden Dissertation identisch.

17.07.2017	
Datum	**Unterschrift**

Dipl.-Ing. Roland Hohl

Process Analytical Technology
for Monitoring of Pharmaceutical Processes
Dissertation

First assessor
Univ.-Prof. Dr. Johannes G. Khinast
Institute for Process and Particle Engineering
Graz University of Technology, and
Research Center Pharmaceutical Engineering GmbH

Second assessor
Ao.Univ.-Prof. Dipl.-Ing. Dr.techn Karl Gatterer
Institut für Physikalische und Theoretische Chemie
Graz University of Technology

Acknowledgement

I am grateful for the scientific supervision of Prof. Johannes Khinast throughout my thesis. The discussions gave valuable insights how to properly tackle difficult problems and how to communicate the results to the scientific community.

I also want to thank Prof. Karl Gatterer for being the second assessor for this work.

My thanks also go to my colleagues of the CPQC group formerly known as QbD/PAT group formerly known as PAT group at RCPE GmbH. I would like to thank Elena Hohl, Patrick Wahl, Otto Scheibelhofer, Daniel Markl, Manuel Zettl, Daniel Koller, Stephan Sacher and Daniel Wiegele as well as students and interns.

My thanks also go to my wife Elena Hohl and my family Karin Hohl, Johann Hohl, Verena Hohl as well as Walter Uhl who always supported me.

Table of Contents

Abstract

In the last years process analytical technologies (PAT) get more important for pharmaceutical industries, this is strongly forced by the regulatory agencies. Here not only spectroscopic methods come to the fore also process simulations gets more important for predicting process behaviours.

For monitoring of different processes multipoint near infrared spectroscopy was used, the fibers were located at different positions in the process vessels. The results of a spray process were compared with discrete element method (DEM) simulations. The implemented algorithms can be used to predict moisture distribution inside granular materials. A hot melt coating process was monitored with a multipoint NIR system the fibers were located at different positions in the process chamber. With this multipoint NIR system inhomogeneities and disturbances in the process chamber were promptly detected and a sensors malfunction was compared and the correct process endpoint could be determined.

Dynamic cross flow filtration is well established process in different industries. The operation performance, limitations and possibilities of the Dynotest were analyzed, for monitoring flux measurements were used. Due to its capacity to handle highly viscous slurries and the easily scale-up possibility the used filtration system is a highly suitable technology for continuous filtration in pharmaceutical industries.

Kurzfassung

Regulatorische Behörden fordern von der pharmazeutischen Industrie verstärkt das Prozessanalytische Technologien (PAT) in den Herstellungsprozessen eingesetzt werden. Mittels spektroskopischen Methoden sondern auch die Prozesssimulation wird verstärkt eingesetzt, denn durch die Simulation von Prozessen können vorhersagen den Prozess betreffend und der Produktqualität getroffen werden.

Die Ergebnisse wurden mit DEM Simulationen verglichen und die Flüssigkeitsverteilung bzw. -aufnahme beurteilt. Ein Multisonden NIR-Spektrometer wurde für die Überwachung eines Hot melt coating Prozess eingesetzt. Mit diesem System war es möglich Störungen im fluid bed bzw. Unregelmäßigkeiten schnell zu erkennen. Ebenfalls ist es möglich mit diesem System Fehlfunktionen eines Sensors auszugleichen und den Endpunkt des Prozesses richtig zu bestimmen.

Querstromfiltration wird in verschiedenen Industrien erfolgreich eingesetzt , dieses System ist aufgrund seiner Fähigkeit, hochviskoser Slurries und des leichten Scale-up eine sehr gut geeignet Technologie für kontinuierliche Filtration in der pharmazeutischen Industrie.

List of Abbreviations

Abbreviation	Meaning
PAT	process analytical technology
QbD	quality by design
FDA	United States Food and Drug Administration
ICH	International Conference on Harmonisation
API	Active pharmaceutical ingredient
NIR	Near infrared
NIRS	Near infrared spectroscopy
PLS	partial least squares
PLSR	partial least squares regression
CV	Cross validation
CV-LOO	Cross validation leave one out
RMSEE	Root mean square error of estimation
RMSEP	Root mean square error of prediction
MVDA	Multivariate data analysis
MLR	multiple linear regression
MF	microfiltration
DEM	discrete element method simulation
CQA	critical quality attribute
KF	Karl-Fischer titration
LOD	loss on drying
SD	standard deviation
MSC	multiplicative signal correction
SNV	standard normal variate
rtd	residence time distribution
CPP	critical process parameters
TPI	Terahertz Pulsed Imaging
LIBS	Laser-induced breakdown spectroscopy
cf	Concentration factor
MSD	Multishaft disk
CFF	Cross flow filtration

1 Introduction

The guidance on PAT was released in by the FDA in September 2004 as a framework for innovative pharmaceutical development, manufacturing, and quality assurance. The goal of the PAT initiative is to enhance process understanding and improved control of the manufacturing process.[1]

The FDA's guidance for industry titled "PAT-A Framework for Innovative Pharmaceutical Development, Manufacturing, and Quality Assurance"[3] was intended to describe a regulatory framework that encourages the implementation and application of innovative techniques to pharmaceutical development, manufacturing, and quality assurance. Goals of process analytical technology (PAT) are

- assurance of pharmaceutical quality and performance through the design of effective and efficient manufacturing processes;
- specifications based on scientific understanding of how formulation and process variables affect product performance and quality;
- continuous real-time quality assurance
- adoption of risk-based regulatory policies that recognize the capability of process control strategies to mitigate the risk of poor quality products. [1]

Process analysis has advanced during the past decades, due to an increasing appreciation for the value of collecting process data. [2]

These measurements can be:

- at-line: Measurement where the sample is removed, isolated from, and analysed in close proximity to the process stream.
- on-line: Measurement where the sample is diverted from the manufacturing process, and may be returned to the process stream.
- in-line: Measurement where the sample is not removed from the process stream and can be invasive or non-invasive. [2]

Process analysers typically generate large volumes of data. Certain data are likely to be relevant for routine quality assurance and regulatory decisions. In a PAT environment, batch records should include scientific and procedural information indicative of high process quality and product conformance [2]. Advances in process analyse makes real time control and quality assurance during manufacturing feasible.

1.1 Near infrared spectroscopy

The discovery of NIR energy is ascribed to Herschel in the 19th century [4], but the first industrial applications only appeared in the 1950s. NIR spectroscopy studies the absorption of EMR in the NIR region, i.e. 700–2 500 nm (14 300–4 000 cm^{-1}). Mid infrared and Far infrared light can be situated in the 2 500–10 000 nm and 10 – 1 000 nm range [3]. The basic principles of NIR spectroscopy are thoroughly described in a review from Reich et

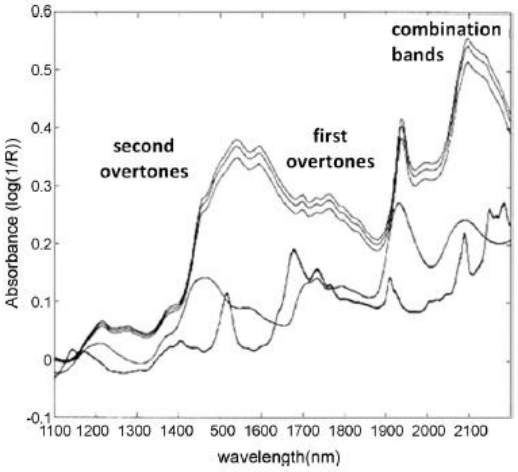

Figure 1-1: Example of NIR spectrum [3]

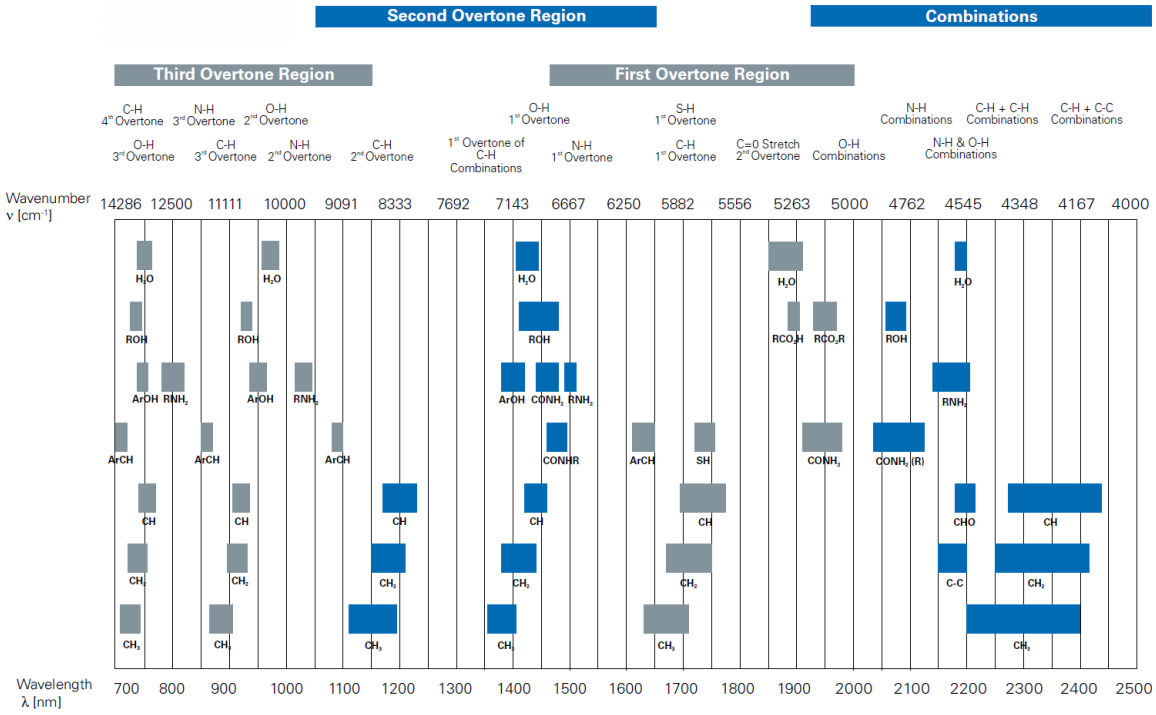

Figure 1-2: NIR band assignment table [6]

al [5]. In Figure 1-1 an example figure of a NIR spectrum is shown and in Figure 1-2 a NIR band assignment table is shown.

Near infrared spectroscopy (NIRS) is one of the most flexible vibrational spectroscopic techniques for the analysis of pharmaceutical products and also one of the most useful tools for the industrial implementation of PAT, at-line, in-line and on-line measurements and a number of measures of physical and chemical properties of samples are possible. Near infrared spectra are influenced by some physical properties of the samples [7]. The influence on the spectra can be by temperature particle density and the particle size. Therefore, an effective method for calibration of the in-line NIR signal is needed [8]. Especially when the environment conditions are changing during the process like in fluid bed granulation when in-line moisture detection is performed [8], but the effects can be suppressed or minimized by using an appropriate spectral pretreatment [7]. Due to its non-destructive nature and its ability to provide immediate results NIRS has a lot of advantages in PAT, the results must be calibrated against a reference [7]. Some of the better known uses of NIRS in the production of solid pharmaceutical forms include chemical raw material identification [9], blend uniformity assessment [10]–[12], granulation monitoring [7], roller compaction monitoring [13], drying end-point determination [14] and coating endpoint and uniformity determinations [7]. Different groups showed the possibility of process monitoring and control via NIRS [3], [10], [11], [15]–[34]. Multivariate data analysis (MVDA) is necessary for building NIR models, this models are necessary for real time control and to ensure product quality.

Figure 1-3: Rotating table Sensor Turn

1.2 Multivariate data analysis[1]

Multivariate data analysis (MVDA) plays a key role in the implementation of PAT and QbD [35] as it enables the transformation of the enormous amount of data generated by process analysers into relevant and crucial process information [36].

[1] Parts of this section are to some extent based on chapter 2 „ Comparison of NIR Spectroscopy with DEM Simulations for Tracing the Spatial Dispersion of Water during Mixing" written by the authors Roland Hohl, Nicolas Heigl, Daniel Koller, Charles A. Radeke

In this sub chapter the building of a model is described for NIR spectrometer. First of all samples with different amount of water were homogeneously distributed on a rotating table (Sensor Turn, WLP-TEC GmbH, Göttingen, Germany), shown in Figure 1-3, which was rotating counter clockwise. The fiberoptic probes were fixed on an acrylic glass disc which was then mounted three millimeters above the rotating material to collect the spectra. The gained data were up loaded to SIMCA 13 P+, and a model has to be built in this program. An example of the raw spectra is shown in Figure 1-4. The raw NIR spectra Figure 1-4 (A) show two water-characteristic bands at 5 150 $cm^{-1}$and 6 875 cm^{-1}, which were assigned to the combination of bending and asymmetric stretching of the O-H (v_3 + v_2) and the symmetric and asymmetric stretching O-H (v_1 + v_3), respectively. As pretreatment for the spectra SNV was used the spectra are shown in Figure 1-4 (B), the increase of the water peak can be seen.
For a predictive model partial least square regression (PLSR) was used. It is a recently developed generalization of multiple linear regression (MLR) [37], [38]. PLSR is of particular interest because, unlike MLR, it can analyse data with strongly collinear correlated, noisy, and numerous X-variables [38]. The PLSR calibration model was validated via segmented cross-validation with leave one out (CV-LOO) in which the spectra of a standard formed a segment. The root mean squared error of estimation (RMSEE) and root mean squared error of prediction (RMSEP) represent the PLSR models prediction accuracies for the calibration samples and the validation samples, respectively, and are given as

$$RMSEE, RMSEP = \sqrt{\frac{\sum_{i=1}^{n}(y_i - \hat{y}_i)^2}{n}} \quad (1)$$

Where y_i is the actual (reference) value of y for object i, $\hat{y}$ is the y-value for object i predicted by the model and n is the number of objects (NIR spectra).

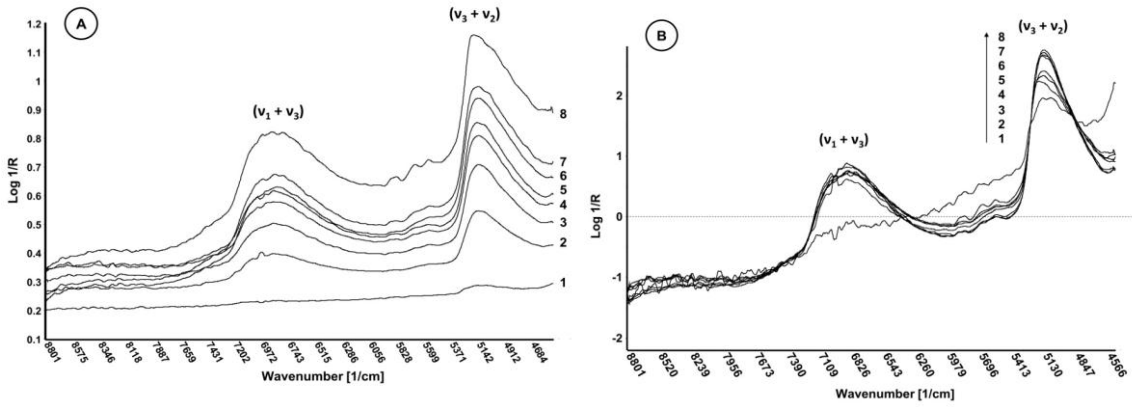

Figure 1-4: (A) raw NIR spectra (B) NIR spectrum after SNV filter

Two PLSR calibration strategies can be followed to predict the % of water via NIRS during the spraying and mixing procedure with more than one sensor:

- all recorded spectra from the different fibers are merged to develop a PLSR model

  or
- individual PLSR models can be developed for each channel with the respectively collected spectra.

In most cases the development of individual models for each channel is more suitable than developing a general model over all channels.

1.3 Fluid bed and hot melt coating[2]

Pharmaceutical coating processes take place in coating pans or fluid bed apparatuses. Most tablets are coated in pans or drums but also fluid bed equipment is in use. Pellet coating is typically performed in a fluid bed [39]. The principle of a fluid bed is to maintain particles in suspension in a close area by blowing air through the powder bed. The state of the fluid bed depends on the air velocity and the powder properties [40], c.f. Figure 1-5. The fluid bed is still a very complex unit operation, mostly because the trajectories of particles in the fluid bed are not predictable. Powders can be classified by their properties and functionality. Geldart's works (1986) have shown that, for the fluidisation process, powders can be classified into four groups Figure 1-6 according to fluid density and the particle size and density [40]. Powders from group C are cohesive and difficult to fluidised, powders from group A present the aeration property required for coating purposes.

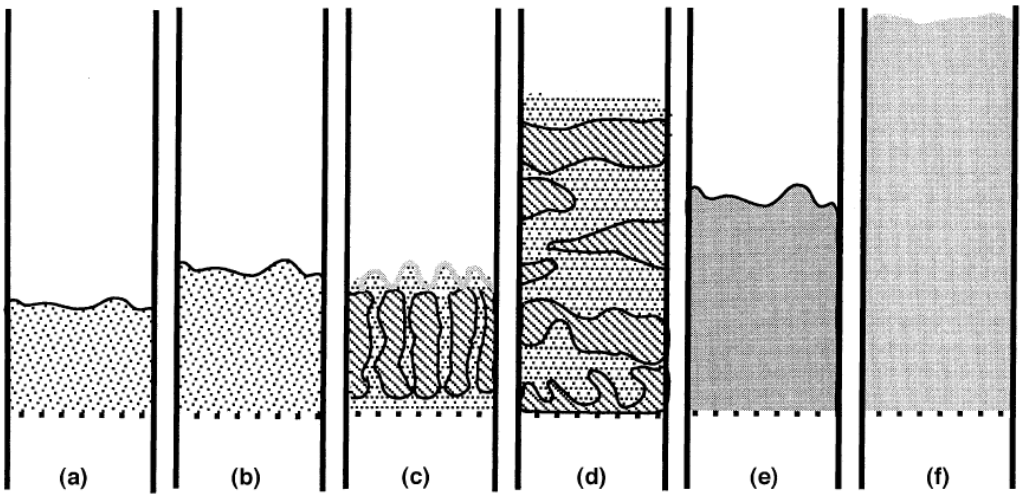

Figure 1-5: Different configurations of a fluid bed: (a) fised bed; (b) expansion; (c) channelling; (d) slugging; (e) stable fluid bed; (f) conveying. [40]

[2] Parts of this subchapter are based on the paper Monitoring of a Hot-Melt Coating Process via a Novel Multipoint Near Infrared Spectrometer

Fluid Beds are a widely used and versatile unit operation in the pharmaceutical industry. Putting to use their property of very large particle to air contact surface, they are an advanced method for drying, coating and more [40]. A great deal of interest has already been invested, concerning the properties of fluid beds, especially their geometry and flow pattern, mostly, this is a field for simulations [41], [42].

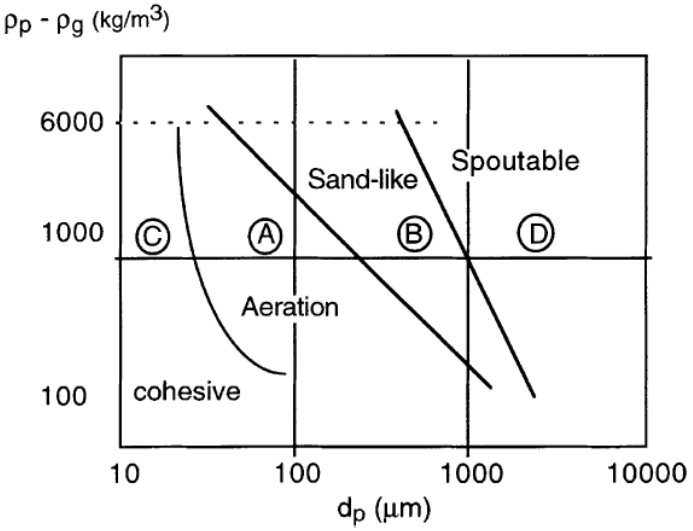

Figure 1-6: Geldart's classification of powders [40]

Nonetheless, the efficiency of fluid beds is often driven by the experience of their operators. This is a result of fluid beds being very sensitive to subtle changes, which can affect the flow pattern significantly, even disenabling the fluid bed process as a whole. Even more so, this increases the difficulty of placing sensors in such an environment, making systematic experimental investigations a delicate work.

Hot-melt coating was performed in an Innojet® laboratory system Ventilus® V-2.5/1 with an Innojet® Hot-Melt-Device IHD-1 (INNOJET HERBERT HÜTTLIN, Germany). Ventilus® V-2.5/1 is a multi-purpose system for granulation, coating and hot melt coating. In this system a bottom spray nozzle was used, sketch and movement of the fluid bed are shown in Figure 1-7.

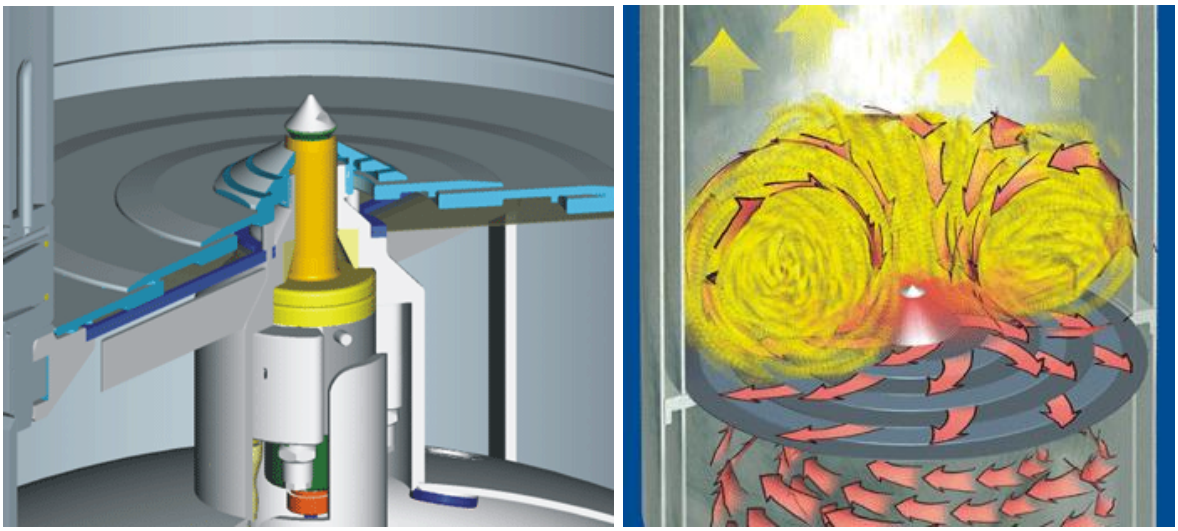

Figure 1-7: Sketch of Ventilus Innojet[3]

In-line NIR measurements for pharmaceutical tablet coating processes in a pan coater were introduced 2005 by Perez-Ramos et al. [43] with univariate calibration and 2008 by Römer et al. with multivariate calibration[19]. In different studies the monitoring of coating process with NIR is shown [44], [45] [46], [47]. With a novel multipoint NIR in-line measurements of the hot melt coating process were performed, the fibers were located at different positions in the production chamber.

[3] http://www.sinomach.com/products/innojet.html

1.4 Dynamic cross flow filtration

The main goal of separation is to get a clear liquid, in pharmaceutical industries the solids are in most cases of interest. These are the active pharmaceutical ingredient (API) and those should be separated from the mother liquor and the impurities. For this task two main types of filters are available on the market first there are filtration systems in which the separation is done batch wise, these are often used in pharmaceutical industries, the second type of filter systems are working continuously. There are several systems on the market such as rotating disk systems, rotating cylindrical membranes and also shear – enhanced filtration system [48]. Rotating disk systems like the multishaft disk (MSD) system are subjects of different studies [49]–[51]. In these studies it could be seen that the permeate flux is strongly influenced by the rotor speeds and the pressure, also the right membrane has to be chosen [52] for getting the highest permeate flux. This means that the membrane resistance has to be minimized but also the membrane fouling has to be prevented the different types of membrane fouling were shown by Belfort et al. [53]. A rotating disk system is the Optifilter CR by Metso Paper (Raisio, Finland) [54] or also in a variation of this concept the DynoFilter manufactured by Bokela GmbH (Karlsruhe, Germany) [54], [55]. Here the DynoTest filter from Bokela was used and characterized. For characterizing this system the influences of different process parameters on the filtration behavior and the CQAs has to be analyzed. CQAs are physical or chemical characteristics, which must be controlled to ensure the quality of the product. Critical process parameters (CPPs) are process inputs, which have a direct and significant effect on CQAs, when they are varied within the experimental range [56].

Figure 1-9: Bokela Dynotest

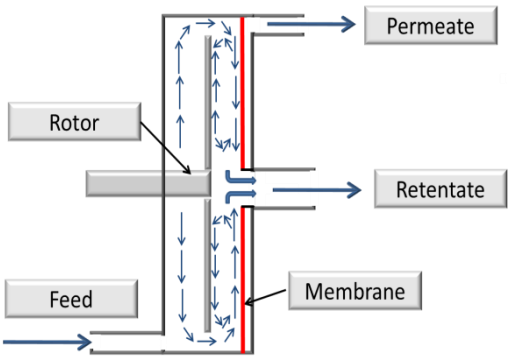

Figure 1-8: Shematic drawing of DynoTest and the flow in the Dynotest

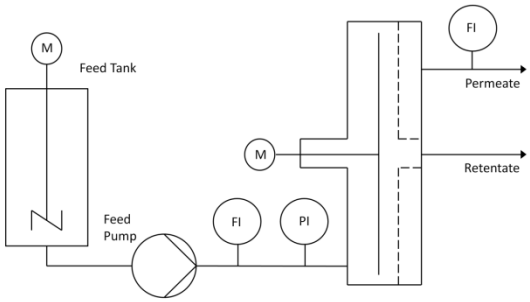

Figure 1-10: Schematic filtration setup

During processing a ceramic membrane with a thickness of 2 mm, pore size of 0.5 µm, inner diameter of 65 mm and outer diameter of 156 mm (Kerafol Keramische Folien GmbH, Germany) is mounted in the front plate, right before the rotor. The residual moisture of the steady-state product was calculated from the feed and permeate flow measurements. Additionally, retentate samples were taken and dried in a thermo-gravimetric balance. The concentration factor (CF) was calculated according to [57] as the ratio of retentate and feed concentration, respectively.

$$\mathrm{Cf} = \frac{c_{\mathrm{retentate}}}{c_{\mathrm{feed}}} \quad (2)$$

The cf gives information about the residual moisture in the retentate, the residual moisture was not measured via NIR here as PAT tool two flow meters were used. Feed throughput was measured uing an electromagnetic flow meter type FSM4000® (ABB GmbH) with ≤0.5% accuracy. Permeate throughput was measured using an electromagnetic flow meter type 008AP001E® (Honsberg Instruments GmbH, Germany) with 2.5% accuracy. To measure filtration pressure, a pressure sensor type 261GS® (ABB GmbH) with ±0.1% accuracy was implemented. A simplified P&I schema is depicted in Figure 1-10.

1.5 Thesis content

The aim of the study presented in chapter 2 is to validate a wet mixing process, where a liquid spray is used to impregnate particles whilst mixing. Here for a near infrared (NIR) sensor instrumented bladed-mixer is utilized in order to compare an experiment with a 1:1 discrete element method simulation (DEM).

The used particles in both cases were absorbing the sprayed liquid over the process time of. With multiple sensors attached to the mixer wall the liquid content of bypassing particles continuously was monitoring. This study has be done because spraying liquids is frequently implemented to the processing of active pharmaceutical

ingredients (APIs) and excipients, e.g. during wet granulation, blending, coating or fluidized bed granulation, in which dispersion of the liquid phase is considered as a critical quality attribute (CQA) [58]. Traditionally, Karl-Fischer titration (KF) and loss on drying (LOD) are employed for the residual water detection, however, both methods show drawbacks, such as long measurement duration, invasive analysis, and no on-line capabilities [59]. In contrast, near-infrared spectroscopy (NIRS) enables highly time-resolved and non-invasive on-line monitoring of water, which was already discussed in chapter 1.1. Furthermore, discrete element method (DEM) simulation was applied to virtually quantify the amount of sprayed fluid onto the spheres when passing the spraying zone. Consequently, the DEM-simulation data was compared with the experimental NIRS data. In contrast to the locally restricted short range NIR sensor analysis, DEM allows the observation of liquid distribution for each individual particle in a simulation over the whole process time.

The aim of the present work in chapter 3 was to demonstrate the advantages of multipoint monitoring of a hot melt coating process. Here for the optical fibers were placed in various positions in the process chamber of a fluid bed device. In our experiments, inhomogeneities and disturbances in the process chamber were promptly detected. In addition, a sensor's malfunction was compensated for, resulting in the product quality assurance and the correct process endpoint determination. Spectroscopic methods are generally based on single probes. Here multipoint NIR was used for predicting the coating amount at different positions in the process chamber. The Coating of solid dosage forms is a typical process step in pharmaceutical manufacturing for various purposes; Including taste masking, increasing the shelf life or tailoring the release profile of the active pharmaceutical ingredient [16], [47], [60]. Multipoint near infrared systems provide better monitoring possibilities and control of the coating process, for example, with regard to controlling homogeneity and determining the end point of a process [61], [62].

The aim of the present work in chapter 4 dynamic cross flow filter was to specify a filtration system which can handle high viscous slurries and is at the same time very flexible, also the modular scale-up possibilities. In this study flow meters and a pressure sensor were used for process monitoring. The residual moisture could be also detected via NIR but for more flexibility so that we also can use other solvents

flow meters were chosen. To evaluate the performance of the filtration system two crystalline material systems which are relevant for the pharmaceutical industry were chosen. The first system was Ibuprofen suspended in water and as second lactose suspended in water. The main focus is the development of a fundamental theoretical model allowing and understanding of the experimental results.

2 Comparison of NIR Spectroscopy with DEM Simulations for Tracing the Spatial Dispersion of Water during Mixing[4]

[4] This chapter is based on on the paper Comparison of NIR Spectroscopy with DEM Simulations for Tracing the Spatial Dispersion of Water during Mixing written by the authors Roland Hohl, Nicolas Heigl, Daniel Koller, Charles A. Radeke, 11.07.2017 accepted in the journal Particuology

Abstract

The aim of the presented work is to validate a wet mixing process, where a liquid spray is used to impregnate particles whilst mixing. A near infrared (NIR) sensor instrumented bladed-mixer is utilized in order to compare an experiment with a 1:1 discrete element method simulation (DEM). The porous particles used in both cases are absorbing the sprayed liquid over a process time of about 18 minutes. Multiple sensors attached to the mixer wall are monitoring the liquid content of bypassing particles continuously. The sensors are modeled accordingly in the simulation and the resulting signals are analyzed and compared. We show that the implemented algorithms for spray and liquid absorption can be used to predict moisture distribution inside granular materials in chemical and pharmaceutical processes. Such simulations can help to save money for resource-intensive experiment plans, equipment design studies, and variations of material parameters and beyond.

2.1 Introduction

Spraying liquids is frequently implemented to the processing of active pharmaceutical ingredients (APIs) and excipients, e.g. during wet granulation, blending, coating or fluidized bed granulation, in which dispersion of the liquid phase is considered as a critical quality attribute (CQA) [58]. Since there has been a growing tendency to use water as a solvent, as it is environmentally friendly and eliminates explosion risk compared to organic solvents, monitoring of water content has become an important task. Moreover, water can have a pronounced impact on the formulations chemical reactivity and stability, and on the final product quality and shelf-life [58], [63]. Traditionally, Karl-Fischer titration (KF) and loss on drying (LOD) are employed for the residual water detection, however, both methods showing considerably drawbacks, such as long measurement duration, invasive analysis, and no on-line capabilities [59].

However, constant advantages have been made in order to enable on-line determination of water content in granular material for the biomass, food and pharmaceutical industry, based on several principles. A robust application is found via capacitance, or impedance methods, based on the high dielectricity of water [64], [65]. Those methods offer the further advantage, that with some computational effort, a tomographic reconstruction (i.e. a soft model) of the water distribution is possible [66].

Naturally, attenuation and phase shift of microwave radiation can be used for moisture determination [67]. Also triboelectric probes were presented, used for determining moisture content during a granulation process at several positions [68].

Additionally, near-infrared radiation shows extremely strong absorption for water, exhibiting two distinct absorption bands in the near-infrared (NIR) region, i.e. the combination of bending and asymmetric stretching of the O-H (v_3 + v_2)from 5100 - 5300 cm^{-1} and the combination of the symmetric and asymmetric stretching O-H (v_1 + v_3) from 6800 - 7100 cm^{-1}, and thus numerous applications have already been shown. [3], [5], [29], [32], [58], [69].

Near infrared spectroscopy offers the possibility of fast and real-time measurements, coupled e.g. with material identification or concentration estimation at the same time. However, compared to e.g. microwave absorption, NIR has the drawback of a very

limited penetration depth into the sample, at the same time however allowing easy access to sealed environments via fiber optics.

In this study we used a lab-scale stainless steel reactor equipped with a spray nozzle and a four-bladed impeller for moisturizing and blending aluminum oxide (Al_2O_3) spheres. Thereby, on-line multipoint NIRS with differently located fiberoptic probes was applied to follow the dispersion of water. Partial least squares regression (PLSR) with loss on drying (LOD) as reference technique was used to develop a linear multivariate model to predict the percentage LOD of the processed Al_2O_3 spheres. Furthermore, discrete element method (DEM) simulation was applied to virtually quantify the amount of sprayed fluid onto the spheres when passing the spraying zone. Consequently, the DEM-simulation data was compared with the experimental NIRS data.

In contrast to the locally restricted short range NIR sensor analysis, DEM allows the observation of liquid distribution for each individual particle in a simulation over the whole process time. Consequently, we use this outstanding capability by modeling and analysis of a 1:1 simulation of the mixing device and the granules.

Classical DEM simulation tools lack the capability of liquid spraying and liquid spread out into powders or particle beds. Therefore we use an in-house code with appropriate extensions to capture the application of a spray nozzle for continuous wetting of a powder whilst mixing.

2.2 Materials and methods

2.2.1 Experimental part

2.2.1.1 Aluminium oxide

Aluminium oxide (Al_2O_3) spheres (SA 52124, UniSpheres®) were purchased from Saint-Gobain Nor Pro (New Jersey, USA). The median sphere diameter is 1.3 mm, surface area is 5.00 m^2/gm, median pore diameter is 0.15 µm, total pore volume (Hg) is 0.30 cm^3/g, packing density is 1040 kg/m^3, chemical purity is < 0.1 % SiO_2 and maximum water absorption level is 30 wt-%. We here used α-Al_2O_3, which is insoluble in acids or bases and shows adequate mechanical stability.

2.2.1.2 Experimental setup

The mixing experiments were carried out using a lab-scale reactor made of stainless steel (id = 10 cm) with a controllable four-bladed steel impeller (Heidolph RZR 2102 control; blade diameter =95 mm, blade width = 25 mm, blade angle = 45 °). Rotating speed was 4 rpm in a counter-clockwise direction. Six different ports, i.e. vision panels made of NIR penetrable sapphire glass, are integrated to connect single fiberoptic probes (Figure 2-1). The blending behavior of this setup was already described in [61]

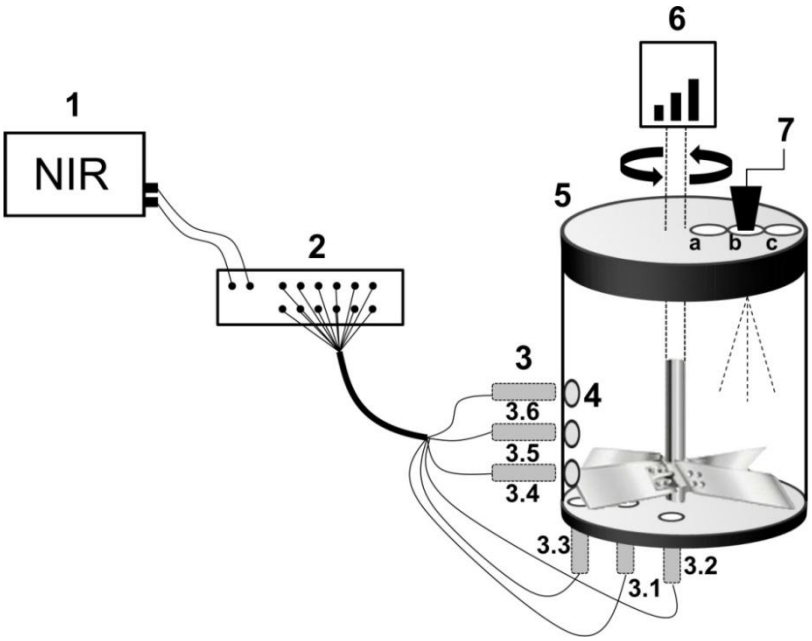

Figure 2-1: Scheme of the experimental setup: (1) NIR spectrometer, (2) fiber switch box, (3.1 – 3.6) single fiberoptic probes, (4) NIR transparent sapphire glass windows, (5) mixing reactor, (6) controllable mixing device with four-bladed impeller, (7) spray nozzle which can be installed at three different positions, (a) inner spray nozzle position, (b) middle spray nozzle position, (c) outer spray nozzle position.

2.2.1.3 NIR instrumentation

NIR spectra were recorded with a FT-NIR400 Spectrometer (PerkinElmer, Brunn am Gebirge, Austria) which was connected to a fiber switch box (FSM2 1× 6, piezosystem jena GmbH, Jena, Germany) enabling successively recording spectra at six different locations. The spectral range was 4100 - 10,000 cm^{-1} and the spectral resolution was 16 cm^{-1}. Recording of a full-range spectrum per fiber probe, or channel, was achieved in about 0.35 seconds. Twelve scans were averaged to gain

adequate signal-to-noise ratio (SNR), leading to a total measurement time of 4.2 seconds per spectrum and channel. Accordingly, total measurement time for the six successively activated channels was 25.2 seconds.

2.2.1.4 NIR calibration

Partial least squares regression (PLSR) with LOD (MLS-N Moisture Analyzer, Kern & Sohn GmbH, Balingen-Frommern, Germany) as a reference method was used to develop a linear multivariate model (SIMCA P+; Umetrics, Umeå, Sweden) for the moisture quantification of the Al_2O_3 spheres. Therefore, calibration standards were prepared by filling 20 g of dry Al_2O_3 into 100 ml plastic bottles and adding predefined amounts of distilled H_2O (TKA, MicroPure UV Reinstwassersytem, Niederelbert, Germany). The moisturized samples were subsequently mixed for two minutes to equally distribute H_2O (Turbula® T2F; Willy A. Bachofen GmbH, Muttenz, Switzerland).The calibration range was limited from 0 to 26 wt-% H_2O, as exceeding moisture contents yielded Al_2O_3 agglomerates. The amounts of sprayed wt-% H_2O and the associated regained % LOD values for the calibration standards are listed in Table 2-1.

Table 2-1: NIR calibration standards with varying amounts of wt-% H_2O. The actual amount of H_2O was confirmed with LOD. (*(n = 3))

Standard	Theoretical wt-% H_2O	Actual mean wt-% H_2O ± SD*	Mean % LOD ± SD*
1	0	0.00 ± 0.00	0.00 ± 0.00
2	5	4.80 ± 0.17	3.78 ± 0.83
3	10	9.68 ± 0.63	8.76 ± 1.50
4	15	13.60 ± 1.10	12.70 ± 1.02
5	17	16.73 ± 0.23	16.47 ± 0.44
6	20	20.31 ± 0.78	20.39 ± 0.87
7	25	22.65 ± 0.38	22.54 ± 0.36
8	26	24.70 ± 0.75	24.80 ± 0.74

In a next step, one standard material after another was homogeneously distributed on a rotating table (Sensor Turn, WLP-TEC GmbH, Göttingen, Germany) which was turned at 42 rpm. The six fiberoptic probes were fixed on an acrylic glass disc which was then mounted three millimeters above the rotating material to collect the calibration spectra. Twelve single NIR spectra were successively recorded for each

of the six channels. Accordingly, a total of 576 NIR spectra, i.e. 8 (standards) × 6 (channels) × 12 (spectra per channel), were used to build a PLSR calibration model. The PLSR calibration model was validated via segmented cross-validation with leave one out (CV-LOO) in which the 12 spectra of a standard formed a segment. The root mean squared error of estimation (RMSEE) and root mean squared error of prediction (RMSEP) represent the PLSR models prediction accuracies for the calibration samples and the validation samples, respectively, and are given as

$$RMSEE\ ,RMSEP\ = \sqrt{\frac{\sum_{i=1}^{n}(y_i - \hat{y}_i)^2}{n}} \quad \textbf{(1)}$$

Where y_i is the actual (reference) value of y for object i, $\hat{y}$ is the y-value for object i predicted by the model and n is the number of objects (NIR spectra).

2.2.1.5 Experimental procedure

First, dry Al_2O_3 was loaded at the mixer to cover the impeller, which corresponds to 110.5 g of material. Two full impeller revolutions were accomplished to equilibrate the system. In a next step, 15 wt-% H_2O was sprayed at 0.75 ml/min during continuous mixing, what equals 20 minutes spray time. Meanwhile, NIR spectra were sequentially collected at channels 3.1 to 3.6 (see Figure 2-1). Consequently, one spectrum per channel was recorded every 25.2 seconds (see section 2.3). Finally, the prior developed PLSR model was used to predict the % LOD by means of the recorded NIR spectra.

2.2.2 Simulation

2.2.2.1 DEM code

In order to achieve faster execution times and higher particle numbers we developed a parallelized DEM code. Our implementation uses the CUDA technology [70]. The program development started already in April 2008 at Prof. F. Muzzios Department for Chemical and Biochemical Engineering of “Rutgers, the State University of New Jersey”.

At this time, with our code one can simulate millions of particles on consumer hardware. The maximum number of particles depends on the memory size of the equipped graphics card. The simulations presented in this paper are executed on an NVIDIA GTX 285 2GB graphics board. At the present development stage it is possible to simulate about two millions of particles per Giga Byte of graphics memory.

2.2.2.2 Implementation

Our numerical model is a 'soft' particle approach where spherical particles exert forces due to their mass m and geometrical overlap δ at the contact points c. The total force F and torque M acting on a particle

$$F = \sum_c f^c + mg \qquad (3)$$

$$M = \sum_c r \times f^c \qquad (4)$$

is the summation of contact forces f^c with other particles or boundaries and gravitational force. Considering Newtons second law, at time t we obtain an acceleration a(t) which can be used for an explicit time step integration with a time step dt in order to obtain new velocities v(t + dt) and positions x(t + dt) for each particle in the system. Here, the classical Verlet integration scheme is employed for positions [71]

$$a(t) = F / m \qquad (5)$$

$$x(t+dt) = 2x(t) - x(t-dt) + a(t)dt^2 \qquad (6)$$

and velocities obtained by central difference approximation

$$v(t+dt) = 1/2dt(x(t+dt) - x(t-dt)) + a(t) \quad \textbf{(7)}$$

The implementation accounts for translational as well as for rotational degrees of freedom. Both are handled separately by the application of the Verlet algorithm (4 - 7) and an Euler integration (8) in the latter case. Total torque M and moment of inertia I are used to obtain the angular acceleration $\dot{\varpi}(t)$

$$\varpi(t) = \frac{M}{I} \quad \textbf{(8)}$$

and the new angular velocity at time t + dt

$$\varpi(t+dt) = \varpi(t) + \dot{\varpi}(t)dt \quad \textbf{(9)}$$

In order to obtain the new particle orientation q(t + dt) the integration of the angular velocity is performed afterward. Here, q(t + dt) is a quaternion representation of particle orientation, details can be found in (Shigeto, Y. & Sakai, M., 2011.). The implemented force laws are linear in normal and tangential direction and follows the implementation suggested in [72].

$$f_n = k_n\delta_n - D_n\dot{\delta}_n - f_{ch} \quad \textbf{(10)}$$

$$f_t = -\min(k_t\delta_t - D_t\dot{\delta}_t, \mu|f_n|) \cdot \mathrm{sgn}(\delta_t) \quad \textbf{(11)}$$

where μ is the static Coulomb friction coefficient, k_n, k_t are spring constants and D_n, D_t account for viscous damping in normal and tangential direction respectively. The cohesive force f_{ch} is only active in the case of liquid bridges.The tangential overlap

$$\delta_t = \delta_t(t) + \delta_t(t-dt) \quad \textbf{(12)}$$

allows for restoring forces if the contact had been existed already in the previous time step. Analogous to sliding friction rolling resistance is implemented.

The boundary conditions (walls) are modeled as DEM standard, where geometric primitives (planes, cylinders) interact with contacting particles by their common normal planes. Impeller blades are modeled using inclined planes adjusted to the measures of the experimental device. The blades are rotated by constant RPM, according to the experiment (table 3).

Where our code is able to simulate a few millions of individual particles, in the presented case we use the computational power to simulate a 16 minutes (!) lasting experiment of 64,000 particles.

2.2.2.3 Particle spray and impregnation modelling

The spray nozzle was modeled by defining a conical spray zone located inside the mixer. Many rays originate in the spray nozzle, which is assumed to be a point source (Figure 2-2).

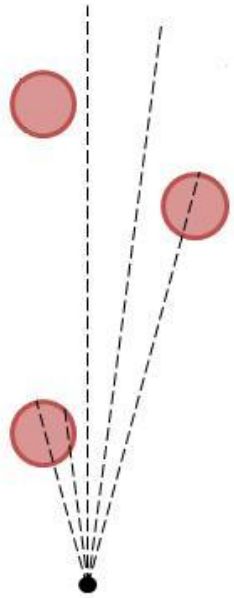

Figure 2-2: 2D-Sketch of the ray-tracing method.

The size of the resulting spray zone depends –as in reality- on the spray cone angle. Each of the rays detects intersecting particles, which increase their liquid content according to their number of ray hits in this time step. The mass of liquid absorbed by the particle increments according to the former time step values, where $m_{abs,i}$ is the mass of absorbed liquid in current time step of particle i, $\dot{n}_{spray}$ is the spray rate of the

nozzle in mL/min , N_{ray} is the number of rays that hit particle i in the time step dt. So the resulting liquid content can be calculated as follows:

$$m_{abs,i} = \frac{N_{ray,i}}{N_{ray,total}} \dot{n}_{spray} dt \qquad \textbf{(13)}$$

.

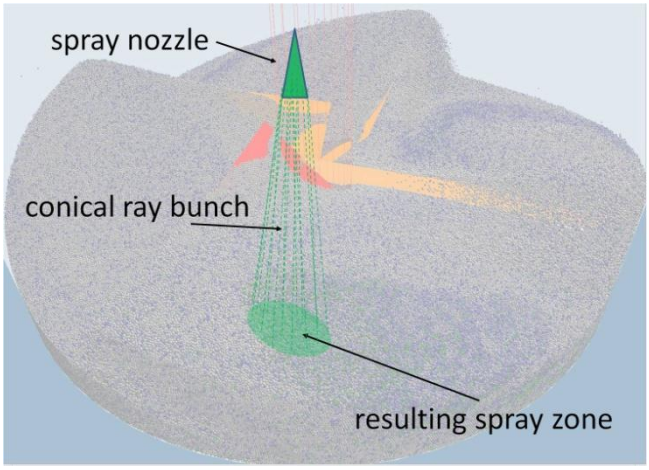

Figure 2-3 Impregnation modeling: Rays running from the spray nozzle through the particle bed and hitting particles in the resulting spray zone.

Thus, particles liquid content is recorded over simulation time. This fast in-line method allows impregnation modeling during the DEM calculation, rather than doing a post-processing. Using this method, particle properties (mass, size, stiffness etc) can be changed over simulation time.

In the simulations of the present work, moisture is not present at particle surface. Therefore, cohesive forces or a change of friction values does not apply. This is coincident with the simulated process, called ‘dry impregnation’, where typically a fine spray fog is used to impregnate particles over a longer period, in order to avoid over-wetting and agglomerate formation.

The mathematical model of the spray nozzle is rather simple and does not include droplet size, droplet distribution or pressure. It assumes an evenly distributed spray fog along with a given spray rate, which results in a homogeneous distributed moisture content for particles in the spray zone. Enhancements of the algorithm for biased droplet distribution and wetting effects (liquid brides, agglomerates etc) are possible, but require validation experiments beyond the scope of the presented work.

2.3 Experiment

2.3.1 Spray nozzle positioning and NIR fiberprobe locations

Generally, the location of the spray nozzle can significantly impact the dispersion of liquids during mixing. In a bladed mixer, mixing is achieved throughout a combination of two mechanisms, a convective part of collective particle streams due to blade rotation and a diffusive part caused by the local interaction of particles with higher granular temperature. Considering the chamber between two blades, one circular convective stream can be observed in-plane of the bottom of the device, directed inverse to the stirrer rotational orientation. The other convection takes place when particles are piling up in front of the inclined blade and stream over the upper blade edge.

Diffusive mixing is expected to occur and to be highest at the range of the blade tips because of the strong increase of circumferential speed in radial direction. Furthermore, the cylindrical wall of the mixer restricts particles spatially and forces the release of their kinetic energy partially in diffusive mixing.

Both mixing effects are superimposed at the blade tips but in our simulations the combined two convective streams in the central radial position area of the blade shows faster mixing. Therefore this central location was chosen for the spray position.

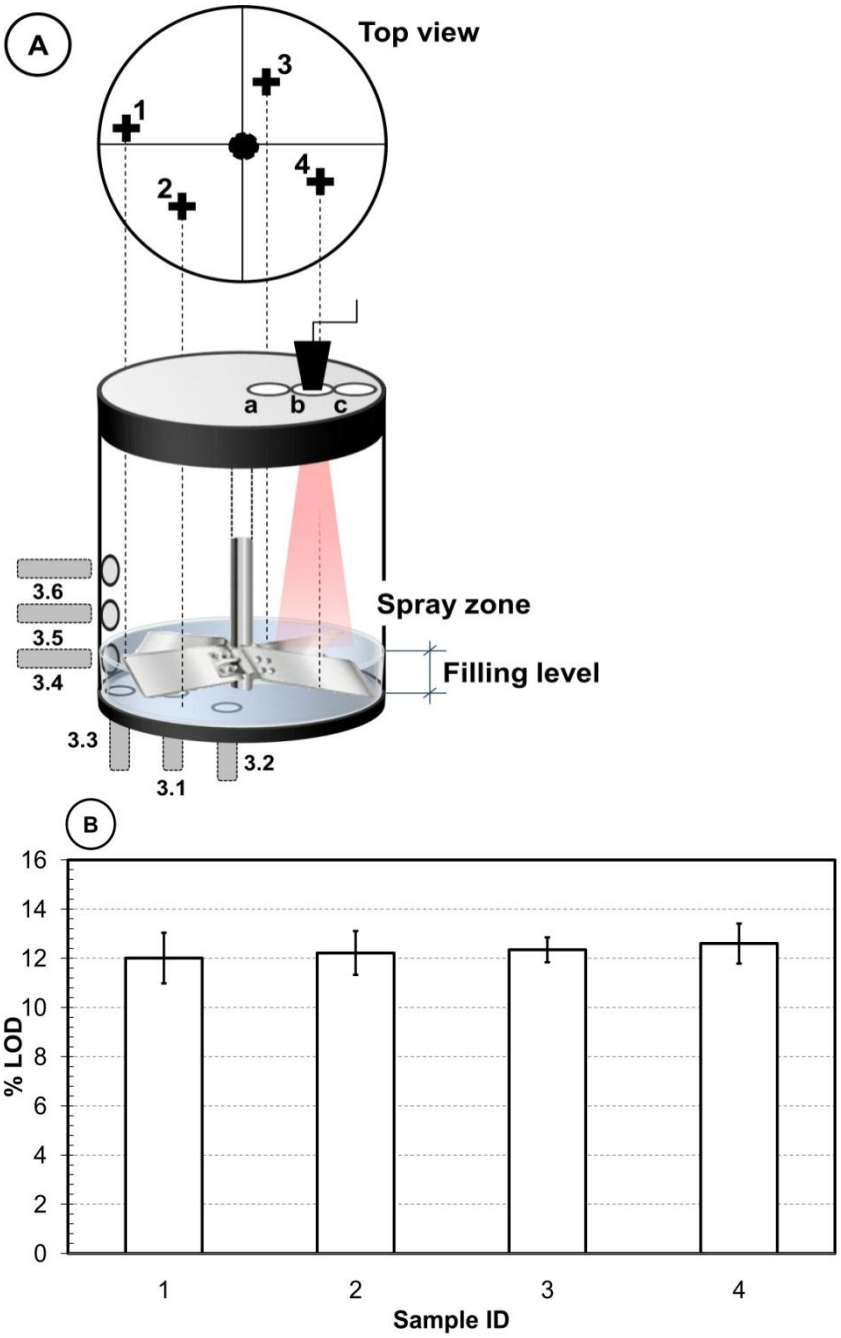

Figure 2-4 Samples were thief-probed at four different bed locations after the spraying and mixing procedure.

To evaluate the homogeneity of H_2O dispersion throughout the Al_2O_3 bed after the spraying and mixing procedure, four individual samples were taken from different bed locations, as displayed in Figure 2-4A, which were subsequently analyzed with LOD. Three individual batches were examined showing satisfactorily reproducibility (Figure 2-4B).

The bars indicate almost equally distributed H_2O throughout the Al_2O_3 bed, whereas the associated error bars (n=3) indicate good batch-to-batch reproducibilities (Figure

2-4B). Due to the relatively low amount of sprayed H2O (15 wt-% ≈ 15 ml, spray rate 0.75 ml/min) compared to the reactor volume (1178 ml), what equals a ratio of 1:78.5, the loss by evaporation and entrainment is supposed to be significant. Here the mean loss for the four sampling positions was 2.71 wt-% H_2O.

Furthermore, due to the rather low filling level only channels 3.1 to 3.4 were evaluated, as channels 3.5 and 3.6 did not provide any signal (Figure 2-4A). Also, some of the Al_2O_3 spheres burst into smaller pieces during the mixing process as they were crushed between the impeller blades and the side wall of the reactor. The resulting fines sedimented at the bottom corners of the reactor but did not significantly bias the NIR measurements.

2.3.2 PLSR modeling

In general, NIR spectra of the same material often show fluctuating signal intensities because of distinct light scattering, which is a result of changing refractive index from solid- to gaseous phase, and light transmission in the samples. With dynamic processes, such as mixing or blending, this effect becomes even more pronounced as the sample distances from the light exit, e.g. fiberoptic probe, additionally change. As a result, primarily a spectral baseline offset (parallel baseline shift), which is a multiplicative effect, or a sloped baseline, which is an additive effect are observed. These often disturbing effects need to be eliminated prior developing calibration models, otherwise erroneous predictions would be the result. Thus normalization algorithms, derivatives and scatter correction methods, such as multiplicative signal correction (MSC) and standard normal variate (SNV), are frequently applied(Reich, G., 2005., Shigeto, Y. & Sakai, M., 2011., Verlet, L., 1967.) In our case, second derivative (Savitzky-Golay, 21 points smoothing) pretreatment effectively corrected the emerging baseline shifts and was therefore used as a standard spectral pretreatment. The raw NIR spectra and the corresponding SNV and 2nd derivative spectra of the eight Al_2O_3 (0 - 26 wt-% H_2O) calibration standards, which were recorded on a rotating sample desk, are illustrated in Figure 2-5 A–C.

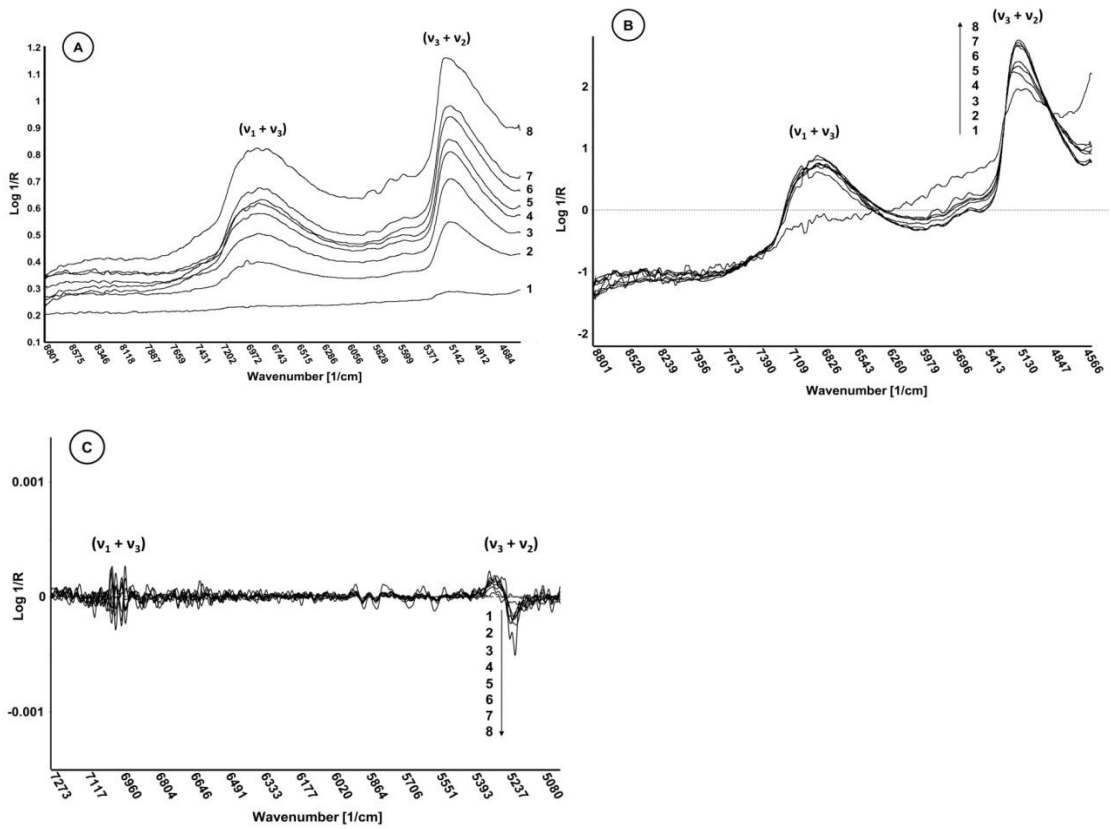

Figure 2-5 NIR spectra of the eight calibration standards with 0 – 26 wt-% theoretical H_2O contents (see Table 1).

In Figure 2-5A the raw NIR spectra show two water-characteristic bands at 5150 cm-[1]and 6875 cm^{-1}, which were assigned to the combination of bending and asymmetric stretching of the O-H (v_3 + v_2) and the symmetric and asymmetric stretching O-H (v_1 + v_3), respectively. SNV effectively corrected for a strong spectral off-set (Figure 2-5 B), thus revealing only subtle Log 1/R increase with increasing H_2O content. Therefore, the second derivative spectra (Figure 2-5C) only exhibited relatively small intensity changes with increasing water content but at the same time a zero baseline, which is beneficial for quantifying the H_2O content as no physical interferences bias the predictions. (1) is for theoretical zero wt-% H2O and (8) is for theoretical 26 wt-% H2O.

Two PLSR calibration strategies were followed to predict the % LOD via NIRS during the spraying and mixing procedure: (i) all recorded spectra from channels 3.1 to 3.4 were merged to develop a PLSR model (termed “general PLSR model” in the following), and (ii) four individual PLSR models were developed for each channel 3.1,

3.2, 3.3 and 3.4 with the respectively collected spectra. Table 2-2 provides the corresponding calibration statistics of the PLSR models.

Table 2-2 PLSR calibration statistics

Model number	Model type	Channel(s)	Spectral pretreatment	PLS-factors	Explained variances (%) **X**, **Y**	RMSEE	RMSEP	R^2	Q^2
1	General	3.1 - 3.4	2nd derivative	3	17.6, 72.3	4.175	6.466	0.723	0.616
2			SNV	5	98.1, 92.3	2.116	21.382	0.923	0.913
3	Individual	3.1	SNV	4	78.8, 96.4	0.722	13.101	0.968	0.987
4		3.1	2nd derivative	2	5.5, 96.8	1.383	5.132	0.966	0.700
5		3.2	2nd derivative	1	3.7, 88.7	2.363	5.698	0.887	0.700
6		3.3	2nd derivative	4	100, 89.7	2.268	6.268	0.897	0.809
7		3.4	2nd derivative	1	7.76, 90.6	2.339	5.233	0.906	0.797

2.4 Simulation procedure

2.4.1 Setup

In order to achieve a 1:1 comparison to the experiment, geometrical dimensions of the mixing device, impeller speed, spray rate and spray frequency are modeled accordingly. The particle properties (size, shape, amount, porosity, fill level) are modeled as close as possible to the experimental data. The simulating parameters are shown in Table 2-3.

Table 2-3 Simulating parameters

Parameter	Value / Unit
Impeller speed	4 rpm
Number of particles	63744
Particle size	1.3 mm
Particle porosity	0.45 % (of Volume)
Spray rate	0.75mL/min (15% weight within 20min)
Impeller diameter	95mm
Blade angle	45 deg
Blade height	25mm
Particle density	1125kg/ m^3

2.4.2 Process simulation

Initially the particles are created at random positions inside the device atop of the blade area. The system was allowed for settling whilst two revolutions. After this initial step the time was set to zero and the onset of spray was started. Then, the simulation runs for 72 revolutions at 4 rpm, which results in a total process time of 18 minutes.

The spray nozzle is fixed at central position (b), directing parallel to the impeller axis according to Figure 2-4A. The spray zone covers a circular area of about 30 mm diameter (varying, depending on impeller passage and bed height).

Particles inside the spray zone are detected by a projection algorithm (ray tracing, Section 2.2.2.3). Every particles' spray zone visit is monitored and leads to a recording of its residence time and the corresponding liquid content under consideration of the constant flow rate. Details of the spray algorithms used to extend the DEM code are not within the scope of the present work and will be presented in a separate paper.

2.5 Results

2.5.1 Alignment of depth of scrutiny of off-line, on-line and simulated data

Naturally, the different presented methods offer a different depth of scrutiny for the interpretation of the process.

Regarding the LOD measurements, happening offline, one is basically free in choosing an appropriate sample size. However, in practice limitations on the amount to be analyzed are given by the measurement equipment, but also by the practical limitations in thieving representative samples from the blender. In the presented case, calibration samples had a mass of approximately 2 g, whereas the thieved samples ended up with 1 g of material. For calibration, the samples were assured to be homogenous, however for the thieved samples it has to be considered, that the samples represent less than roughly 1.2% of the total filled mass inside the blender.

For the NIR based measurements, it is safe to assume, that the penetration into the powder is no more than one particle layer. Hence, based on the diameter and aperture of the optical fiber, the acquisition time and number of scans, and assuming a particle speed equal to the tip speed of the impeller, one ends up with an estimated scanned volume of 0.075 ml. This is equal to the volume of 6.8 particles, and at the same time representing approximately 0.1% of the total (particle occupied) volume in the vessel.

In order to obtain sensor data comparable to the experimental procedure, the location and the near field of the sensors is modeled accordingly. The particles are detected in a half-spherical sensing field in front of a sensors position. A mean value of 3.6 (0.95 STDEV) particles are entering the near field for the channels 3.1 and 3.2 on the bottom. For sensor 3.4 we observe only a mean value of 2.8 particles with a higher STDEV of 1.2. This is because of the stronger fluctuation of the bed surface, which passes the sensing area at the location of sensor 3.4 (Figure 2-1).

Thus the estimations on the experimental part, and the simulated results, regarding the number of particles scanned are in good agreement, considering that likely the particles move at slower speed than the impeller tip, and the bulk density in the vicinity of the blade is slightly decreased due to particle movement.

For quantifying, the water content in the simulation, for all of the detected particles in the sensing area, their liquid content is accumulated and divided by the number of particles in this near field.

Hence, the comparison of experimental and simulated results is possible rather straightforward, as the same volumes (or particle numbers) are compared. Furthermore, the fundamental error when sampling particle systems caused by the finite particle number in the sample [73] is of lesser concern to us, as the Al_2O_3 spheres do not represent a binary system (with wet and dry spheres), but carry a continuous expression of amount of moisture.

Evidently, the obtained water content obtained via NIR measurements, as well as probed in the simulation, show the same order of magnitude in their fluctuations. Both are higher than the observed deviations within the thieved samples analyzed via LOD, reflecting the differences in sample size probed in the NIR measurement, the simulation, and the LOD method.

This is already reflected in the observed larger error of the NIRS calibration based on to the LOD reference measurement. Based on the fact, that only a majority of the variation is explained by the finally chosen chemometric model (see Table 2-2), that large fluctuations in the observed spectra lead to a bad model performance. These might include the actual position and reflection of the rather large particles in front of the probe, leading to distortions in the spectra. Although this is corrected for by spectral pretreatments, such effects cannot be eradicated completely.

It has to be noted here, that the used optical probes are most simply, and just consist of a cupped bifurcated fiber, as those were costume made to fit into the blending vessel. Alternative probes, which could enable a more homogeneous illumination and a wider area of detection, would permit to mean over the individual particle positions and improve the spectral interpretation.

2.5.2 Comparison and explanation of theoretical and experimental results

Previous simulations predicts a central spray zone location, at the middle of the impeller radius for optimum liquid distribution in the bed. Therefore, experiments for different locations a, b, c (Figure 2-4A) were made in order to verify this prediction. Spraying at the inner position a can be discarded because of resulting wetting of the stirrer and impeller blades in this case. For position c the blades will not be wetted but partially the cylindrical wall. This leads to sticking particles and agglomerates forming. Additionally, the comparison of the liquid content evolution shows much stronger fluctuations than in the case of central spray location (Figure 2-6). Stronger

fluctuations corresponds to less homogeneous liquid distribution inside the particle bed, so the central spray location is the optimum for our process.

Figure 2-6 to Figure 2-9 show the comparison of DEM liquid evolution with the measured evolution via NIR. The data sets were verified with a chi-squared test, Table 2-4 shows the results of chi-square test. For sensor 3.1 and 3.2 the null hypothesis is true, which means that sensor 3.1 and 3.2 can be compared with the simulation data.
Sensor 3.4 did not pass the chi-square test. The reason is the position of this sensor, the comparison of this sensor and simulation data is shown in Figure 2-7. The sensor is located in a height in which also the blades of the impeller are measured, c.f. Figure 2-1. This leads to higher fluctuations during the measurements and the null hypothesis has to be rejected.

Table 2-4 Values of chi-squared test from DEM simulation data and NIR data.

Channel	χ^2-Test p-Wert
3.1	0.98179
3.2	0.99999
3.4	0.03408

The measured fluctuations depicted in Figure 2-7 to Figure 2-9 sometimes show a mirrored behavior (Figure 2-7, between 30 – 50 rev.). This can be explained by a phase-shift between simulation and experiment, when blades and pure particles are passing the sensor. Here, a synchronous angular constellation of the impeller in simulation and experiment cannot be warranted. Similarly, the sensor electronic schedules sensors in a multiplex logic, where data are delivered asynchronous to the simulated sensors.

2.5.3 Results for different measurement and spray locations

In Figure 2-6 the comparison of different spray locations, central (b) and outside (c evolution of monitored liquid content at sensor 3.2, (bottom, 34mm radial distance) is shown. Higher fluctuations represent more inhomogeneous liquid distribution inside the bed. The central spray location yields smoother liquid content increase.

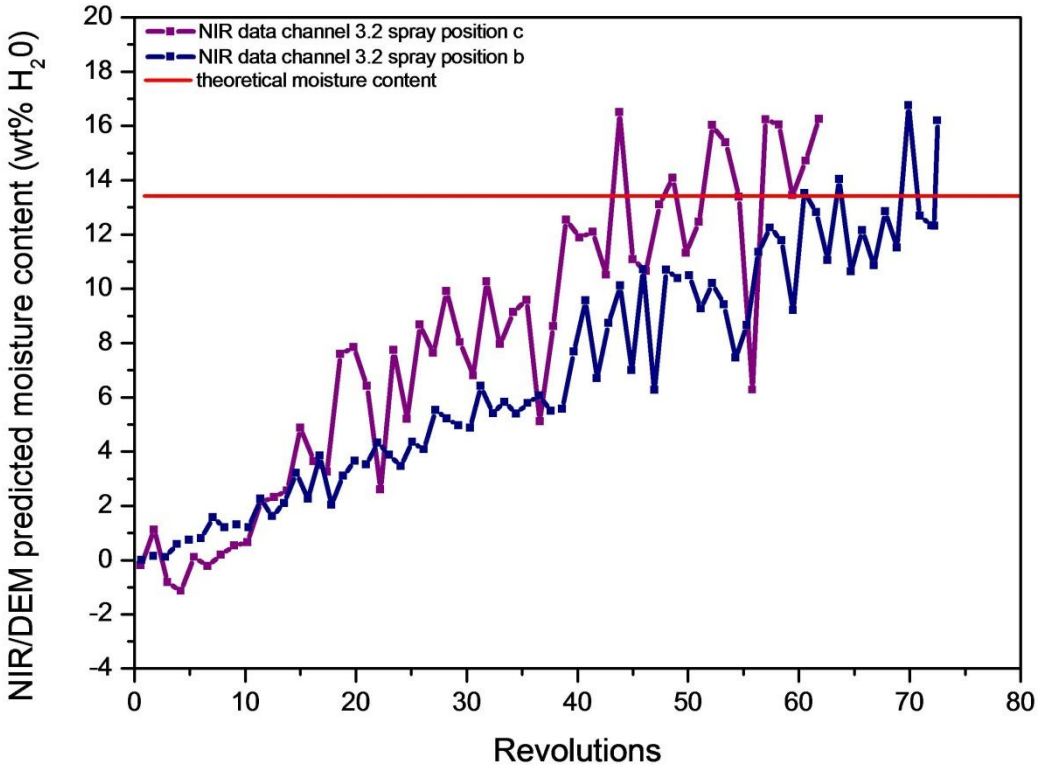

Figure 2-6 Comparison of different spray *locations*, central (b) and outside (c).

In Figure 2-7 evolution of monitored liquid content at sensor 3.2 at the bottom, 20 mm radial distance (central spray position). Both curves depicts a fluctuation of liquid content within the same range. Here, the liquid content is slightly under-predicted by the simulation until 60 revolutions; the final saturation is equal to the experimental data.

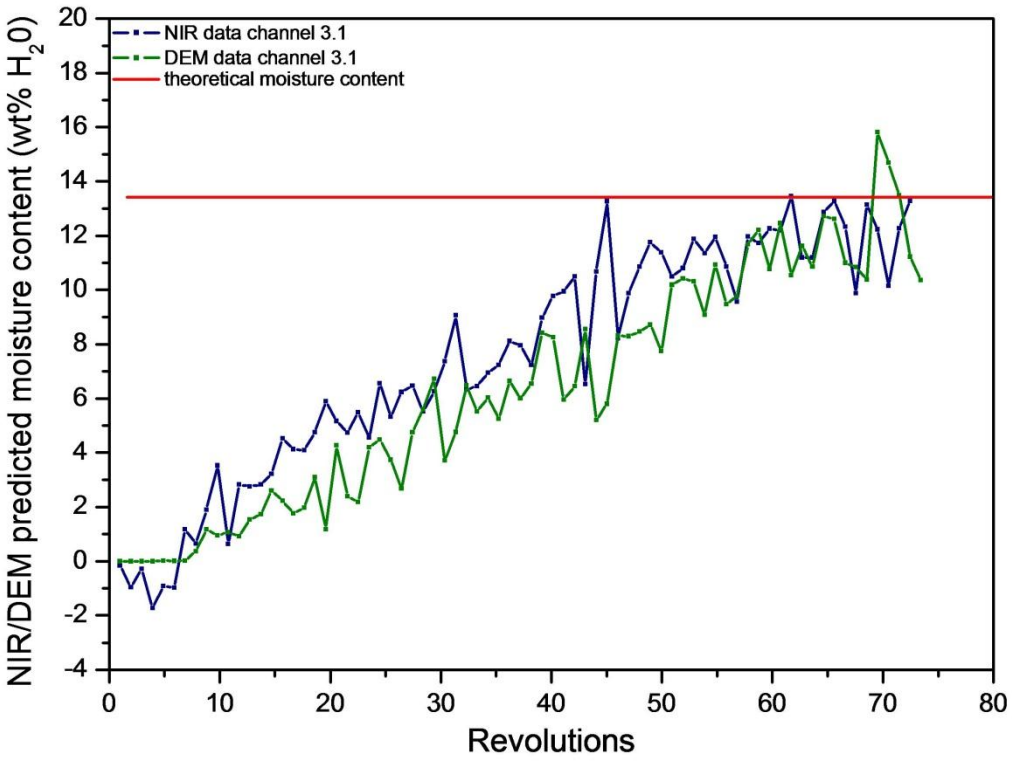

Figure 2-7 Evolution of monitored liquid content at sensor 3.1

In Figure 2-8 evolution of monitored liquid content at sensor 3.2 at the bottom, 34 mm radial distance (central spray position) is shown. Excellent agreement of both data sets until the theoretical moisture content has been reached.

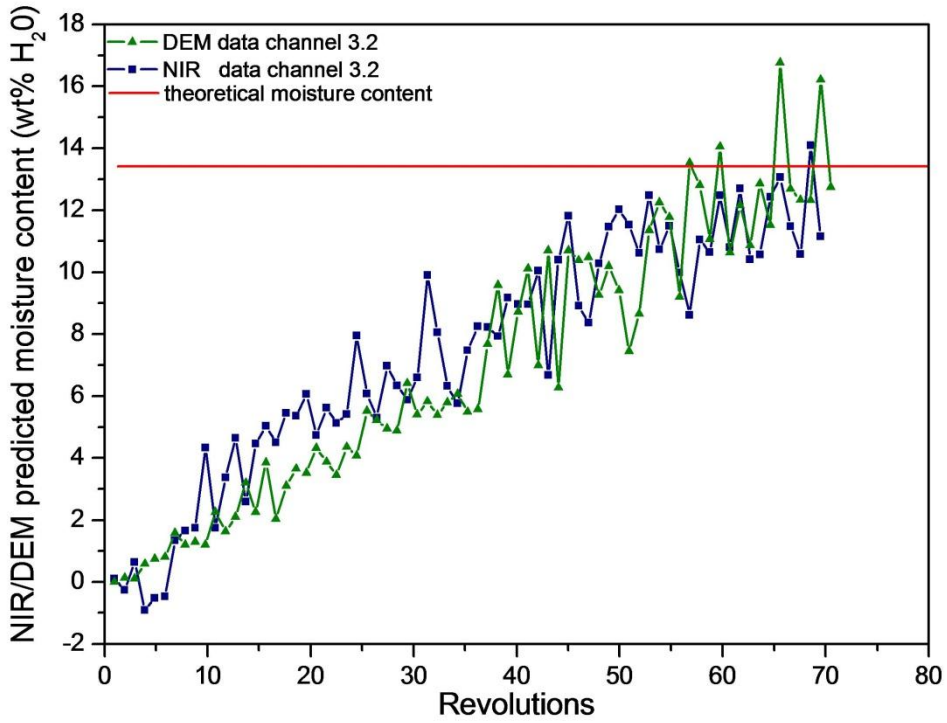

Figure 2-8 Evolution of monitored liquid content at sensor 3.2.

In Figure 2-9 evolution of monitored liquid content at sensor 3.4 at the side wall, 20 cm vertical distance (central spray position) is shown. The agreement here is poor, because of the improper location of the sensor, where no continuous measurements are possible.

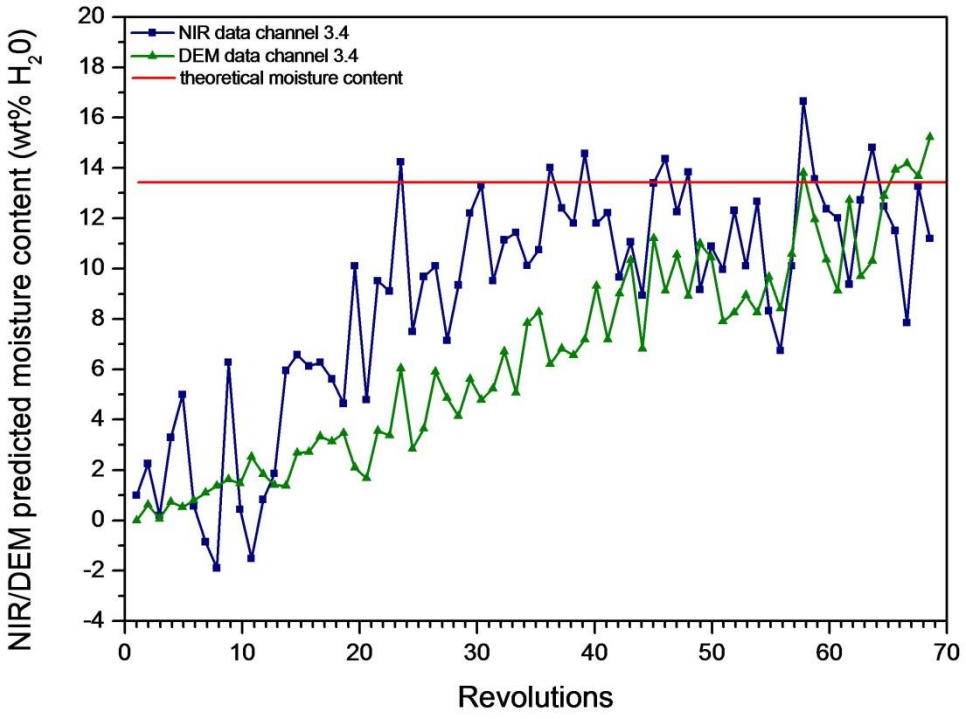

Figure 2-9 Evolution of monitored liquid content at sensor 3.4.

Residence time and liquid content are evolving in tandem. That is first: Because of the fact, that particles are receiving a constant amount of sprayed liquid per time spending in the spray zone which is equal to the flow rate of the nozzle. Second: The porous particles are not over-wetted, because their absorption rate is higher than the spray rate. In that case, particles cannot transfer liquid throughout wet contacts or by a liquid film, because they do not arise.

As known from statistical theory, summarizing any random values lead to a Gaussian density distribution. So this observation has to be assumed for our particle residence time distribution as well [74].

With increasing process time the typical Gaussian shape of the distribution function develops, shown in Figure 2-10. After 50 revolutions, it becomes fairly symmetric and shifts towards larger residence times as a whole, with an increasing number of revolutions. That indicates a stationary flow regime of the mixing process.

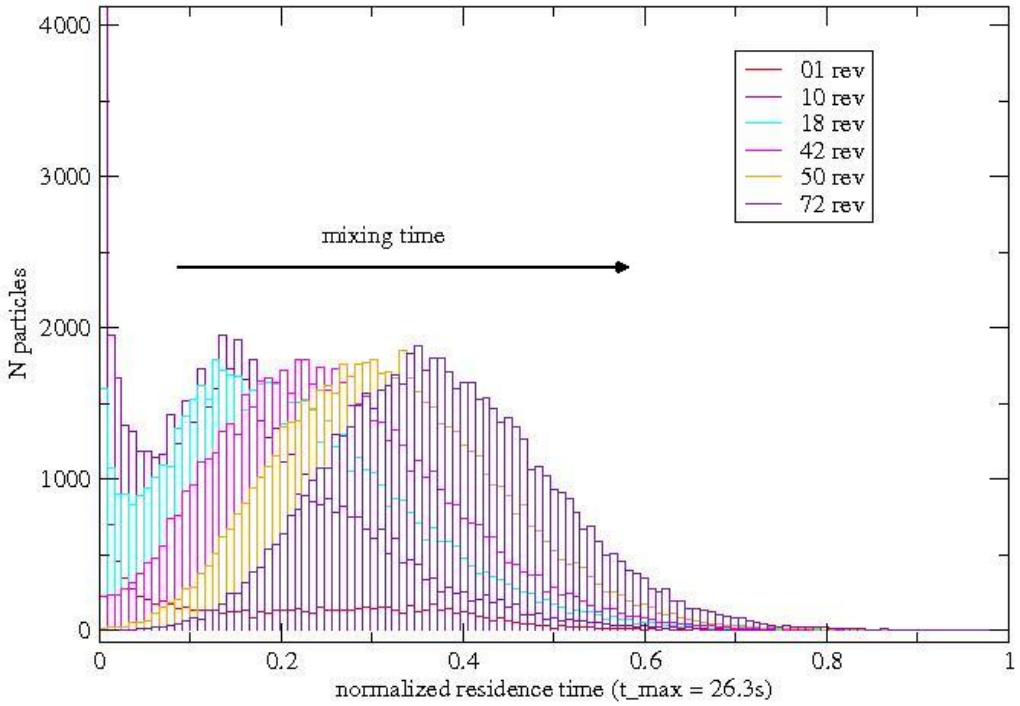

Figure 2-10 Residence time distribution of particles visiting the spray zone.

2.6 Discussion and outlook

The analysis of our results shows very good agreement for the quantitative liquid content evolution of the simulation data compared to the experimental data. Where in the experiment only spot-like analyses are accessible via NIR sensors which have advantages of revealing local variations, in numerical simulations the information of the liquid content is available for all particles in the system at any time. In order to evaluate the quality of our simulation, we compared the liquid content of the experimentally measured sensor data with 'virtual sensors', accordingly placed in the simulation and identified statistically reasonable sensor locations (3.1 and 3.2) for our process.

Based on the available total information in the simulation data, the mixing-time dependent residence time distribution (rtd) was analyzed (Figure 2-10). We remark that this analysis cannot be carried out at all without numerical simulations. The

excellent agreement of the sensor data confirms that we have simulated the rtd of experiment as well.

Acknowledgements

This work has been funded by the Austrian COMET Program under the auspices of the Austrian Federal Ministry of Transport, Innovation and Technology (bmvit); the Austrian Federal Ministry of Economy, Family and Youth (bmwfj); and the State of Styria (Styrian Funding Agency SFG). COMET is managed by the Austrian Research Promotion Agency FFG.

3 Monitoring of a Hot-Melt Coating Process via a Novel Multipoint Near Infrared Spectrometer[5]

[5] This chapter is based on the paper: Monitoring of a Hot Melt Coating Process via a Novel Multipoint Near-Infrared Spectrometer; R. Hohl, O. Scheibelhofer, E. Stocker, S. S. Behzadi, D. Haack, K. Koch, P. Kerschhaggl, D. Lochmann, S. Sacher, and A. Zimmer, *AAPS PharmSciTech*, 2016.

3.1 Abstract

The aim of the present work was to develop a PAT strategy for the supervision of hot-melt-coating processes. Optical fibers were placed at various positions in the process chamber of a fluid bed device and experiments were performed to determine the most suitable position for in-line process monitoring, taking into account such requirements as a good signal to noise ratio, the mitigation of dead zones, the ability to monitor the product over the entire process, and reproducibility. The experimental evidence suggested, that the position at medium fluid bed height, looking towards the center, i.e. normal to particle movement, proved to be the most reliable position. In this study the advantages of multipoint monitoring are shown, and an in-line-implementation was created, which enables the real-time supervision of the process including the fast detection of inhomogeneities and disturbances in the process chamber, and the compensation of sensor malfunction. In addition, a model for estimating the particle size distribution via NIR was successfully created. This ensures that the quality of the product and the endpoint of the coating process can be determined correctly.

3.2 Introduction

Coating of solid dosage forms is an important process step in pharmaceutical manufacturing for various purposes, including taste masking, increasing the shelf life or tailoring the release profile of the active pharmaceutical ingredients (API) [16], [47], [60]. In addition, a second API can be delivered to patients by active coatings (i.e., an API is incorporated in the coating) [75]. Depending on the purpose of the coating and on the substrate particles (e.g., tablets or pellets), typically pan coating or fluid-bed coating are used to apply a thin continuous layer on the substrate. Dependent on the size of the substrate particles pan coating (widespread used for tablets) or fluid-bed coaters (usually used for pellets and mini-tablets) are preferred. Several different implementations of fluid-bed coaters exist, whereas bottom-spray fluid-bed technology is one of the most established methods for pellet coating [60]. Typically, an aqueous polymer-containing solution is sprayed onto pellets. However, solvent-free systems have been developed as well. For example, hot-melt coating (HMC) has been used for many materials, such as paper or textiles, since the early 1940s. In the pharmaceutical industry hot-melt coating has been applied since the 1980s [76]. One of the advantages over conventional coating techniques is that no solvent is required, since the coating material is applied to a substrate in the molten state, reducing the energy costs associated with evaporation and the (expensive) need for solvent recovery and explosion proofing in case of organic solvents. Moreover, HMC can be performed in modified conventional coating systems (e.g., fluid bed coaters) [76]. An excellent understanding and a precise control of the HMC process is required to successfully manufacture and to reduce product variability. The critical process parameters (CPP) are the melt temperature, the air flow rate, the molten lipid spray rate and the atomizing air pressure (a detailed discussion on the CPPs will be found in Stocker E, Salar-Behzadi S, Hohl R, et. al. Applying ICH Q9 quality risk management methods and tools to encourage process development for hot-melt coated particles; in preparation) as they significantly affect the critical quality attributes (CQA) of the product, including taste masking, effectively. Therefore, the quality of the coating layer is an important and critical parameter for the performance of the drug product.

In general, the coating quality is characterized by the coating thickness and its uniformity. These parameters should be monitored by sensors providing real-time information about the process state, thus enabling control of the process. Several studies investigated process analytical technology (PAT) applications for the monitoring of coating processes. Most techniques directly rely on the detection of the coating material, including near infrared spectroscopy (NIRS) [44], [46], [77], [78], Raman spectroscopy [43], [79], [80], and Terahertz pulsed imaging [39]. In a series of papers we recently reported the use of optical coherence tomography (OCT) as a powerful method for in-line measurement of coating thickness and variability [81]–[83]. Alternatively, the particle growth due to coating can be monitored, e.g. with spatial filter velocimetry [84].

Being non-destructive and fast, NIRS and Raman spectroscopy are established PAT tools for monitoring of coating processes [44]–[46], [77], [78], [85]. However, the fluorescence of certain coating materials can be a major obstacle with regard to Raman spectroscopy [43], [79], [80]. Using a correct data pre-treatment and reference analytics, successful real-time prediction of coating thickness, uniformity and drug release via NIRS were reported [44], [45]. NIRS was also extensively investigated in connection with fast and non-destructive particle size monitoring during granulation processes, typically combined with moisture content determination [86].

All mentioned methods are usually based on point sampling, i.e. the area of measurement is usually in the range of a few µm² (OCT), up to some mm² (for infrared). Hence, correct positioning of a probe is critical. This is especially true for processes, where spatial gradients exist (e.g. the particle size varies with the fluid bed height).

In the current study, a novel multipoint near-infrared system was used for simultaneous measurements of the coating thickness at various positions in the process chamber of a fluid-bed hot-melt coater. A single probe may fail or may become useless due to several reasons; very common is the occurrence of fouling. Thus, a multipoint system provides a better monitoring quality and control of the coating process, for example, with regard to coating homogeneity and end point control of a process [61], [62], [87]. Different positions inside the coating vessel were evaluated regarding their susceptibility for fouling and their reliability.

3.3 Materials and methods

3.3.1 Hot-melt coating

Hot-melt coating was performed in an Innojet® laboratory system Ventilus® V-2.5/1 with an Innojet® Hot-Melt-Device IHD-1 (Romaco Innojet, Steinen Germany). The Ventilus® V-2.5/1 is a multi-purpose system for granulation, coating and hot melt coating.

A stable fluidized bed of the substrate crystals is established by the air stream forcing the crystals to follow a helical path inside the process chamber. The process chamber has volume of 2.5 liters and is topped by a filter tower. The spray nozzles for the molten coating are situated at the bottom of the process chamber and eject the molten material in a low angle into the process chamber, in all radial directions.

The substrate crystals were provided by Hermes Arzneimittel GmbH, Germany and were coated with Compritol ATO 888 (Glattefossé, Nanterre Cedex, France).The coating process was performed for 30 minutes at a constant product temperature of 55°C. Atomizing air pressure was set to 1 bar. These settings were applied in all experiments.

3.3.2 Near infrared spectroscopy and probe positioning

A new spectrometer prototype, Helios EyeC Multifiber, provided by EVK (EVK DI Kerschhaggl GmbH, Raaba, Austria) was used to monitor the process. The spectrometer is based on available hyperspectral imaging systems. The MCT-sensor chip (mercury-cadmium-telluride) allows to detect a spectral range in the near-infrared region of 1000 – 2250 nm effectively. A special optical unit maps up to 25 probes, which can be attached via typical SMA905-ports to the spectrometer, to the entrance slit of the imaging system. Thus this enables the simultaneous acquisition of all probes. With this setup, acquisition of spectra can be done very fast, and spectral drifts between several probes are not occurring.

In each coating run, measurements were performed simultaneously at three positions. One sensor was permanently fixed at level 2 and looking in radial direction during all experiments. This sensor was defined as main sensor. The other sensors were placed at different levels, as shown in Figure 3-1. These sensors are termed further control sensors.

The three probes used consisted of bifurcated fibers, capped with a sapphire window (Ocean Optics Inc., Dunedin, USA). They were mounted inside the process chamber at different positions and were pointed in different directions, as shown in Figure 3-1. The height levels of the sensor positions are marked 1 to 3. The directions of the sensors were chosen to be in circumferential direction (C), in the upward (U) direction, downwards-looking (D) onto the fluid bed and in radial (R) direction, i.e. from the vessel rim towards the center of the fluid bed.

The spectra were acquired with an integration time of 1500 µs and a frequency of 105 Hz. After every 5.3 s, the recording was interrupted for about 8 s to flush the working memory, resulting in about 60000 spectra during the process time of half an hour. The interpretation of spectra was performed with MATLAB R2011b (version 7.13.0.546, TheMathWorks Inc., Natick, Massachusetts, USA) and using the Statistical Toolbox., for off-line analysis as well as SIMCA and SimcaOnline respectively (SIMCA version 13.02, SimcaOnline version 13.01, Umetrics, Umeå, Sweden) for in-line analysis. Since all spectra were recorded by one single CCD chip of the EyeC system, typical setbacks associated with multiple spectrometers (e.g., the need for individual models, time delays, differences in the resolution) were eliminated.

Right before the coating process was started, white and dark reference spectra were recorded; for creating dark reference the sensors were disconnected from the spectrometer and for white reference Spectralon® (Labsphere, North Sutton, NH) was used in a distance of 2 mm from the probes. The direction and position of the main sensor (R) was not changed, during the experiments. The control sensors were used at different height levels and different directions. Many positions proved to be vain, due to having a too low particle density, or not enough movement in front of the sensor, to give reliable results. Three experiments will be discussed in detail in this manuscript, which are listed in in Table 1.

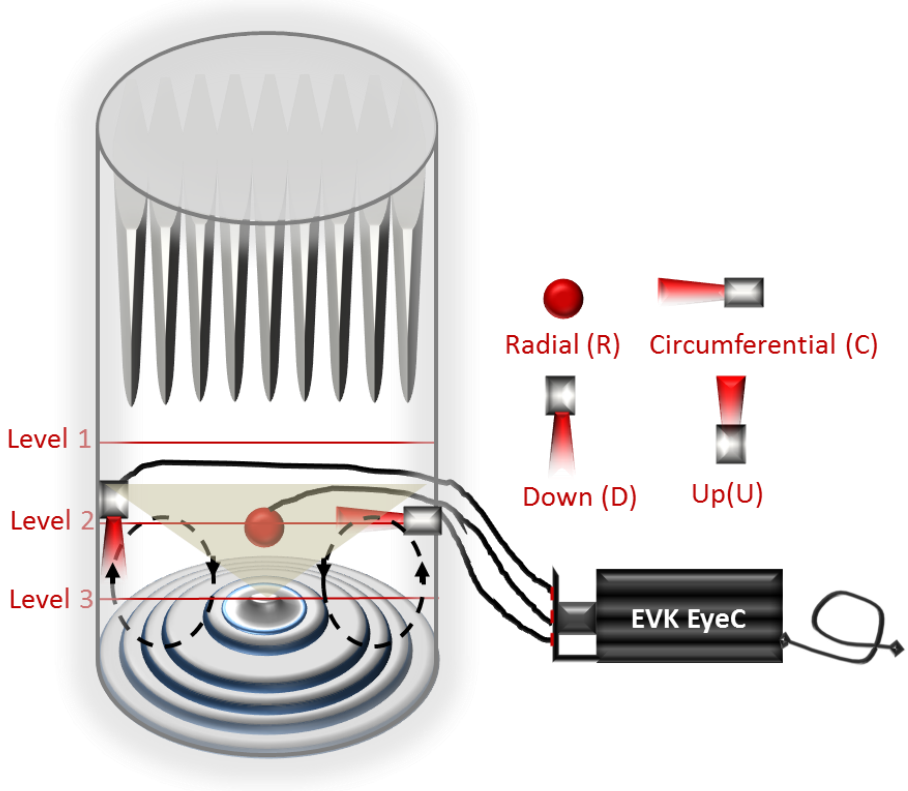

Figure 3-1: Fluid bed vessel with a bottom spray nozzle and EVK system Helios EyeC. NIR optical fiber probes were turned in different directions: (C) circumferential, (U) upwards, (D) downwards and (R) in radial direction towards the center.

Table 3-1: Dependent on the size of the substrate particles pan coating (widespread used for tablets) or fluid-bed coaters (usually used for pellets and mini-tablets) are preferred.

	Main sensor	Control sensor 1	Control sensor 2
Experiment 1	Level 2 (R)	Level 2 (D)	Level 2 (C)
Experiment 2	Level 2 (R)	Level 1 (D)	Level 2 (C)
Experiment 3	Level 2 (R)	Level 3 (U)	Level 1 (C)

3.3.3 Compensating for window fouling

Another crucial issue associated with HMC is window fouling, which can render the sensors ineffective. For example, the end point can be detected too early due to coating material deposited on the sensor head. Window fouling occurs when the molten lipid recrystallizes on the capping of the NIR fibres rather than on the particles in the process chamber or when abrasion of the coated particles takes place. As such, window fouling can be different at different positions. To compensate for window fouling, extended multiplicative signal correction can be used (EMSC) [88]. As proposed in [89] the collected spectra were separated according to:

$$A_{measured} = a \cdot A_1 + b \cdot A_{crystal} + c \cdot A_{coating} + d \cdot A_\lambda + e \cdot A_\lambda^2 + R \qquad (14)$$

The parameters a, b, c, d, e are calculated for every time step but are constant over the considered spectral region. A_1, is a constant value across all wavelengths, which mainly reflects the influence of the crystal distance. $A_{crystal}$ is the characteristic spectrum (taken off-line) of pure substrate crystals. Therefore, if crystals are near the probe window, and give a notable absorption spectrum, b is high. Since a and b depend on the crystal distance, they show a correlation. $A_{coating}$ describes spectral content attributed to coating. It was obtained by taking off-line spectra of the samples collected during the coating process. A_λ and A_λ^2 represent linear baseline offset and quadratic curvature.

By taking into account the existing correlations between a, b, and c; i.e. the geometrical based relation of crystal distance, and crystal and coating proportion in the spectra, it is possible to distinguish between the coating, adhered to crystals, and coating adhered to the probe window [89]. Thus the increase of coating on the crystals, and on the NIR probes can be followed separately. The obtained corrected EMSC coefficient is then directly proportional to the detected coating mass.

This calculation is performed for every time step (i.e. with 105 Hz). To avoid cluttering, in the following figures the mean value over 0.57 s, and the corresponding standard deviations over the same time period are indicated. Numerical values are given relative to the coating target value.

3.3.4 Off-Line measurement of the particle size distribution

Particle size distribution was measured using the QICPIC dynamic picture analysis instrument with the RODOS dry dispersion unit and the VIBRI vibrating conveyor from Sympatec (Sympatec GmbH, Clausthal-Zellerfeld, Germany). QICPIC is a high-speed camera with a stroboscopic light source, which can take up to 450 pictures per second of dispersed particles moving through the measurement zone. The associated software WINDOX 5.6.0.0 calculates the PSD and shape factor distributions of the measured particles by evaluating their projected area in the pictures. The particle diameters x_{10}, x_{50} and x_{90} were determined for the particle volume distributions.

3.3.5 Coating prediction via PLS

The calibration of the NIR setup was performed off-line, using samples taken every 5 minutes during a coating process. Samples were distributed homogeneously on a rotating table (Sensor Turn, WLP-TEC GmbH, Göttingen, Germany). The table rotated to mimic particles passing the probe and to avoid subsampling. To collect the calibration spectra, the three fiber optic probes were fixed on an acrylic glass disc mounted 2 mm above the rotating material. For the in-line measurements it was also necessary to develop a PLS (projection to latent space) model for the prediction of the coating mass. The model is similar to the one presented in [90]. The model was developed by recording several batches during the whole process time. Afterwards, only those batches, which performed successful (as determined afterwards by drawing samples and analyzing them off-line were considered for being included in the model. Off-line-analysis happened via dynamic picture analysis, as described in section 2.4. It was assumed that the increase in particle diameter over process time can be attributed to the growth of the coating layer on the particles. This was supported by microscopic images (taken with a Leica DM 4000 equipped with a Leica DFC 290 camera), which allowed to distinguish the coating layer from the substrate material optically. The score plot for a single calibration batch is shown in Figure 3-2.

As target variable the batch maturity, i.e., the normalized process time, is used. Thus, the end-point of a successfully coated batch is 1. More details on such batch models

can be found in literature [91], [92]. For the prediction of coating, SNV normalized spectra over nearly the whole spectral range (1100 – 1800 nm) were used. Three PLS components were used, resulting in a model with a RMSECV of 0.033 (in units of normalized time, i.e. root mean square error for predicting the batch maturity of the cross-validation batches is approximately 1.5 minutes). The regression vectors indicate, that the increase of coating material, and the decrease of substrate material in the obtained spectra are the variables relied on.

As this model just gives a regression vector for the obtained spectra (i.e., is sensitive to the increase of coating material in the obtained spectrum), the validity of this model can only be guaranteed, for one position and reproducible fouling over several batches (as window fouling is intrinsically calibrated into the model). Hence, the model can only be applied, when the correction in section 3.2.3 has shown, that fouling occurs as expected.

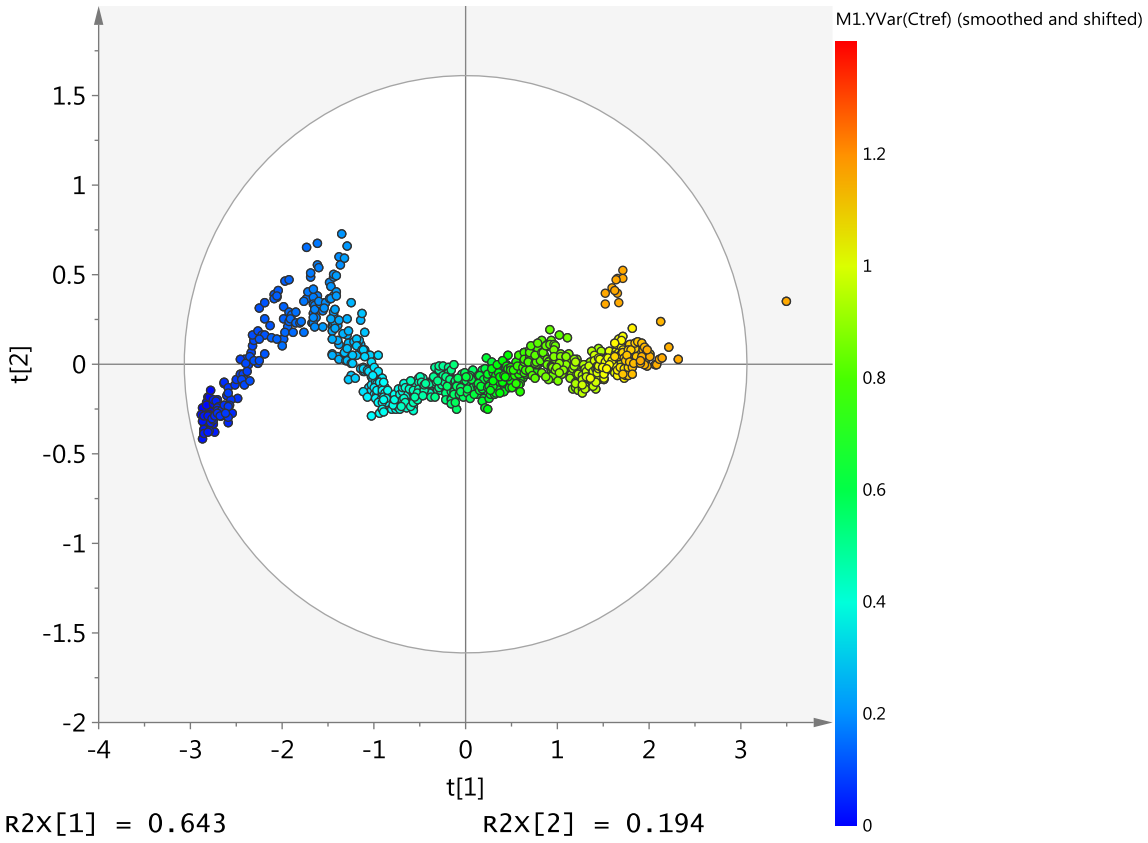

Figure 3-2: Score scatter plot of a calibration batch for the PLS model. The color indicates time, hence it can be seen that the HMC processes wander from left to right, until they are finished. Whereas the first component nicely increases with time, the second component has to compensate some fluctuations, maybe due to badly controlled coating feed.

3.3.6 Set-up for In-line monitoring

An FPGA (field programmable gate array) chip housed in the spectrometer is used for control of the spectrometer. In principal the FPGA can be used to perform calculations on the acquired spectra at high speed [93]. In the current application, however, no further steps are performed on the FPGA, but the raw detected intensity is exported. The multipoint spectrometer was set to an automatic mode for in-line-monitoring, to regularly acquire and save the detected intensity data into files. This has the additional advantage that the original spectral data is preserved (and thus archived) as demanded by the regulators.

In an intermediate step, the folder containing the spectral data is supervised remotely and newly written files are loaded and processed further in an in-house developed program. The first step is the conversion of the recently acquired intensity I(t) to absorbance, by including the previously determined white I_{white} and dark I_{dark} reference, via

$$A(t) = -\log_{10}\left(\frac{I(t)-I_{dark}}{I_{white}-I_{dark}}\right) \quad \textbf{(15)}.$$

For off-line analytics, the absorbance spectra are then used as described in section 3.3.3 to correct for window fouling. For in-line supervision, a mean absorbance over 5 seconds is calculated. These values are then written to an OPC server, running on the same machine, as illustrated in Figure 3-3. OPC (Object Linking and Embedding for Process Control) is a standardized software interface for the exchange of plant data in between instruments and controllers of different manufacturers.

A third computer serves as the final supervision station. Here, the data are imported regularly from the OPC server via two different APIs (application programming interfaces) that serve as OPC clients, namely the Batch Table Wrapper API and OPC SIM API. The communication between OPC server and clients on different PCs is a delicate task, regarding communication protocols and data safety; details are omitted here. The data are then used in a real-time prediction system (i.e., SimcaOnline). This systems performs the chemometric analysis of the data, based on the

chemometric model, which was established beforehand, and gives a status report and possible warnings to the user.

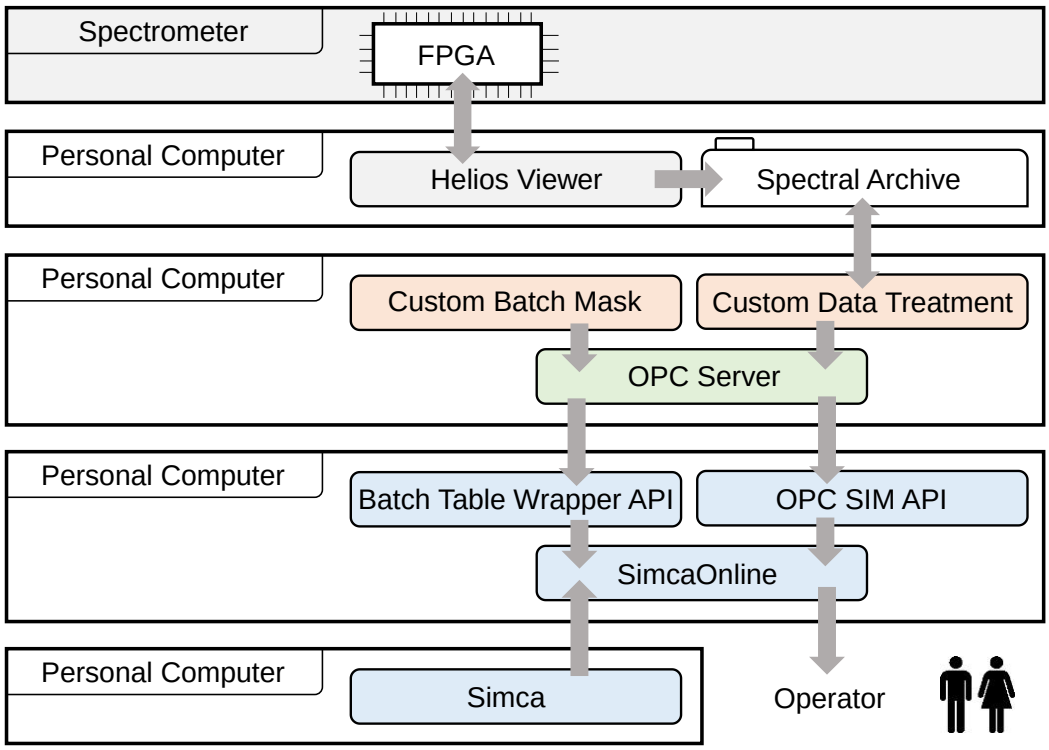

Figure 3-3: Schematic overview of the data flow. Grey fields are performed on the spectrometer, and the accompanying computer. Orange fields represent our custom program, used for entering batch data and handling of spectra respectively. Green marks the OPC server (MatrikonOPC, Köln, Germany). Blue fields are products from the company Umetrics AB. APIs are used by SimcaOnline for communicating with the OPC server and administrating the batch data. SIMCA itself is used to prepare the chemometric model.

3.4 Results

3.4.1 NIRS measurements

Experiments were performed with sensor positions given in Table 3-1. For all shown experiments the applied coating is shown as ratio to a target coating level. Hence a coating ratio level of 0 represents the lack of coating, and a value of 1 roughly a coating thickness of 75 µm. A usual coating process should end at a range of 1. In Figure 3-4 the experiment 1 according to table 1, is shown, the higher coating ratio

reported by the sensors is caused by window fouling of the sensors during the process time.

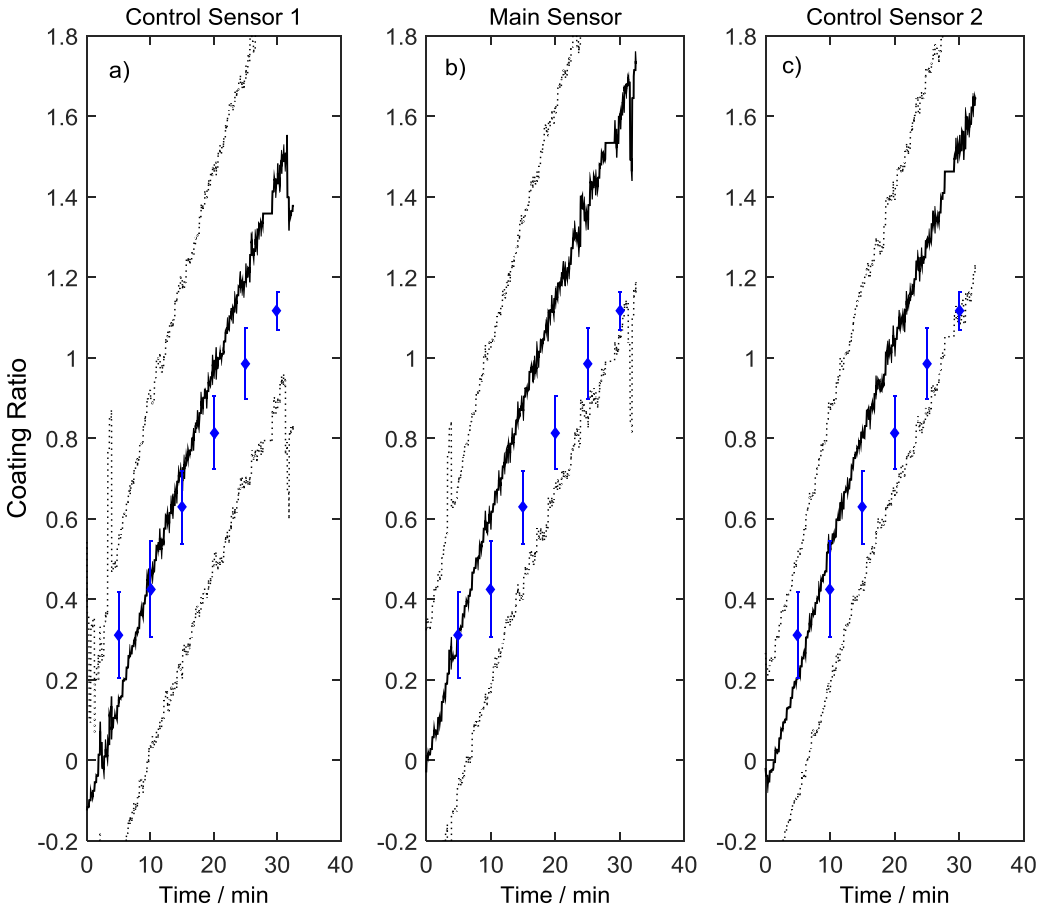

Figure 3-4: Experiment 1 according to table 1, coating ratio vs. time without correcting for window fouling (solid line). The dotted line is the standard deviation of the coating ratio. Blue dots represent the off-line measured values. As can be seen, the off-line measurement show a lower coating ratio. The higher coating ratio reported by the sensors is caused by window fouling of the sensors during the process time.

In Figure 3-5 the same process data are presented, now with the correction for window fouling. As can be seen, the NIR-measured coating ratio decreased and a final value of approximately 1 was reached, which is in good agreement with the off-line samples; the off-line calibration samples are within the standard deviation of the in-line measurement. Therefore, by using the off-line calibration and without applying the presented signal correction, the process would potentially be stopped too early before reaching the final coating ratio.

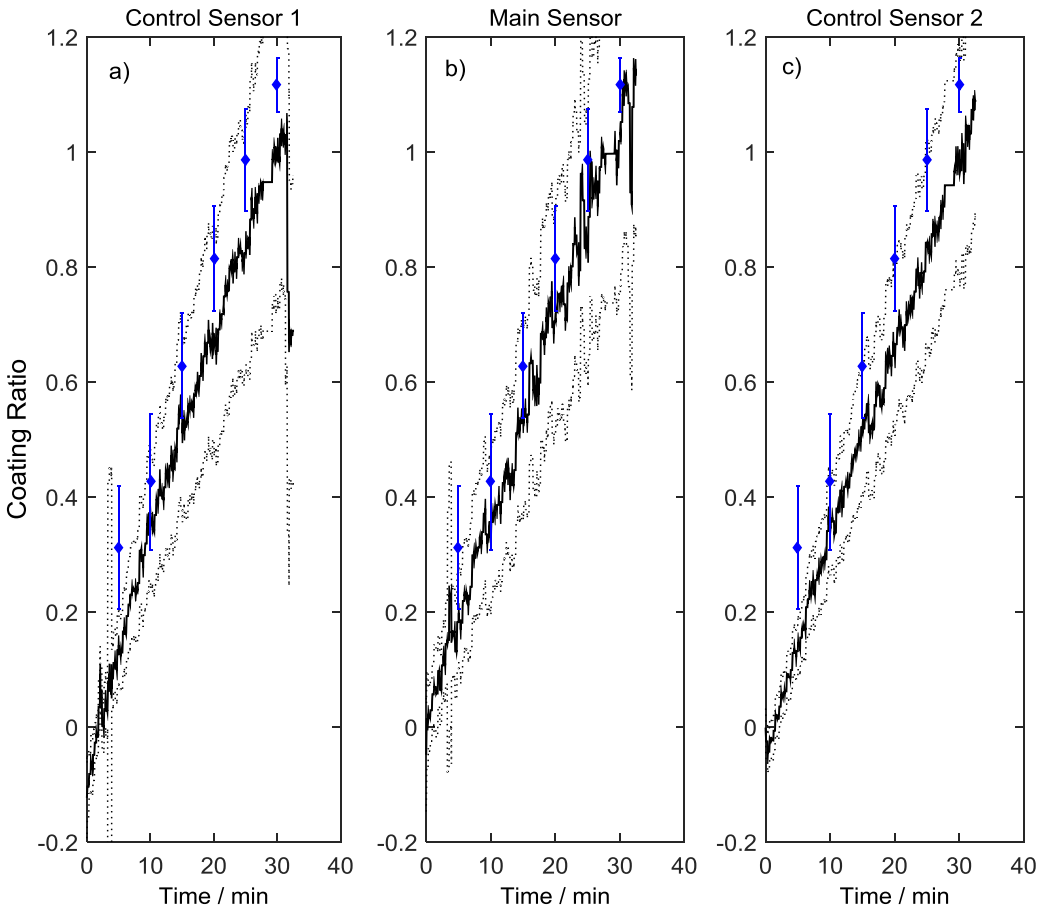

Figure 3-5: Experiment 1 according to table 1 coating ratio vs. time after correcting for window fouling. The dotted line is the standard deviation of the coating ratio. Blue dots represent the off-line measured values. At minute 34, the process was stopped, and depending on the direction of the probes their ability to still see particles in the settled bed is different, hence the different values of coating ratio at the very end.

The results of experiment 2 are shown in Figure 3-6. In this experiment control sensor 1 was fixed at an unsuitable position above the fluid bed at level 1. This sensor was not able to see the product adequately, because the product stream was too far away, only window fouling was detected. In contrast the main sensor and control sensor 2 were mounted at level 2. The same increase of the coating ratio can be observed at both positions indicating that particles are coated homogeneously.

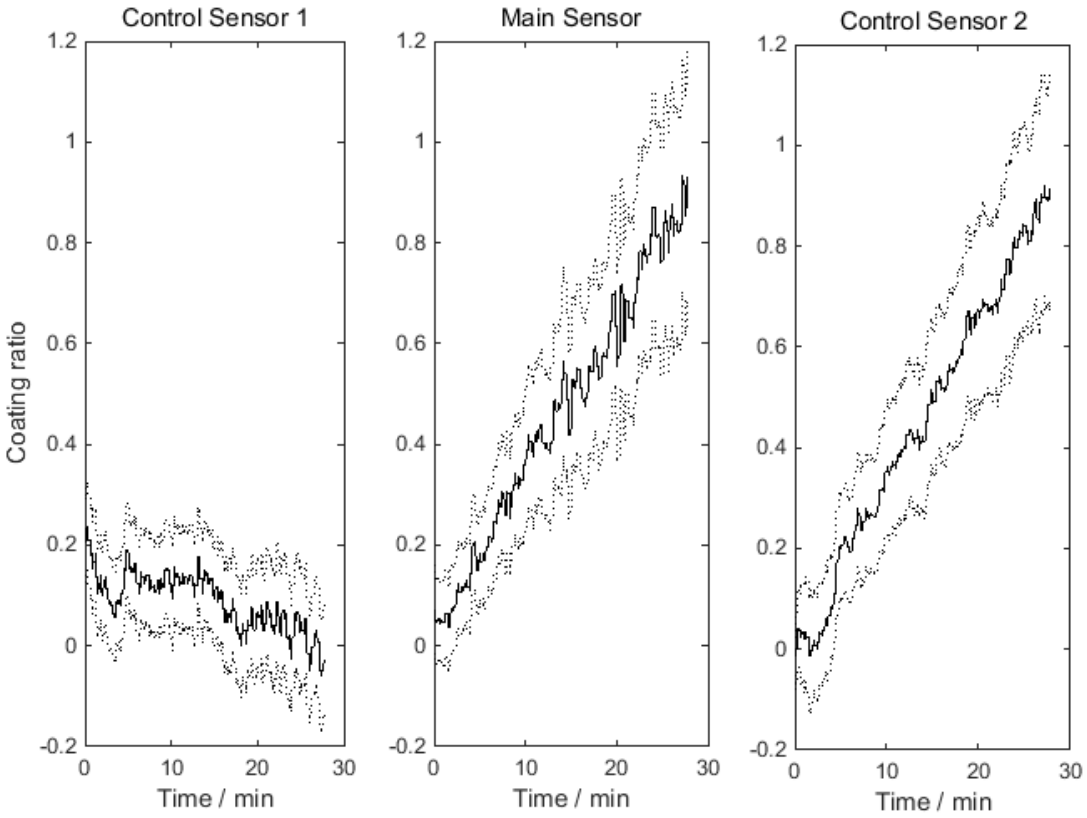

Figure 3-6: Experiment 2 according to table 1, coating ratio vs. time for experiment 2. The solid line represents coating ratio and the dotted lines are the standard deviations. The sensor in the left chart was mounted at an unsuitable position.

Additionally, a rough spatial assignment and a detection of disturbances are possible by considering the different sensor positions and directions, as shown in Figure 3-7. The disturbances detected by main sensor and the control sensor 2 might be caused by substrate crystals falling down from the filter. Control sensor 1 shows no disturbance at this specific process time. This might be due to the facts that this sensor was looking downwards from top to bottom, and the disturbance was rather short and local in the fluid-bed.

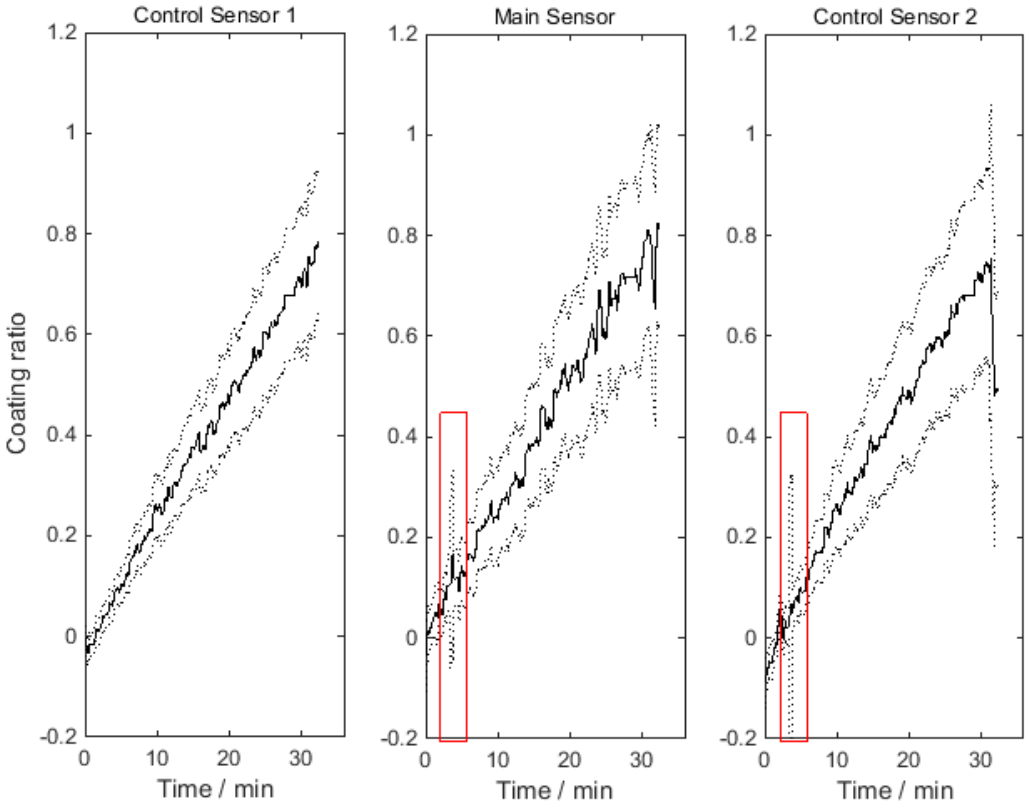

Figure 3-7: Coating ratio recorded by the three sensors over time. The black lines are the measured-to-desired coating ratio, the black dotted lines are the standard deviation of the coating ratio. The main sensor and the control sensor 2 detect a process upset at the same time, marked with a red rectangle.

In the experiment 3 according to Table 3-1, shown in Figure 3-8, control sensor 1 was fixed at level 3 at the bottom of the process chamber and control sensor 2 above the fluid-bed at level 1. The Control sensor 1 was not able to follow the coating, because in front of the sensor a dead zone was created where no particle movement happened. Control sensor 2 was not able to see a product because it was too distant. With the main sensor the process could be followed, as it was mounted at level 2.

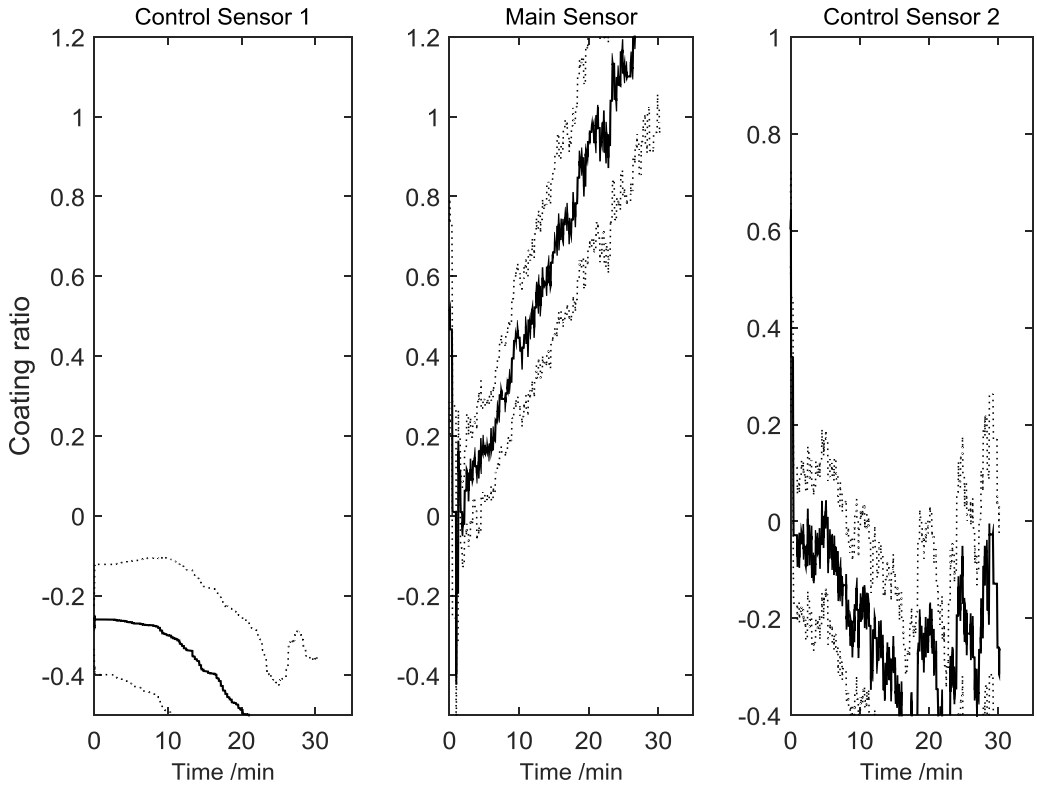

Figure 3-8: Experiment 3 according to table 1, coating level recorded by the three sensors over time. The solid lines are the coating ratio, the dotted lines are the standard deviation. Both control sensors (left and right graph) fail, due to their unsuitable positioning.

All other possible positions for control sensor 1 and control sensor 2 were tested. The best position for the sensors is level 2 in the process chamber. At this level the process could be followed with all three sensors. For all following experiments the sensors were mounted at level 2.

3.4.2 In-line prediction of particle size distribution

The reference measurements were generated by drawing samples, and measuring them with NIR as described in section 3.3.2, followed by QicPic measurements for several batches. As can be seen in Figure 3 – 9, the predictions are successful, yet scatter wildly. The color is according to the DModX value [94], indicating that some of the measurements differ in their spectral response.

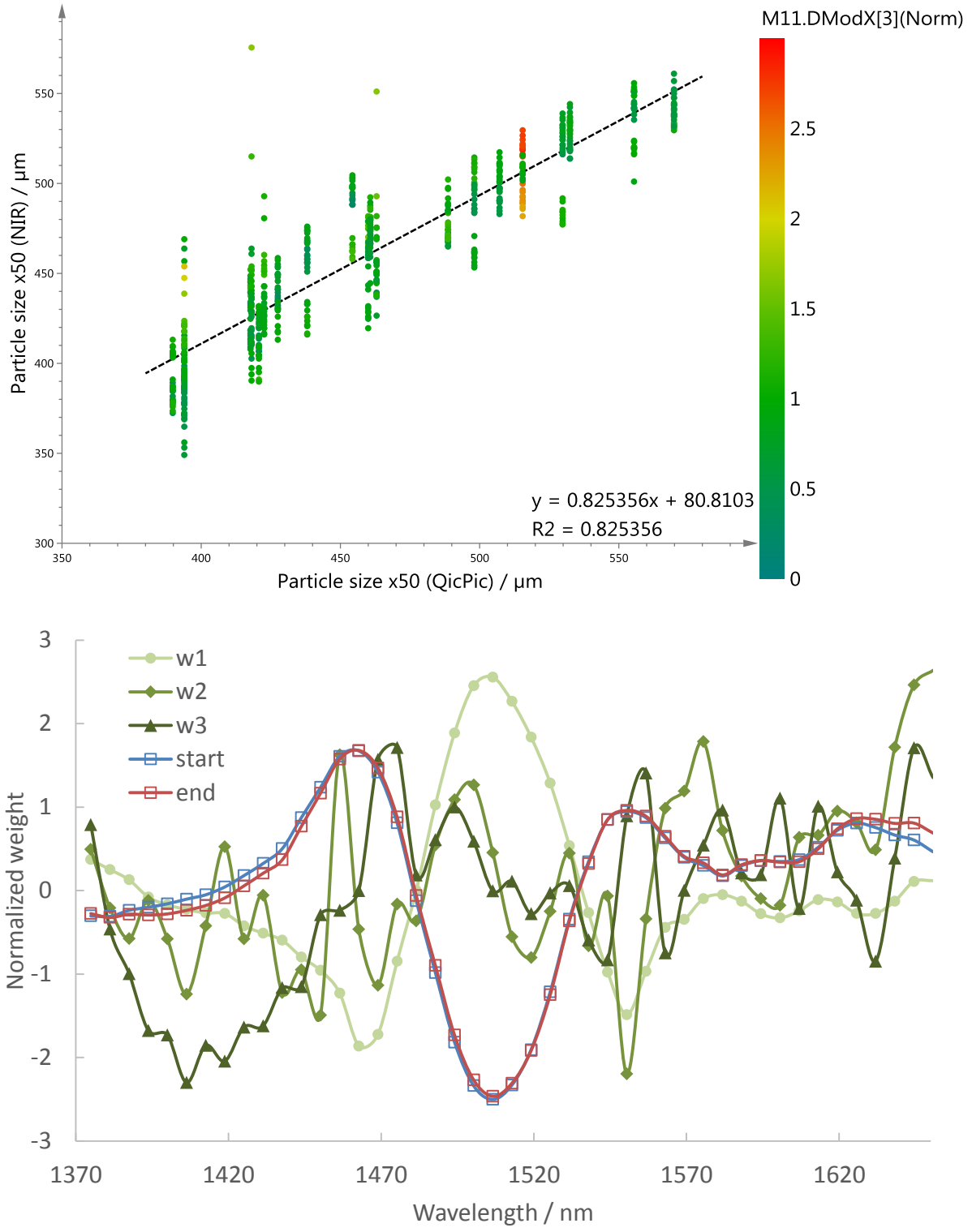

Figure 3-9: Top: Predicted and reference values for NIR and particle size parameter x_{50} obtained by QicPic. Bottom: The three PLS weights for the first three components are shown (w1, w2, w3). Additionally, the 2nd derivative spectra from process start and end are depicted. Note, that those have been scaled, in order to make them comparable.

The PLS-model is based on the 2nd derivative of the spectral range between 1375 – 1650 nm. Three PLS components are used; Taking a look at the PLS weights, it is

clear that the first component reflects the diminishing of the substrate material during the coating process, whereas the second and third component represent contributions of the peak flanks. Hence, the particle sizes were determined, based on chemical information, which is insensitive to variations of the particle-sensor distance. The cross validation groups are distinct batches. The obtained root mean square error for cross validation (RMSECV) for the prediction of the x50 parameter was below 30 µm. The predicted values during the process (with NIRS) and reference values (with QicPic) for the calibration measurements can be seen in Figure 3 – 10.

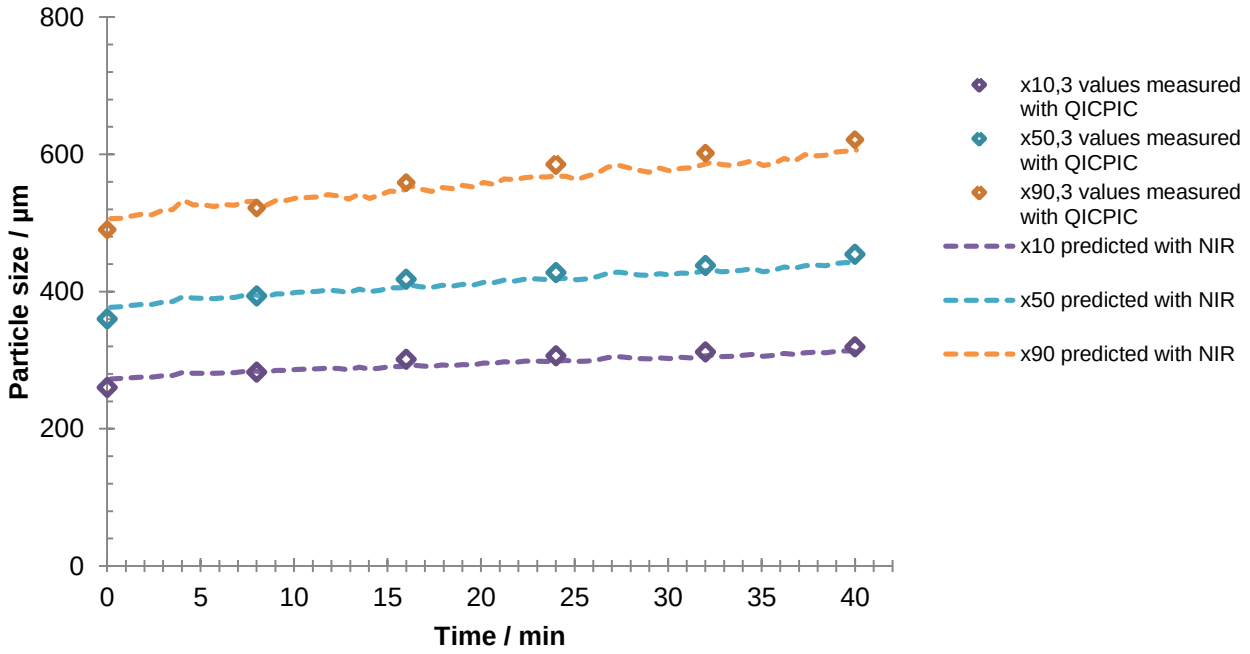

Figure 3-10: Predicted value and reference value for the calibration measurement of the particle size x_{50}.

Additionally, different size parameters (i.e., x_{10} and x_{90}) can be modeled the same way. However, as those share the same calibration samples, the relationship in the predictions between different particle size parameters is nearly linear.

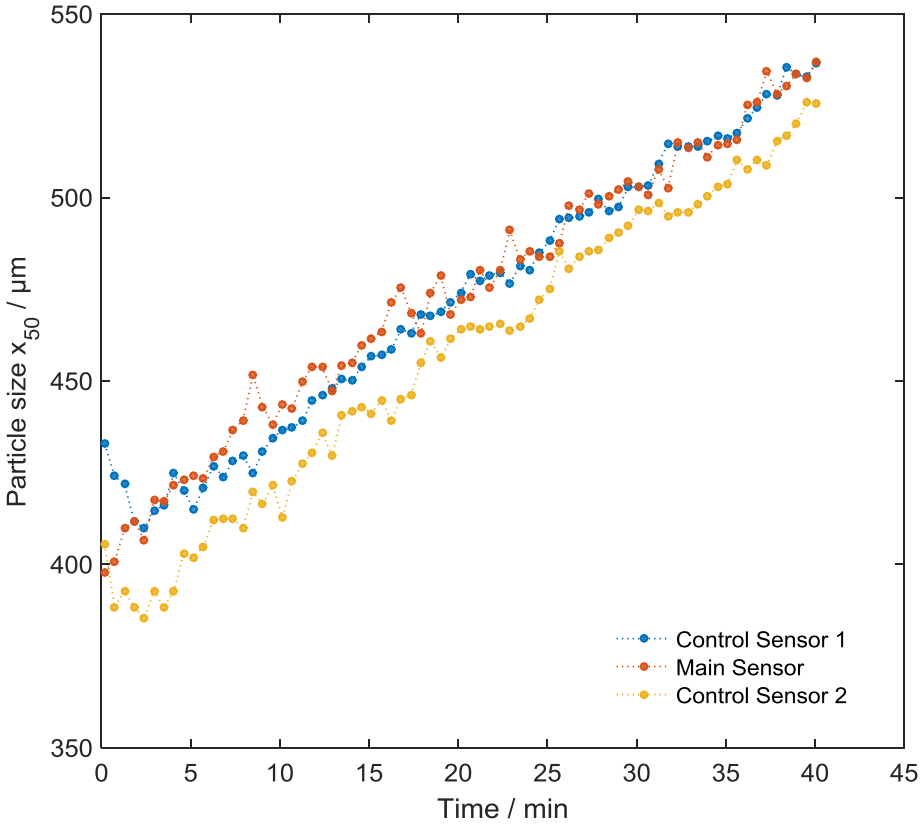

Figure 3-11: Prediction of the particle size during the coating process. Evidently, the particle size increases as the particles gain coating mass over time. However, different positons give slightly different results. The Sensors were mounted according to experiment 1.

In Figure 3-11 the predicted particle diameter is shown over process time. Hence, it is possible to follow the particle size over time. Additionally, it can be seen, that the obtained particle size slightly varies depending on the sensor position. In this experiment the probes were arranged like in experiment 1 and thus it can be concluded that the particles are slightly separated inside the fluid bed.

3.4.3 In-line monitoring of the hot-melt coating process

The crucial step for enabling in-line control is the real-time implementation of the analysis - hitherto performed off-line - into an in-line system. The spectrometer represents the data in a hypercube, which incorporates the obtained intensity values, dependent on position, wavelength, and time. Hence a second of measurements results in a cube with dimensions of 25 ×256 ×105 (25 channels, not all are used; 256 distinct wavelengths, and an acquisition rate of 105 Hz).

Whenever those values are written as a complete file into the supervised folder by the spectrometer software, those files are read again using our custom program. The 3 used measured positions are extracted from the 25 channels. Additionally, the program performs the necessary spectroscopic steps, i.e., conversion of intensity to absorbance by including background spectra. Furthermore a mean of 525 spectra over a time step of 5 seconds is taken. These data are then written by an OPC client on the defined OPC server.

Hence, a number of 3x256 spectral variables are present on the OPC server. Additionally, some control variables are stored on the OPC server (e.g., batch information as batch number and start time, timestamps of the spectra, control variables that the spectrometer is online, and the custom program is running OK, etc.). The data are persistent on the OPC server, hence available whenever the data are questioned, and only replaced by newer data.

The data are then read by SIMCA-online in a regular interval of 5 seconds (chosen in our setup). The data are consecutively interpreted by a chemometric model, developed in SIMCA beforehand. Thus, selection of spectral bands and projection into an existing PLS model are performed via SimcaOnline.

In a last step, an overall maturity parameter, indicating the process state via a single variable, is created via hierarchical modelling. The already described PLS model for coating thickness prediction serves as bottom model. The obtained scores in these models, for the first two latent variables, and for every channel, thus six variables, serve as input for a top model. This top model is again a PLS model and is regressed towards a maturity parameter ranging from 0 at process start, to 1 for achieving the desired coating thickness at all three channels. That means, the large original data set has been condensed down into a single variable, indicating the progress of the hot-melt coating process, which can be interpreted by operators, and serve as decision indicator.

Finally, it is necessary to define limits for 1) determining a successful process end, and 2) deciding if a process is out of specification. For determining a successful process end, the predicted coating level of all three positions has to be within 1 to 1.1 of the desired coating level, at all three positions at the same time, and no other

alarm must have occurred. The limits for detecting an out-of-bounds process, or confirming a still successful process, are the following:

- A confidence limit for the desirability variable was established by previous batches. As this variable contains all three probes, a deviation in any probe will lead to deviation in this variable.
- Hard alarm limits were set in the predicted coating amount for all three channels, as well as on the score values of the individual measurement positions.
- The DModX-value (i.e., the residual between the reconstructed spectra in the PLS model, and the actual measured spectra) is supervised. Here, a large value indicates that the obtained spectra have a different structure then expected, and investigation is needed.

A process monitored with SimcaOnline, showing the indicator variables over time, can be seen in the screenshot in Figure 3-12. Problems appeared, as sometimes only a portion of a spectrum was transmitted, before the reading process started, and thus was mixed with the previous spectrum. These pieced-together spectra led to a high DModX-value and could not be interpreted correctly. With new software versions, this problem should be avoided, as a spectrum is treated as a vector, and not an array of independent numbers anymore.

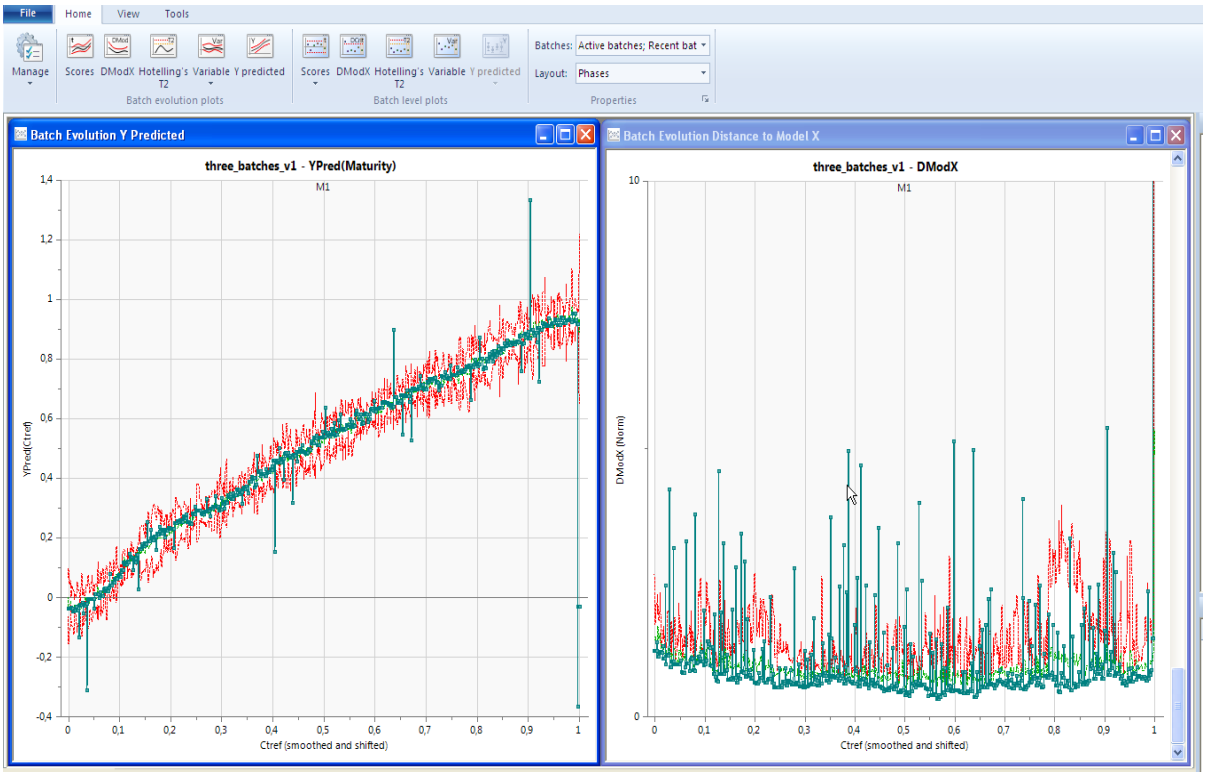

Figure 3-12: Screenshot of a hot-melt coating process monitored with SIMCA-Online. On the left hand side, the running maturity variable, and the allowed corridor are shown. On the right hand side, the DModX variable is plotted. It can be noticed, that the process is running smoothly, but singular outliers appeared. An investigation unveiled, that those outliers were caused not by real measured events, but by incompletely transferred spectra to the OPC server.

3.5 Discussion

3.5.1 Probe positioning and multiple probes

The examples shown in section 3.4.1 highlight the fact that the sensor positions have to be chosen carefully. If only one sensor is used, and its position is not chosen carefully, in-line monitoring will ultimately fail.

The sensor performance at different levels provides a judgement on the different positions. As expected, the central level (level 2) is feasible for process monitoring. Regarding the lower level (level 3), the problem that the sensor was completely covered by crystals arose (though not in all experiments). This also happened once at level 2 for an up-looking (U) sensor. Hence, one has to be careful not only to avoid fouling of the sensors by coating, but also the substrate crystals themselves can clog

the sensor, if the position is unsuitable. Both problems occur individually and in combination when positioning the sensor at the lowest level (level 3). However, sometimes this positons worked remarkably well, in most occasions, the number of crystals observed was too few, to give reliable results. This indicates that the effective height of the fluid bed varies from process to process (although the experimental settings are the same). This may be caused by environmental variables, changes in the raw material properties, and more. Consequently it also shows that a single experiment is not reliable in deciding for or against suitable measurement positions in fluidized systems.

By using a multiple-sensor approach, process disturbances, such as those shown in Figure 3 – 6 can be detected and corrective actions may be initiated, bringing the process back in the desired operating space. Moreover, malfunction of one sensor can be compensated. With regard to a hot-melt coating process, the corrective actions could, for example, be an increase/decrease of process time and spray rate.

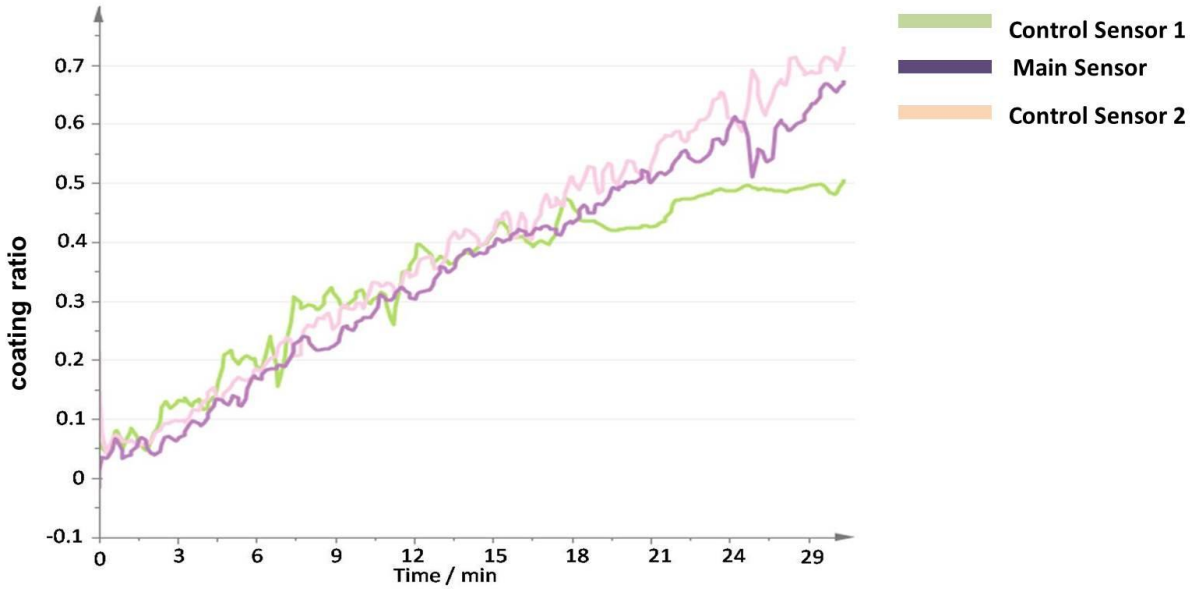

Figure 3-13: Signals of the three sensors. Only two predicted the coating level correctly.

Figure 3-13 (sensor positions according to Table 3-1, Experiment 1) shows the coating ratio for the three sensors. It can be observed that control sensor 1 follows the trajectory of the coating process until the process reaches a coating value of 0.45

after 18 minutes. After this time sensor 1 shows no further increase of the coating mass. Thus, sensor 1 needs to be checked after the process regarding its function and position. With the two other sensors the coating growth was monitored correctly. With the positioning of the three sensors the endpoint can be determined also in the case of one sensor failing.

3.5.2 Process monitoring

The set-up described in the sections 3.3.6 and 3.4.3 indeed enables the in-line control of the hot-melt coating process. The operator can follow the coating trajectory over time, and out of specs occasions can be detected in real-time. An example of a frequently occurring event (in our set-up) is the clogging of the tube, transporting the molten coating from the heating element to the spray nozzle. Corrective actions by the operator can be the elongation of the spraying time, or the increase in feed rate, after the tube has been cleaned.

An interesting example of a possibly faulty process is shown in Figure 3-14. Here, the sensor did not notice the increase in coating over time, due to an unsuitable measurement position. At the process end, however, the powder bed developed enough height, to render the probe successful, and it indicated a regular process. In this questionable case, if the in-line monitoring had already been in place at that time, the process would have been stopped. Having only the usual end-control would have indicated a successful process nonetheless. In contrast, having the full knowledge over time renders this batch out-of-specs. This is a warning, that the usual opinion of having more data being beneficial is only true if the additional data are of high quality, and can be interpreted correctly.

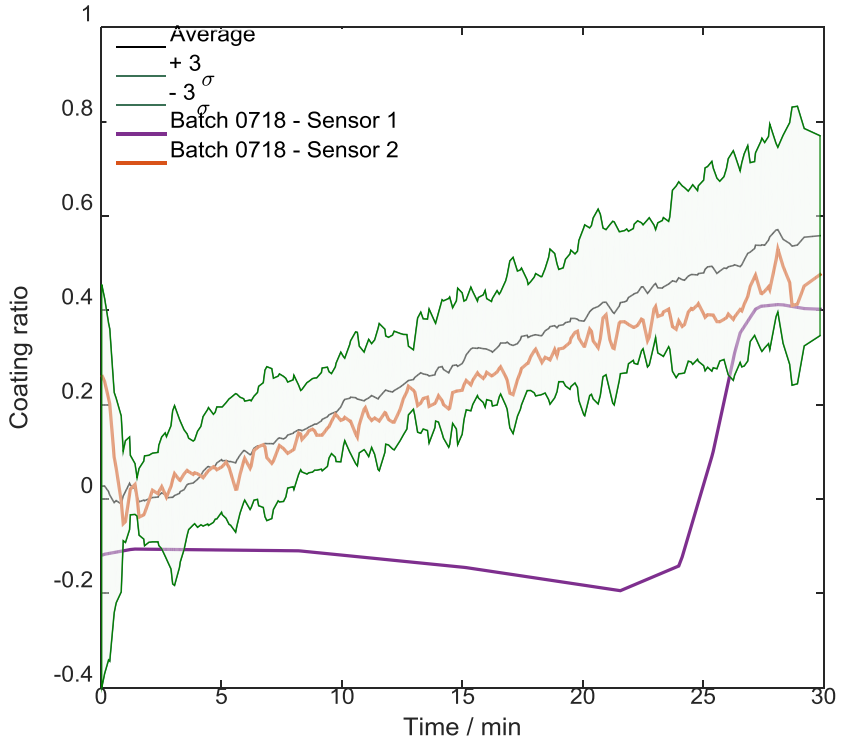

Figure 3-14: Questionable case of a coating process with one sensor at an unsuitable measurement position. At the process end a regular process in indicated.

3.6 Conclusions

This study demonstrates the advantages of using a multi-point near infrared system for hot-melt coating process monitoring. The CQA coating ratio was determined in different positions, and disturbances or inhomogeneities in the process chamber were promptly detected. Proper monitoring of the process and correct endpoint determination can be performed effectively with three sensors, and in the case of a breakdown of one of these sensors the quality of the batch and the endpoint can be determined with the others. Window fouling has also to be taken into consideration. Moreover, although particles in the fluid bed move very fast and often only void space was in front of the sensor, the appropriate quality of spectra was ensured due to the system's high acquisition speed.

Furthermore, an in-line-implementation was created, that enabled the real-time supervision of the process, thus facilitating the correct determination of the coating time, and the fast detection of problems during the running process.

Acknowledgements

This work has been funded by the Austrian COMET Program under the auspices of the Austrian Federal Ministry of Transport, Innovation and Technology (bmvit), the Austrian Federal Ministry of Economy, Family and Youth (bmwfj) and the State of Styria (Styrian Funding Agency SFG). COMET is managed by the Austrian Research Promotion Agency FFG. The authors thank Manuel Zettl, Petra Hofstadler and Moritz Gratzer for their help with operating the fluid bed.

4 Dynamic Cross-Flow Filtration: Enhanced Continuous Small-Scale Solid-Liquid Separation [6]

[6] This chapter is based on the paper Dynamic Cross-Flow Filtration: Enhanced Continuous Small-Scale Solid-Liquid Separation by Johannes Gursch, Roland Hohl, Diana Dujmovic, Jörg Brozio, Markus Krumme, Norbert Rasenack, Johannes Khinast *Drug Dev. Ind. Pharm.*, pp. 1–8, Oct. 2015

4.1 Introduction

While there is a wide variety of technologies available for high-volume throughputs (e.g., drum pressure filters, belt filters, decanters, and so on), for continuous small-throughput filtration only a few systems are readily available. Meanwhile, the demand for such equipment is increasing. For example, in the pharmaceutical industry continuous production of small-quantity products is on the rise due to the trend towards continuous manufacturing and highly specialized patient-centered drugs.[97] Although some ready-to-use continuous equipment is available, the achievable final solid concentrations are often rather low (i.e., 20 vol.% [110]), making the process of solid-liquid separation inefficient.

In our previous study,[111] we reported the use of a commercially available dynamic cross-flow device and demonstrated that it is suitable for producing highly concentrated slurries in a continuous operation mode. While industrial sectors, such as the food and chemical industries have long established continuous manufacturing lines, the pharmaceutical sector has only recently begun to adopt continuous manufacturing (CM) methods [112]. One of the advantages of CM is that time-consuming scale-up can often be avoided. By simply increasing the process time, the same equipment can be used both during the development phases and in the final production [98], enabling a faster product development and a shorter time-to-market for new drugs [96]. Together with real-time release testing and model-based control strategies, products of consistently high quality can be produced in less time. This way, rejection of large batches can be avoided, resulting in a substantial decrease in quality-associated costs and in the length of the supply chain [95], [96], [113], [114].

In our previous study [111], dynamic cross-flow filtration was shown to be suitable for continuous operation of small throughputs, even at high initial solids concentrations. A schematic of the system is shown in Figure 4-1.

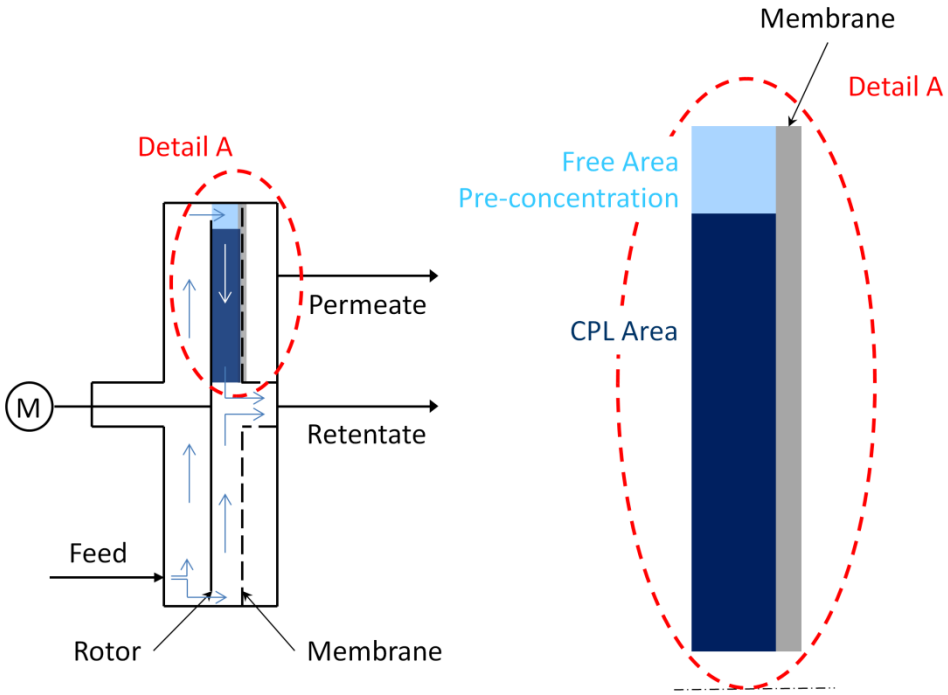

Figure 4-1: Schematic of the filter system and a possible concentration polarization layer (CPL) structure as presented in [111]

However, the tested setup had one major restriction: a constant (material-depending) concentration factor (CF) that could not be changed by modifying process conditions (e.g., for Ibuprofen a CF = 2 was obtained). The concentration factor is defined as:

$$\mathrm{CF} = \frac{\text{product solid concentration}}{\text{feed solid concentration}} \qquad \textbf{(2)}$$

Thus, concentration of a feed with low solids loading takes several consecutive steps. For instance, with a concentration of 1 wt% six subsequent steps need to be carried out to concentrate the suspension up to 64 wt%, with each step requiring a complete set of supporting equipment, such as process analytical tools (PAT), pumps, etc. This results in high investment costs and creates additional complexity associated with developing a control strategy for multiple independent process steps.

Therefore, strategies for improving the process effectiveness have to be developed, i.e., by increasing the achievable permeate flow rates and the concentration factors. Various approaches can be identified by considering Darcy's equation. According to classical filtration theory, the permeate flux (J) can be calculated as a function of

transmembrane pressure (Δp), dynamic viscosity (η), membrane resistance (R_m) and concentration polarization layer (CPL) or cake layer resistance (R_C) [107]:

$$J(t) = \frac{\Delta p}{\eta * (R_m + R_C)} \quad \textbf{(16)}$$

The following strategies can be considered:

(1) Reduction of CPL or cake layer resistance R_c: In many cross-flow applications, the filtered material itself forms a limiting barrier to the flow of liquid through the membrane. In dynamic cross-flow filtration, the limiting barrier is reduced or completely eliminated by shear that is generated either by the material flow itself or the moving parts, e.g., disks or propellers. An increase in the shear rate thus leads to a decrease in layer thickness and an increase in the permeate flow rate [50], [54], [115], [116].

(2) Change of filter medium: Sub-optimal filter media can create substantial problems due to filter blockage. Choosing filter media suitable for a specific filtration task (e.g., particle size, solvent polarity, etc.) significantly improves permeate flow rates if membrane resistance R_m represents the rate-limiting step.

(3) Increase in filtration pressure: An increase in the pressure difference as the main driving force in cross-flow filtration leads to an increase in the permeate flow rates, as long as other effects (e.g., flow reduction due to compaction of the filter cake) can be avoided.

As shear rates were already set to maximal levels (option one) and optimal filter media were already chosen (option two) during our previous study [111] only option three, i.e., an increase of filtration pressure, remains to be addressed. As reported earlier, the tested dynamic cross-flow equipment can alternately open and close the retentate (i.e., the highly concentrated slurry outlet) exit, leading to a pulsating flow at the outlet. During the closed time period, the chamber pressure rises and higher permeate flow rates can be achieved. This oscillating, quasi-continuous operation mode can also be implemented in the equipment manufacturer's larger filtration devices and is already successfully used in industrial applications.

In the fully continuous operation mode (i.e., retentate valve open at all times), the filtration pressure was constant throughout all tested ranges of feed solid concentration and feed rates [111]. The observed constant pressure level (1.41 bar) results from the nature of free suspension flow through the equipment in the open continuous mode and a very low flow resistance of the tested equipment itself. Increasing the resistance of flow through the device, e.g., by adding a constriction at the retentate exit, increases the filtration pressure. However, constrictions may cause blockage of the retentate exit at higher concentrations and thus, are not technically feasible.

Another method of increasing the pressure is to establish a pressurized zone at the retentate exit. However, a continuous discharge of the retentate from a pressurized zone has to be established. Such locks are difficult to engineer and are error-prone.

Another option is to increase the driving pressure difference by reducing the pressure level behind the membrane by adding a vacuum pump to create a limited under-pressure on the permeate side. In this study we investigated approaches to increase the concentration factors and/or the permeate flow rates in a straightforward manner. This paper provides experimental results for vacuum-enhanced dynamic cross-flow filtration in comparison with the established pulsation operation mode. Additionally, for comparison reasons results for open operation mode as presented in [111] are highlighted.

4.2 Materials and methods

4.2.1 Filtration equipment

The Dynotest® by Bokela GmbH, Germany was used as filtration equipment. The unit has a 0.55 kW/ 400 V motor that drives a directly-coupled rotor in line with the axis of the filter disk. The cooled process chamber can be opened for cleaning and changing the membrane, as shown in Figure 4-2. The filtration area is 130 cm2. The maximum filtration pressure is 7 bar (absolute).

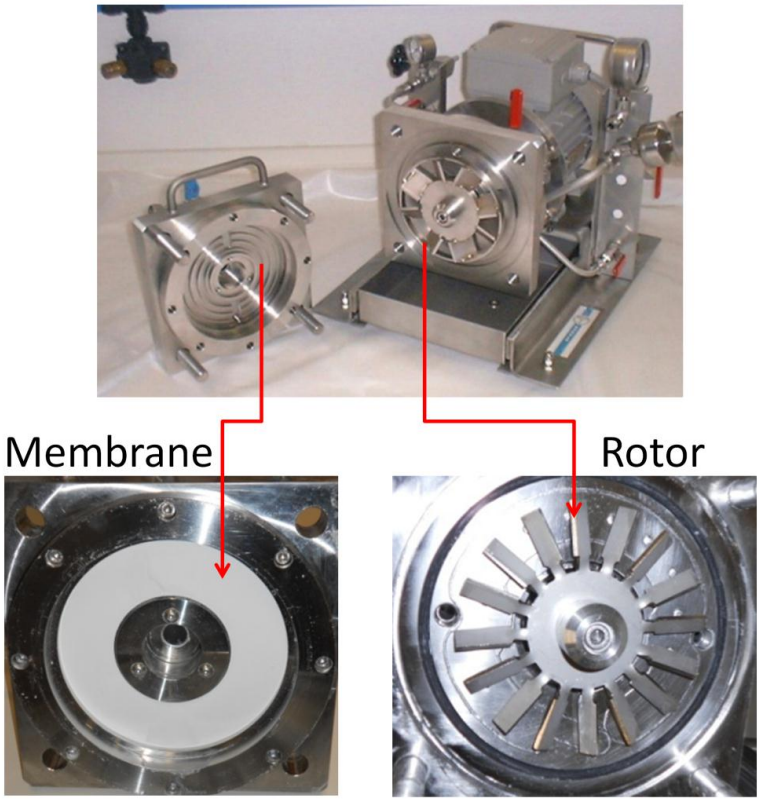

Figure 4-2. CFF (Dynotest® by Bokela GmbH) with rotor and a ceramic membrane

A progressive cavity pump type MX10S-10/20® (Knoll Maschinenbau GmbH, Germany) was used to feed material into the process chamber. The feed throughput was measured with smaller than 0.5% accuracy using an electromagnetic flow meter type FSM4000® by ABB GmbH. Permeate throughput was measured with 2.5% accuracy using an electromagnetic flow meter type 008AP001E® by Honsberg Instruments GmbH, Germany. To measure the filtration pressure, a pressure sensor type 261GS® by ABB GmbH with ±0.1% accuracy was installed. To enhance permeate flow rate, a peristaltic pump type ISM920® by Ismatec, Switzerland was added at the permeate outlet. A simplified P&I schema is provided in Figure 4 – 3.

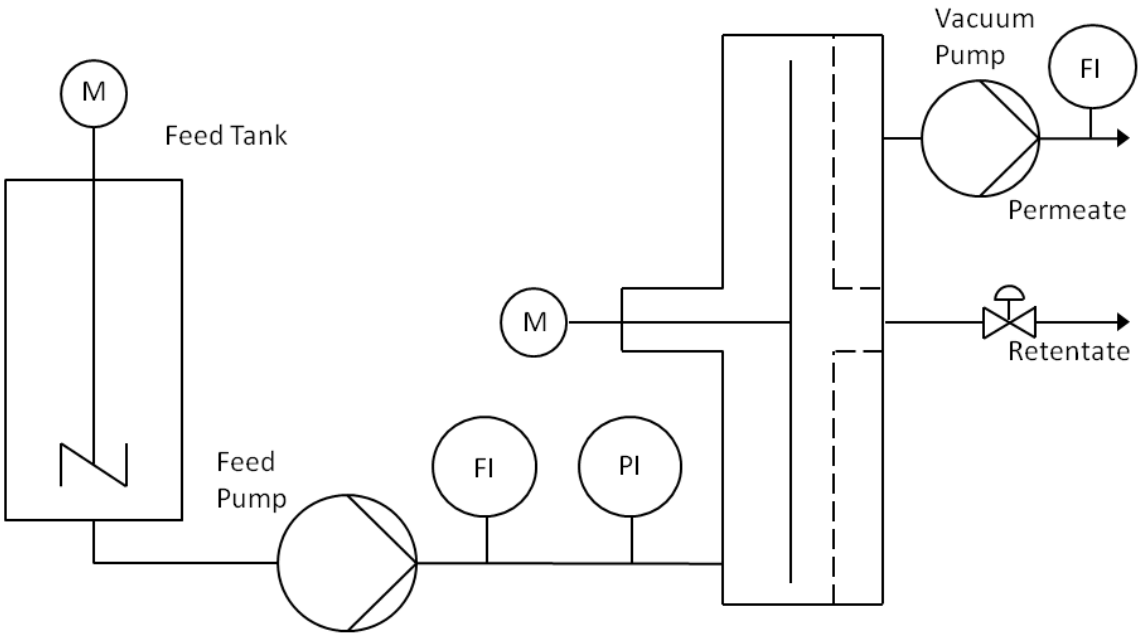

Figure 4-3 Schematic of the filtration setup

4.2.2 Materials

In our study, alpha-lactose monohydrate (Granulac_230® donated by Meggle AG, Austria) with a volume mean particle size of 19 µm was dispersed in water. To prevent particle size or shape changes due to dissolution, we used water saturated with pre-dissolved lactose (180 g/l). Ibuprofen with the volume mean particle size of 32 µm (BASF Switzerland) was also dispersed in water. In the case of Ibuprofen, 8 g sodium pyrophosphate tetrabasic (SPT) provided by Sigma-Aldrich were pre-dissolved per liter of water to ensure uniform dispersion. Solubility effects of Ibuprofen in water are negligible. As membranes, aluminum oxide disks with mean pore size of 0.5 µm, inner diameter of 65 mm, outer diameter of 156 mm and thickness of 2 mm provided by Kerafol Keramische Folien GmbH, Germany were used.

4.2.3 Material characterization

Raw materials and products were thoroughly characterized. Q3 particle size distribution (PSD) was determined using laser diffraction with Helos® (Sympatec

GmbH, Germany, dry dispersing unit Rhodos®) equipped with Sympatec Software, WINDOX 5.6.0.0®. The dispersion pressure was 1.5 bar.

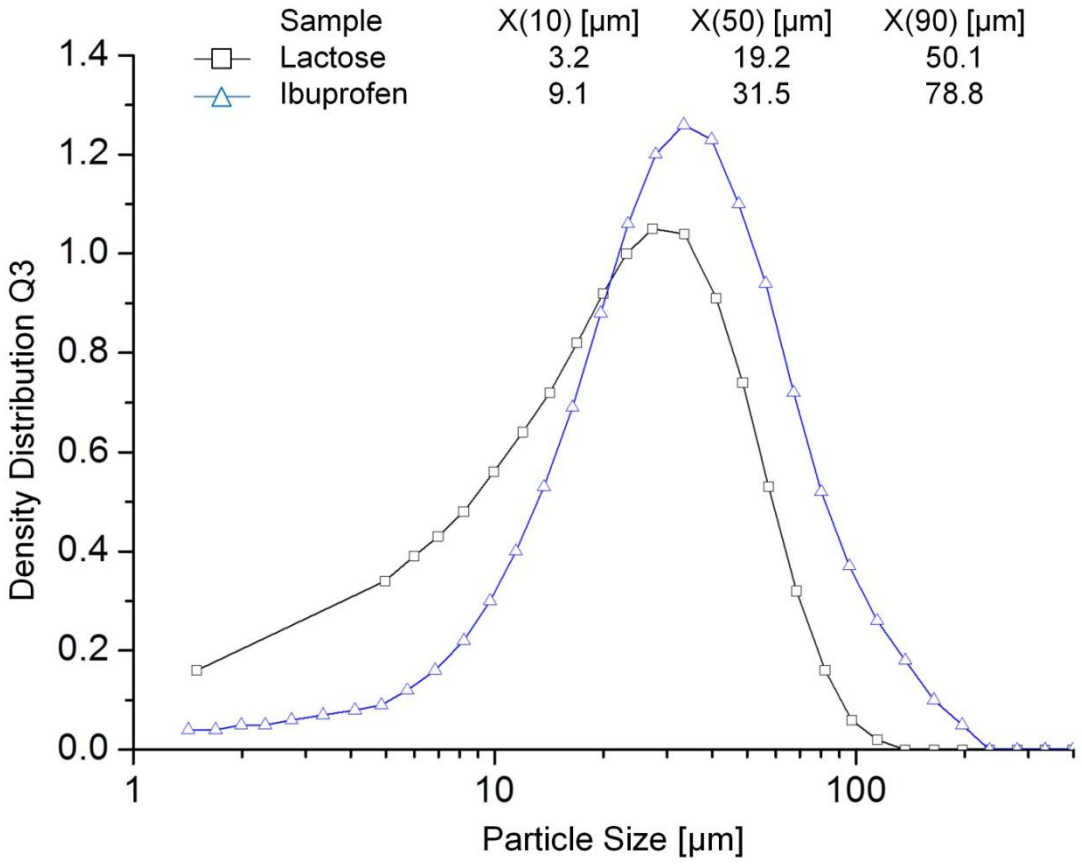

Figure 4-4 PSD of raw materials

Residual moisture was analyzed via a thermo-gravimetric method (MLS_N Version 2.0, Kern & Sohn GmbH, Germany). The drying temperatures for lactose and the Ibuprofen-SPT mixtures were kept constant at 105 °C and 65 °C, respectively. The final residual moisture content was determined once the weight did not change more than 1 mg within 4 minutes, which corresponds to approximately 0.05‰ of relative weight change (based on 20 g sample size).

4.2.4 Methods

To avoid partial blockage of the membrane due to air enclosed in the internal membrane structure, prior to use all membranes were wetted in water for an hour. After assembly, the SFD was vented and rinsed with water for an hour to ensure evacuation of all air. During this time, the outlet valve was opened and a continuous operation mode was established in the vacuum-enhanced operation mode. In the pulsation operation mode, the outlet valve was kept closed during venting and rinsing. Subsequently, the feed was switched from water to suspension. Suspension was prepared in a continuously stirred tank and fed to the SFD via a progressive cavity pump.

In the vacuum-enhanced operation mode, the rotation speed of the peristaltic pump (permeate side) was increased stepwise to prevent exceeding the maximal solid concentration levels as defined by a ramp-up test, which would lead to blockage of the rotor. At the maximum rotation speed of the vacuum pump (130 rpm) an additional pressure difference of approximately 0.54 bar could be achieved. The additional pressure difference was calculated using equation16, and the permeate flow and the membrane resistance were measured with water only. The measured chamber pressure of 1.41 bar was typical for the open operation mode [111]. Thus, a total pressure difference of 0.95 bar were achieved by the vacuum pump speed of 130 rpm and the SFD rotor speed of 1400 rpm.

In the pulsation mode, the retentate valve was designed to open once a material-specific rotor load set point was reached. For lactose and ibuprofen, the opening set points were 71.5 W and 60.5 W, respectively, with open valve intervals of 0.7 s in both cases. These set points were determined by ramp-up tests, during which the retentate valve was kept closed and the suspension was continuously fed to the chamber. As the permeate continuously exits the process chamber, both the suspension’s solid concentration in the chamber and the rotor load (measured via frequency converter) increased. As shown in Figure 4-5, in the beginning of the ramp-up test, the rotor load increased slowly. Once a certain solid concentration in the process chamber was reached, a rapid rise in the rotor load occurred. The rotor load set point was chosen in the beginning of the rapid load increase. After this point,

a slight increase in the solid concentration led to a fast increase in the rotor load. To minimize the risk of rotor blockage, the rotor load set point should not be exceeded.

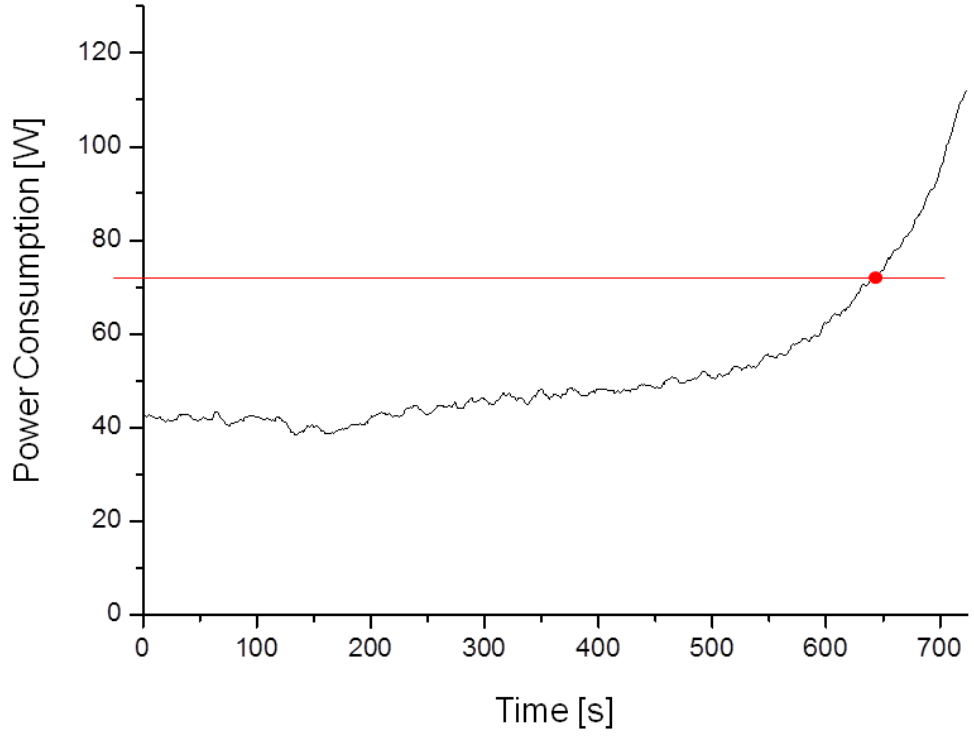

Figure 4-5 Ramp-up test for lactose to determine rotor load set point

Tests were performed for all three operation modes, as shown in Table 4-1. Since rotor blockage occurs once a certain solid concentration in the filtration chamber is exceeded (50wt % for Ibuprofen and 76 wt% for lactose), a low level of feed solid concentration was chosen to demonstrate the possibility of achieving high CFs. Therefore, suspension concentrations range from 10-20 wt%. The feed flow rate was set to 4 kg/h, which is a typical low throughput. However, sedimentation in the feed pipes is still prevented in our lab setup. The rotor speed was set to 1400 rpm (the maximal rotation speed) to ensure the most efficient CPL removal and the highest permeate rates and retentate solid concentrations.

The residual moisture of the steady-state product was calculated based on the feed and permeate flow measurements. Additionally, product samples were dried in a thermo-gravimetric balance. The concentration factor (CF) was calculated according to equation 2 [57] as the ratio between product and feed concentration.

4.3 Results

A summary of the results as well as the tested parameter range is shown in Table 4-1.

Table 4-1 Tested parameter range with resulting retentate solid concentration and concentration factor (CF)

Substance	Operation mode	Feed flow [l/h]	Feed solid concentration [wt%]	Retentate solid concentration [wt%]	CF
Lactose	Open mode	4	10	17	1.7
	Vacuum-enhanced open mode	4	20	70	3.5*
	Pulsation mode	4	10	76	7.6*
Ibuprofen	Open mode	4	10	20	2.0
	Vacuum-enhanced open mode	4	20	52	2.6*
	Pulsation mode	4	10	50	5.0*

* Concentration factors for the pulsation and vacuum-enhanced operation modes strongly depend on the feed concentration. In order to reach a specific maximal concentration defined by the rotor load set point, in the pulsation mode retentate valve opening is controlled and in the vacuum-enhanced operation mode vacuum pump speed is adapted.

4.3.1 Open operation mode

In the open operation mode, a material-dependent, yet otherwise constant CF (1.7 for lactose; 2 for Ibuprofen) is obtained. As reported in [111], typical startup times to reach steady-state are from 45 minutes to an hour. In all open mode runs, the trans-membrane pressure reached a constant level of 1.41 bar after the startup phase, with centrifugal forces of the rotor causing the largest fraction of the measured pressure level.

4.3.1.1 Vacuum-enhanced operation mode

In the vacuum-enhanced open mode, maximal pressure difference was 0.95 bar (1.41 bar measured chamber pressure plus vacuum). Fluctuations in the permeate flow (Figure 4-6 and Figure 4-7) result from variations in the vacuum pump rotation speed that were introduced in order to keep CF high but to avoid transcending maximal solid concentration levels as defined by a ramp-up test. Additional adaptations of vacuum pump rotation speed were necessary to compensate for air leakage into the vacuum system. Air leakage caused a decrease of vacuum conditions as well as deviations in the permeate flow measurement. Achievable CFs in the vacuum-enhanced open mode were approximately 3.5 for lactose and 2.6 for Ibuprofen, and thus 2.1 and 1.3 higher than in the open mode, respectively. CF values are calculated using initial feed solid concentrations. As the vacuum level was adapted to achieve maximal retentate solid concentrations (as determined by a ramp-up test) calculated CF values would be higher for lower feed solid concentrations.

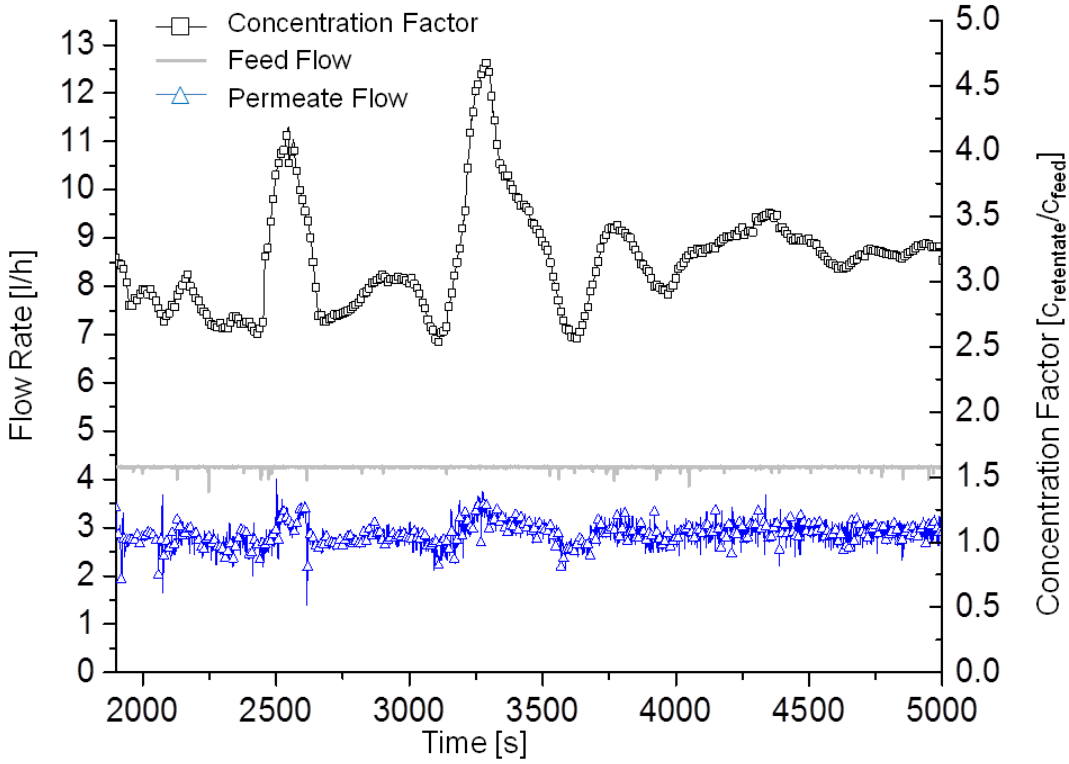

Figure 4-6 Experimental results for the vacuum-enhanced open operation mode with lactose (only every 10th data point plotted). The fluctuations in the permeate flow and in CF from 2000 to 4000 s result from variations in the vacuum pump speed. During this time span, the vacuum pump speed was manually manipulated to maximize CF while avoiding transgression of maximal solid concentration levels as defined by a ramp-up test.

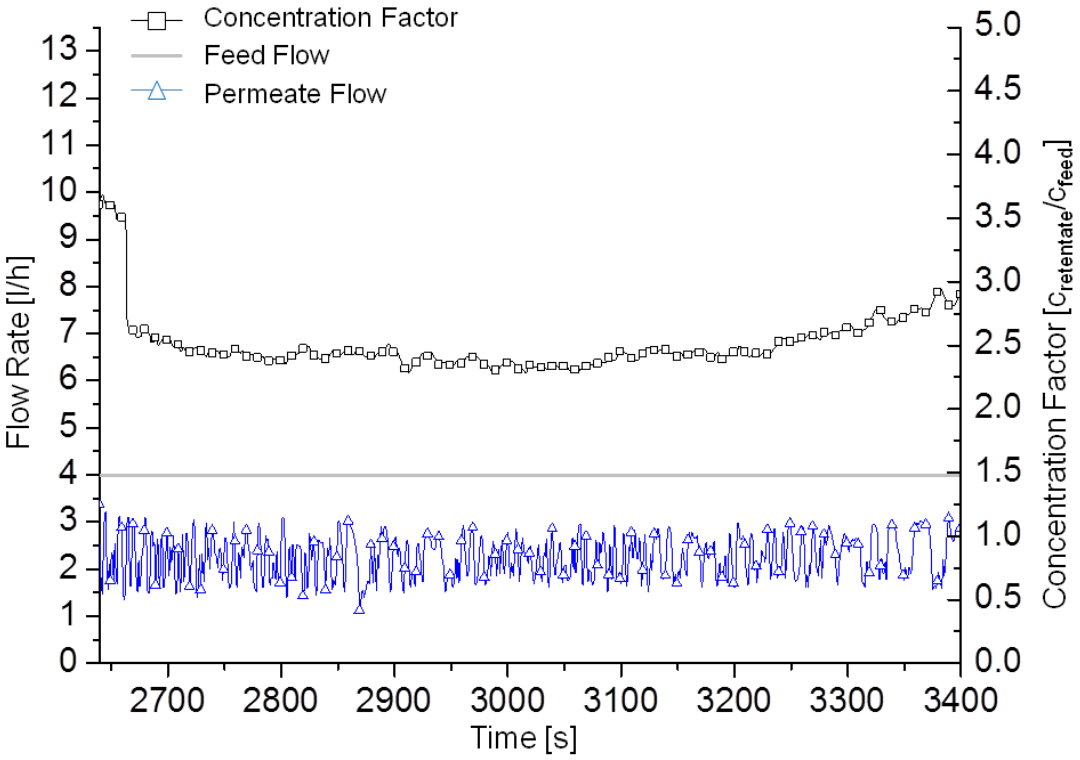

Figure 4-7 Experimental results for vacuum-enhanced open operation mode with Ibuprofen (only every 10th data point plotted)

4.3.2 Pulsation operation mode

In the pulsation mode, the pressure remained at 1.4 bar for lactose, as shown in Figure 4-8. However, an additional test run performed at an elevated feed rate of 8 kg/h resulted in a pressure increase of 1.8 bar. For Ibuprofen, even at a feed rate of 4 kg/h, a rise in the pressure to approximately 2 bar was observed Figure 4-8. Achievable CFs in the pulsation mode were 7.6 for lactose and 5 for Ibuprofen. As retentate solid concentration solely depends on a material-dependent rotor load set point determined in a ramp-up test, calculated CF values only depend on feed solid concentrations. As for the vacuum enhanced operation mode, achievable CF values would be higher for lower feed solid concentrations.

In Figure 4-8 and Figure 4-9 measured chamber pressure difference is shown instead of CF. As retentate solid concentrations reached a constant value right from the start (76 wt% for Lactose and 50 wt% for Ibuprofen), CF values were also constant. In contrast, chamber pressure was subjected to constant pressure rises and decreases due to repeated opening and closing of the retentate valve.

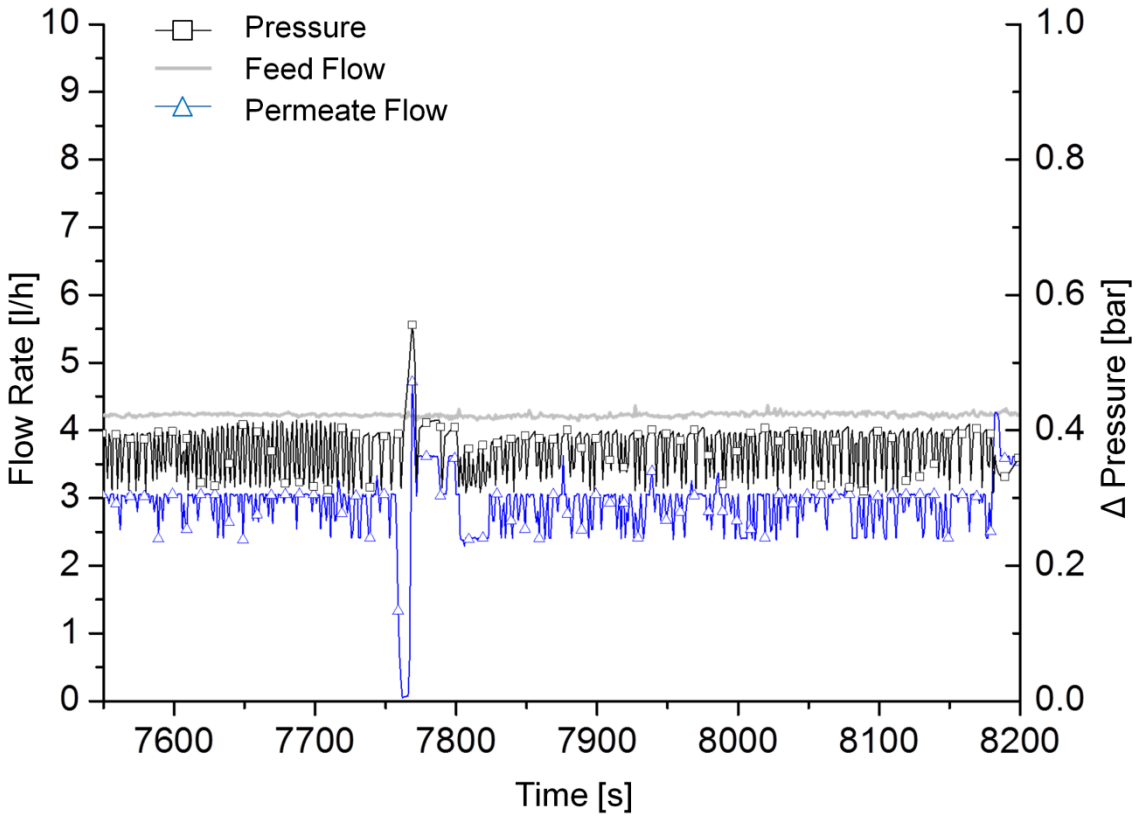

Figure 4-8 Experimental results for the pulsation operation mode for lactose (only every 10th data point plotted) The peak measured at 7760 seconds results from a short term material congestion at the retentate valve. However, the subsequent pressure rise sufficiently removed the congestion

4.4 Discussion

As reported in [111], the open operation mode requires long start-up times for obtaining a constant concentration polarization layer (CPL). During the start-up phase, variations in the concentration factor, i.e., variations in the retentate fluid concentration, can be expected. Depending on the feed rate, this can lead to a large

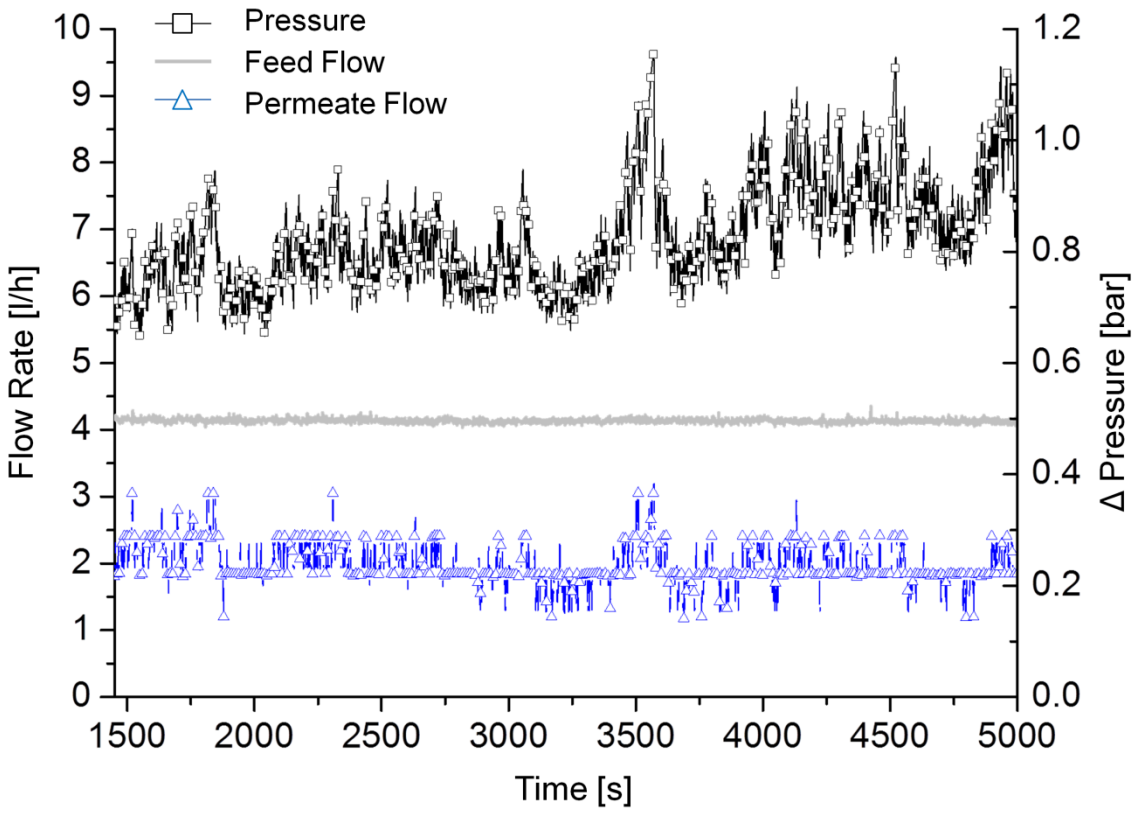

Figure 4-9 : Experimental results for Ibuprofen in the pulsation operation mode (only every 10th data point plotted)

amount of reject material or material that needs to be re-treated. However, once the steady state is reached, a stable flow and a constant CF is obtained. Since the CFs depend exclusively on the material, they are constant over a wide range of flow rates and feed concentrations, as described in [111]. This means that filtration, which involves achieving a significant concentration increase, may require a high number of subsequent filtration steps. This requires additional production equipment or time-consuming recycling steps and results in a large amount of reject material during each start-up phase.

Time to steady state can be significantly reduced in the vacuum-enhanced open mode. For the manually operated vacuum system, a slow stepwise increase in the vacuum level was required to avoid transcending maximal solid concentration levels as defined by a ramp-up test and subsequent blockage of the filter rotor (Figure 4-6 from 2000 to 4000 seconds). Shorter times to steady state can be expected when setting up an automated control of the vacuum system. In addition, by ensuring a constant vacuum level, fluctuations in the permeate flow can be reduced. In our experiments, air slip into the vacuum system caused a decline in the vacuum conditions and deviations in the permeate flow measurement. Less permeate flow fluctuations can be expected when using a vacuum pump type other than the implemented peristaltic pump. Since the vacuum system can be used to control the permeate flow, in a fully automated system a constant CF can be achieved from the start of operation, i.e., only a small amount of initial retentate will have to be discarded (or re-treated). This small amount results from the fact that the implemented system has to be prefilled for degassing purposes; therefore, initial retentate consists of a mix of prefilled liquid and feed material. As shown in Table 4-1, the achievable concentration factors were quite high, and the final solid concentration matched the maximum final solid concentration determined during the ramp-up tests.

In the vacuum-enhanced operation mode, one filtration step was enough to reach the maximum final concentration levels. Thus, compared to the open mode operation, an increase in the CF for most materials (as was the case for all tested substances) and less filtration equipment or recycle steps can be expected.

Start-up time in the pulsation mode depends solely on the feed rate: the faster the filtration chamber is filled, the sooner the pre-determined rotor load set point is reached and the retentate valve opens. Due to the regulated product discharge, the maximal final solid concentration is reached in one step and the retentate has a constant solid concentration right from the beginning. Due to the intermittent closure of the retentate valve and the retention of the concentrated product, the system pressure rises. According to equation16, a rise in the pressure results in an increased permeate flow rates, as long as there are no additional effects, such as the

compaction of the CPL layer. During our experiments, a pressure rise to approximately 2 bar was observed before the system stabilized. Although the pulsing nature of the retentate flow may cause variations in subsequent manufacturing steps, e.g., drying and mixing, its direct integration into downstream steps without buffers may be feasible. For this purpose, the retentate stream has to be well characterized, i.e., the retentate flow rate has to be precisely determined. Calculation of retentate flow rate from permeate measurement is inaccurate (calculation with mean values), therefore retentate flow rate has to be measured directly. For most flow measurement devices this is difficult to achieve at low flow rates, especially if the monitored fluid is a highly concentrated slurry.

4.5 Conclusion

Three operation modes were tested using the same continuously or semi-continuously operating cross-flow filtration device and two model substances. Process stability, the ability to integrate with downstream steps and the filtration efficiency (high achievable suspension concentration) are key factors in choosing an operation mode.

Fluctuating feed rates and concentrations cannot be compensated in the open operation mode since the only controlling parameter is the CPL layer or rather the CPL layer build up [111]. Fast fluctuations cannot be compensated quickly by variations in the CPL layer. As such, variations in the feed flow will result in variations in the retentate composition. In the vacuum-enhanced operation mode, the vacuum level can be adapted by a control system, reacting to the changing feed conditions. Thus, changes in the feed concentration and feed flow rate can be accounted for and variations in the retentate composition can be avoided.

Since in the pulsing mode the retentate valve only opens once a given rotor load/chamber solid concentration is reached, retentate composition does not depend on the feed conditions and the only variation in the retentate is the resulting flow rate over time. The pulsating output flows (flow rate and pressure) of this operation mode pose challenges for integration in subsequent manufacturing steps. Buffering might be needed, or retentate flow rates have to be measured directly. However, flow rate measurement of fast changing high-viscosity suspensions at low throughput volumes

is challenging. In contrast, retentate flow rates in the open and vacuum-enhanced operation modes can be characterized using the permeate flow rates. Even direct measurement of the retentate stream is possible due to the constant flow through cross-flow filtration equipment.

In terms of achievable CFs, the pulsation and vacuum-enhanced operation modes are superior to the open operation mode. Minimizing the number of required filters decreases not only the investment costs, but also possible sources of malfunctions and process upsets. In this context, the open operation mode seems to be the least beneficial: for example, low feed concentrations would necessitate a large number of filtration steps or filtration cycles. Depending on the filtered substance, the vacuum-enhanced operation or pulsation operation modes with the increasing filtration pressure may result in higher CFs. For several substances permeability of the concentration polarization layer is known to decrease once a certain vacuum or pressure level is reached. For the tested lactose and Ibuprofen-water mixtures no significant differences could be observed with driving pressure forces reaching approximately the same values (vacuum enhanced mode: 1.95 bar; pulsation mode: 1.8 bar for lactose and 2 bar for Ibuprofen). Therefore, both operation modes seem feasible, according to the specific filtration characteristic of the treated substance.

Overall, the vacuum-enhanced operation mode appears to be the most promising one in terms of achievable CFs for a large number of substances. Easy integration into subsequent manufacturing steps, straightforward flow monitoring and fast reaction to changes in the feed conditions make this operation mode promising for enhanced continuous small-scale filtration.

4.6 Acknowledgements

This work was funded through the Austrian COMET Program by the Austrian Federal Ministry of Transport, Innovation and Technology (BMVIT), the Austrian Federal Ministry of Economy, Family and Youth (BMWFJ) and by the State of Styria (Styrian Funding Agency SFG). We would like to acknowledge the support of Manuel Zettl, Daniel Wiegele, Arlin Gruber and Daniel Kaiser and thank Bokela GmbH for their assistance, Meggle AG for donating lactose and Novartis Pharma AG Basel for financial contribution.

5 Outlook and summary

In chapter 2, the comparison of the experimental data and the simulated date show very good agreement. In order to evaluate the quality of our simulation, we compared the liquid content of the experimentally measured sensor data with ‘virtual sensors’, accordingly placed in the simulation and identified statistically reasonable sensor locations (3.1 and 3.2) for our process.

- The analysis of our results shows very good agreement for the quantitative liquid content evolution of the simulation data compared to the experimental data.

- In the experiment only spot-like analyses are accessible via sensors, in numerical simulations the information of the liquid content is available for all particles in the system at any time.

- Based on the available total information in the simulation data, the mixing-time dependent residence time distribution (rtd) was analysed.

In chapter 3 the advantages of using a multi-point near infrared system for hot-melt coating process monitoring are demonstrated.

- The CQA coating ratio was determined indifferent positions.

- Disturbances or inhomogeneities in the process chamber were promptly detected.

- Proper monitoring of the process and correct endpoint determination can be performed effectively with three sensors in the case of a breakdown of one of the sensors, the quality of the batch and the endpoint can be determined with the sensors.

In chapter 4, a membrane filtration system was investigated which can handle a wide range of feed rates and feed concentrations.

- The materials showed a linear relationship between the feed and the permeate rate.

- A constant concentration factor was reached for the different model substances.

- The linear relationship and the constant CF makes it easy to predict filtration performance.

- Once the material-specific CF value is known, the developed one-parameter model suffices to describe the filtration process.

- Here, feed rates of 36 l/h were set as the upper limit, due to the equipment's use as small-scale production equipment.

- Maximum final solid concentrations were very high (60 wt% for Ibuprofen and 76 wt% for lactose).

- The low throughput range renders the CFF the most favorable choice for continuous production.

- Its closed-chamber design allows for treatment of toxic solvents and APIs, which is a must in pharmaceutical production.

The implementation of PAT in pharmaceutical processes gets more important, especially real time analysis of the production processes. Different measurement systems can be used for the online control and prediction of those processes. The importance of simulations for process understanding and also the use of non-

spectroscopic measurement systems which generate univariate data could be clearly shown in this thesis.

6 References

[1] R. W. Bondi and J. K. Drennen, “Quality by Design and the Importance of PAT in QbD,” *Sep. Sci. Technol.*, vol. 10, no. September 2004, pp. 195–224, 2011.

[2] FDA, “Guidance for Industry Guidance for Industry PAT — A Framework for Innovative Pharmaceutical,” no. September, p. 19, 2004.

[3] T. De Beer, a. Burggraeve, M. Fonteyne, L. Saerens, J. P. Remon, and C. Vervaet, “Near infrared and Raman spectroscopy for the in-process monitoring of pharmaceutical production processes,” *Int. J. Pharm.*, vol. 417, no. 1–2, pp. 32–47, 2011.

[4] W. Herschel, “To subscribe to Phil. Trans. R. Soc. Lond. , go to: http://rstl.royalsocietypublishing.org/subscriptions,” 1800.

[5] G. Reich, “Near-infrared spectroscopy and imaging: basic principles and pharmaceutical applications.,” *Adv. Drug Deliv. Rev.*, vol. 57, no. 8, pp. 1109–43, Jun. 2005.

[6] “Brucker Optics, ‘Guide for Infrared Spectroscopy,’” 2011.

[7] J. G. Rosas, M. Blanco, J. M. González, and M. Alcalà, “Real-time determination of critical quality attributes using near-infrared spectroscopy: A contribution for Process Analytical Technology (PAT),” *Talanta*, vol. 97, pp. 163–170, 2012.

[8] J. Rantanen, E. Räsänen, O. Antikainen, J. P. Mannermaa, and J. Yliruusi, “In-line moisture measurement during granulation with a four-wavelength near-infrared sensor: An evaluation of process-related variables and a development of non-linear calibration model,” *Chemom. Intell. Lab. Syst.*, vol. 56, pp. 51–58, 2001.

[9] M. Blanco and M. a Romero, “Near-infrared libraries in the pharmaceutical industry: a solution for identity confirmation.,” *Analyst*, vol. 126, pp. 2212–2217, 2001.

[10] A. S. El-Hagrasy, H. R. Morris, F. D’Amico, R. a. Lodder, and J. K. Drennen, “Near-infrared spectroscopy and imaging for the monitoring of powder blend homogeneity,” *J. Pharm. Sci.*, vol. 90, no. 9, pp. 1298–1307, 2001.

[11] S. S. Sekulic, H. W. Ward, D. R. Brannegan, E. D. Stanley, C. L. Evans, S. T. Sciavolino, P. a Hailey, and P. K. Aldridge, “On-line monitoring of powder blend homogeneity by near-infrared spectroscopy.,” *Anal. Chem.*, vol. 68, no. 3, pp. 509–513, 1996.

[12] H. Wu, M. Tawakkul, M. White, and M. a. Khan, “Quality-by-Design (QbD): An integrated multivariate approach for the component quantification in powder blends,” *Int. J. Pharm.*, vol. 372, pp. 39–48, 2009.

[13] A. Gupta, G. E. Peck, R. W. Miller, and K. R. Morris, “Nondestructive Measurements of the Compact Strength and the Particle-Size Distribution after Milling of Roller Compacted Powders by Near-Infrared Spectroscopy,” *J. Pharm. Sci.*, vol. 93, no. 4, pp. 1047–1053, 2004.

[14] G. Reich, “Near-infrared spectroscopy and imaging: Basic principles and pharmaceutical applications,” *Adv. Drug Deliv. Rev.*, vol. 57, pp. 1109–1143, 2005.

[15] M. Andersson, M. Josefson, F. W. Langkilde, and K. G. Wahlund, “Monitoring of a film coating process for tablets using near infrared reflectance spectrometry,” *J. Pharm. Biomed. Anal.*, vol. 20, pp. 27–37, 1999.

[16] J. D. Kirsch and J. K. Drennen, “Determination of film-coated tablet parameters by near-infrared spectroscopy.,” *J. Pharm. Biomed. Anal.*, vol. 13, no. 10, pp. 1273–81, Sep. 1995.

[17] J. Aaltonen, K. Kogermann, C. J. Strachan, and J. Rantanen, “In-line monitoring of solid-state transitions during fluidisation,” *Chem. Eng. Sci.*, vol. 62, pp. 408–415, 2007.

[18] J. Aaltonen, K. C. Gordon, C. J. Strachan, and T. Rades, “Perspectives in the use of spectroscopy to characterise pharmaceutical solids,” *Int. J. Pharm.*, vol. 364, pp. 159–169, 2008.

[19] M. Römer, J. Heinämäki, C. Strachan, N. Sandler, and J. Yliruusi, “Prediction of tablet film-coating thickness using a rotating plate coating system and NIR spectroscopy.,” *AAPS PharmSciTech*, vol. 9, no. 4, pp. 1047–1053, 2008.

[20] J. Märk, M. Karner, M. Andre, J. Rueland, and C. W. Huck, “Online process control of a pharmaceutical intermediate in a fluidized-bed drier environment using near-infrared spectroscopy,” *Anal. Chem.*, vol. 82, no. 10, pp. 4209–4215, 2010.

[21] E. Räsänen, J. Rantanen, J. P. Mannermaa, J. Yliruusi, and H. Vuorela, “Dehydration studies using a novel multichamber microscale fluid bed dryer with in-line near-infrared measurement,” *J. Pharm. Sci.*, vol. 92, no. 10, pp. 2074–2081, 2003.

[22] R. L. Green, G. Thurau, N. C. Pixley, A. Mateos, R. a. Reed, and J. P. Higgins, “In-line monitoring of moisture content in fluid bed dryers using near-IR spectroscopy with consideration of sampling effects on method accuracy,” *Anal. Chem.*, vol. 77, no. 14, pp. 4515–4522, 2005.

[23] F. J. S. Nieuwmeyer, M. Damen, A. Gerich, F. Rusmini, K. Van Der Voort Maarschalk, and H. Vromans, “Granule characterization during fluid bed drying by development of a near infrared method to determine water content and median granule size,” *Pharm. Res.*, vol. 24, no. 10, pp. 1854–1861, 2007.

[24] P. a. Hailey, P. Doherty, P. Tapsell, T. Oliver, and P. K. Aldridge, “Automated system for the on-line monitoring of powder blending processes using near-

infrared spectroscopy part I. System development and control," *J. Pharm. Biomed. Anal.*, vol. 14, pp. 551–559, 1996.

[25] A. S. El-Hagrasy and J. K. Drennen, "A process analytical technology approach to near-infrared process control of pharmaceutical powder blending. Part III: Quantitative near-infrared calibration for prediction of blend homogeneity and characterization of powder mixing kinetics," *J. Pharm. Sci.*, vol. 95, no. 2, pp. 422–434, 2006.

[26] Z. Shi, R. P. Cogdill, S. M. Short, and C. a. Anderson, "Process characterization of powder blending by near-infrared spectroscopy: Blend end-points and beyond," *J. Pharm. Biomed. Anal.*, vol. 47, pp. 738–745, 2008.

[27] Y. Sulub, B. Wabuyele, P. Gargiulo, J. Pazdan, J. Cheney, J. Berry, A. Gupta, R. Shah, H. Wu, and M. Khan, "Real-time on-line blend uniformity monitoring using near-infrared reflectance spectrometry: A noninvasive off-line calibration approach," *J. Pharm. Biomed. Anal.*, vol. 49, pp. 48–54, 2009.

[28] Y. Sulub, R. LoBrutto, R. Vivilecchia, and B. W. Wabuyele, "Content uniformity determination of pharmaceutical tablets using five near-infrared reflectance spectrometers: A process analytical technology (PAT) approach using robust multivariate calibration transfer algorithms," *Anal. Chim. Acta*, vol. 611, pp. 143–150, 2008.

[29] J. Rantanen, E. Räsänen, J. Tenhunen, M. Känsäkoski, J. Mannermaa, and J. Yliruusi, "In-line moisture measurement during granulation with a four-wavelength near infrared sensor: an evaluation of particle size and binder effects.," *Eur. J. Pharm. Biopharm.*, vol. 50, no. 2, pp. 271–6, Sep. 2000.

[30] H. Wikström, P. J. Marsac, and L. S. Taylor, "In-line monitoring of hydrate formation during wet granulation using Raman spectroscopy," *J. Pharm. Sci.*, vol. 94, no. 1, pp. 209–219, 2005.

[31] T. R. De Beer, M. Alleso, F. Goethals, a Coppens, Y. V Heyden, H. L. De Diego, J. Rantanen, F. Verpoort, C. Vervaet, J. P. Remon, and W. R. Baeyens, "Implementation of a process analytical technology system in a freeze-drying process using Raman spectroscopy for in-line process monitoring," *Anal. Chem.*, vol. 79, no. 5, pp. 7992–8003, 2007.

[32] J. Mantanus, E. Ziémons, E. Rozet, B. Streel, R. Klinkenberg, B. Evrard, J. Rantanen, and P. Hubert, "Building the quality into pellet manufacturing environment--feasibility study and validation of an in-line quantitative near infrared (NIR) method.," *Talanta*, vol. 83, no. 2, pp. 305–11, Dec. 2010.

[33] J. Rantanen, H. Wikström, R. Turner, and L. S. Taylor, "Use of in-line near-infrared spectroscopy in combination with chemometrics for improved understanding of pharmaceutical processes," *Anal. Chem.*, vol. 77, no. 2, pp. 556–563, 2005.

[34] A. C. Jørgensen, J. Rantanen, P. Luukkonen, S. Laine, and J. Yliruusi, “Visualization of a pharmaceutical unit operation: Wet granulation,” *Anal. Chem.*, vol. 76, no. 18, pp. 5331–5338, 2004.

[35] S. M. Mercier, B. Diepenbroek, M. C. F. Dalm, R. H. Wijffels, and M. Streefland, “Multivariate data analysis as a PAT tool for early bioprocess development data,” *J. Biotechnol.*, vol. 167, no. 3, pp. 262–270, 2013.

[36] T. Kourti, “The Process Analytical Technology initiative and multivariate process analysis, monitoring and control,” *Anal. Bioanal. Chem.*, vol. 384, pp. 1043–1048, 2006.

[37] a Höskuldsson and A. Hoskuldsson, “PLS Regression Methods,” *J. Chemom.*, vol. 2, no. November 1987, pp. 211–228, 1988.

[38] S. Wold, M. Sjöström, and L. Eriksson, “PLS-regression: A basic tool of chemometrics,” *Chemom. Intell. Lab. Syst.*, vol. 58, pp. 109–130, 2001.

[39] K. Knop and P. Kleinebudde, “PAT-tools for process control in pharmaceutical film coating applications,” *Int. J. Pharm.*, vol. 457, no. 2, pp. 527–536, 2013.

[40] E. Teunou and D. Poncelet, “Batch and continuous fluid bed coating - Review and state of the art,” *J. Food Eng.*, vol. 53, pp. 325–340, 2002.

[41] M. A. van der Hoef, M. Ye, M. van Sint Annaland, A. T. Andrews, S. Sundaresan, and J. A. M. Kuipers, “Multiscale Modeling of Gas-Fluidized Beds,” *Adv. Chem. Eng.*, vol. 31, pp. 65–149, 2006.

[42] W. Du, X. Bao, J. Xu, and W. Wei, “Computational fluid dynamics (CFD) modeling of spouted bed: Assessment of drag coefficient correlations,” *Chem. Eng. Sci.*, vol. 61, no. 5, pp. 1401–1420, Mar. 2006.

[43] S. Romero-Torres, J. D. Pérez-Ramos, K. R. Morris, and E. R. Grant, “Raman spectroscopic measurement of tablet-to-tablet coating variability.,” *J. Pharm. Biomed. Anal.*, vol. 38, no. 2, pp. 270–4, Jun. 2005.

[44] C. Gendre, M. Genty, M. Boiret, M. Julien, L. Meunier, O. Lecoq, M. Baron, P. Chaminade, and J. M. Péan, “Development of a Process Analytical Technology (PAT) for in-line monitoring of film thickness and mass of coating materials during a pan coating operation,” *Eur. J. Pharm. Sci.*, vol. 43, no. 4, pp. 244–250, 2011.

[45] C. Gendre, M. Boiret, M. Genty, P. Chaminade, and J. M. Pean, “Real-time predictions of drug release and end point detection of a coating operation by in-line near infrared measurements.,” *Int. J. Pharm.*, vol. 421, no. 2, pp. 237–43, Dec. 2011.

[46] M. Lee, C. Park, A. Kim, B. Kwon, K. Bang, Y. Cho, M. Jeong, and G. Choi, “Dynamic Calibration for the In-Line NIR Monitoring of Film Thickness of Pharmaceutical Tablets Processed in a Fluid-Bed Coater,” *J. Pharm. Sci.*, vol. 99, no. 1, pp. 325–335, 2010.

[47] M.-J. Lee, D.-Y. Seo, H.-E. Lee, I.-C. Wang, W.-S. Kim, M.-Y. Jeong, and G. J. Choi, “In line NIR quantification of film thickness on pharmaceutical pellets during a fluid bed coating process.,” *Int. J. Pharm.*, vol. 403, no. 1–2, pp. 66–72, Jan. 2011.

[48] M. Y. Jaffrin, “Dynamic shear-enhanced membrane filtration: A review of rotating disks, rotating membranes and vibrating systems,” *J. Memb. Sci.*, vol. 324, pp. 7–25, 2008.

[49] Z. Tu and L. Ding, “Microfiltration of mineral suspensions using a MSD module with rotating ceramic and polymeric membranes,” *Sep. Purif. Technol.*, vol. 73, no. 3, pp. 363–370, Jul. 2010.

[50] G. He, L. H. Ding, P. Paullier, and M. Y. Jaffrin, “Experimental study of a dynamic filtration system with overlapping ceramic membranes and non-permeating disks rotating at independent speeds,” *J. Memb. Sci.*, vol. 300, pp. 63–70, 2007.

[51] S. S. Lee, a Burt, G. Russotti, and B. Buckland, “Microfiltration of recombinant yeast cells using a rotating disk dynamic filtration system.,” *Biotechnol. Bioeng.*, vol. 48, no. 4, pp. 386–400, Nov. 1995.

[52] A. Pessoa and M. Vitolo, “Evaluation of cross-flow microfiltration membranes using a rotary disc- filter,” *Process Biochem.*, vol. 33, no. 1, pp. 39–45, 1998.

[53] B. Georges, P. Joseph M., G. Anthony, and K. Y. Chung, “Diagnosis of membrane fouling using a rotating annular filter.” Journal of Membrane Science, pp. 1–22, 1993.

[54] M. Y. Jaffrin, “Dynamic filtration with rotating disks, and rotating and vibrating membranes: An update,” *Curr. Opin. Chem. Eng.*, vol. 1, no. 2, pp. 171–177, 2012.

[55] R. Bott, T. Langeloh, and E. Ehrfeld, “Dynamic cross flow filtration,” *Chem. Eng. J.*, vol. 80, no. 1–3, pp. 245–249, Dec. 2000.

[56] P. Marchetti, A. Butté, and A. G. Livingston, “Quality by Design for peptide nanofiltration: Fundamental understanding and process selection,” *Chem. Eng. Sci.*, vol. 101, pp. 200–212, Sep. 2013.

[57] M. W. Jornitz and T. H. Meltzer, Eds., *Filtration and Purification in the Biopharmaceutical Industry*, 2nd ed., vol. 28. Informa Healthcare, 2007.

[58] C. C. Corredor, D. Bu, and D. Both, “Comparison of near infrared and microwave resonance sensors for at-line moisture determination in powders and tablets.,” *Anal. Chim. Acta*, vol. 696, no. 1–2, pp. 84–93, Jun. 2011.

[59] Y. Roggo, P. Chalus, L. Maurer, C. Lema-Martinez, A. Edmond, and N. Jent, “A review of near infrared spectroscopy and chemometrics in pharmaceutical technologies.,” *J. Pharm. Biomed. Anal.*, vol. 44, no. 3, pp. 683–700, Jul. 2007.

[60] L. K. Wang, P. W. S. Heng, and C. V. Liew, “Online monitoring of particle mass flow rate in bottom spray fluid bed coating--development and application.,” *Int. J. Pharm.*, vol. 395, no. 1–2, pp. 215–21, Aug. 2010.

[61] O. Scheibelhofer, N. Balak, D. M. Koller, and J. G. Khinast, “Spatially Resolved Monitoring of Powder Mixing Processes via Multiple NIR-Probes,” *Powder Technol.*, vol. 243, pp. 161–170, 2013.

[62] O. Scheibelhofer, N. Balak, P. R. Wahl, D. M. Koller, B. J. Glasser, and J. G. Khinast, “Monitoring Blending of Pharmaceutical Powders with Multipoint NIR Spectroscopy.,” *AAPS PharmSciTech*, Dec. 2012.

[63] C. R. Dalton and B. C. Hancock, “Processing and storage effects on water vapor sorption by some model pharmaceutical solid dosage formulations,” *Int. J. Pharm.*, vol. 156, no. 2, pp. 143–151, Oct. 1997.

[64] E. E. Moura, P. A. Berbert, M. A. Berbert-Molina, and M. T. R. Oliveira, “Performance analysis of RF dielectric models for density-independent estimation of moisture content in sorghum,” *Powder Technol.*, vol. 246, pp. 369–378, 2013.

[65] H. G. Wang, P. R. Senior, R. Mann, and W. Q. Yang, “Online measurement and control of solids moisture in fluidised bed dryers,” *Chem. Eng. Sci.*, vol. 64, no. 12, pp. 2893–2902, 2009.

[66] M. S. Beck and R. A. Williams, “Process tomography: a European innovation and its applications,” *Meas. Sci. Technol*, vol. 7, pp. 215–224, 1996.

[67] J. Austin, S. Rodriguez, P. F. Sung, and M. Harris, “Utilizing microwaves for the determination of moisture content independent of density,” *Powder Technol.*, vol. 236, pp. 17–23, 2013.

[68] F. Portoghese, F. Berruti, and C. Briens, “Continuous on-line measurement of solid moisture content during fluidized bed drying using triboelectric probes,” *Powder Technol.*, vol. 181, no. 2, pp. 169–177, 2008.

[69] D. M. Koller, A. Posch, G. Hoerl, C. Voura, N. Urbanetz, S. D. Fraser, W. Tritthart, F. Reiter, M. Schlingmann, and J. G. Khinast, “Continuous Quantitative Monitoring of Powder Mixing Dynamics by Near-infrared Spectroscopy,” *Powder Technol. Submitt.*, 2010.

[70] Y. Shigeto and M. Sakai, “Parallel computing of discrete element method on multi-core processors,” *Particuology*, vol. 9, no. 4, pp. 398–405, Aug. 2011.

[71] L. Verlet, “Computer ``Experiments'' on Classical Fluids. {II}: Equilibrium Correlation Functions,” *Phys. Rev.*, vol. 165, no. 1, pp. 201–214, 1967.

[72] S. Luding, “Collisions & Contacts between two particles,” in *Physics of dry granular media - NATO ASI Series E350*, 1998, p. 285.

[73] P. Minkkinen, “Practical applications of sampling theory,” *Chemom. Intell. Lab. Syst.*, vol. 74, no. 1, pp. 85–94, Nov. 2004.

[74] A. M. Abouzeid and D. W. Fuerstenau, “Flow of Non-Homogeneous Particulates in Rotating Drums,” vol. 28, no. 28, pp. 155–166, 2010.

[75] B. Cuq, N. Gontard, and S. Guilbert, “Edible films and coatings as active layers,” in *Active Food Packaging*, M. L. Rooney, Ed. New York: Springer US, 1995, pp. 111–142.

[76] V. Jannin and Y. Cuppok, “Hot-melt coating with lipid excipients.,” *Int. J. Pharm.*, vol. 026, Oct. 2012.

[77] M. Andersson, S. Folestad, J. Gottfries, M. O. Johansson, M. Josefson, and K.-G. Wahlund, “Quantitative Analysis of Film Coating in a Fluidized Bed Process by In-Line NIR Spectrometry and Multivariate Batch Calibration,” *Anal. Chem.*, vol. 72, no. 9, pp. 2099–2108, May 2000.

[78] Y. Roggo, N. Jent, a Edmond, P. Chalus, and M. Ulmschneider, “Characterizing process effects on pharmaceutical solid forms using near-infrared spectroscopy and infrared imaging.,” *Eur. J. Pharm. Biopharm.*, vol. 61, no. 1–2, pp. 100–10, Sep. 2005.

[79] S. Romero-Torres, J. D. Pérez-Ramos, K. R. Morris, and E. R. Grant, “Raman spectroscopy for tablet coating thickness quantification and coating characterization in the presence of strong fluorescent interference.,” *J. Pharm. Biomed. Anal.*, vol. 41, no. 3, pp. 811–9, Jun. 2006.

[80] J. F. Kauffman, M. Dellibovi, and C. R. Cunningham, “Raman spectroscopy of coated pharmaceutical tablets and physical models for multivariate calibration to tablet coating thickness.,” *J. Pharm. Biomed. Anal.*, vol. 43, no. 1, pp. 39–48, Jan. 2007.

[81] D. Markl, M. Zettl, G. Hannesschläger, S. Sacher, M. Leitner, A. Buchsbaum, and J. G. Khinast, “Calibration-free in-line monitoring of pellet coating processes via optical coherence tomography,” *Chem. Eng. Sci.*, vol. 125, no. 0, pp. 200–208, Mar. 2015.

[82] D. Markl, G. Hannesschläger, A. Buchsbaum, S. Sacher, J. G. Khinast, and M. Leitner, “In-line quality control of moving objects by means of spectral-domain OCT,” *Opt. Lasers Eng.*, vol. 59, no. 0, pp. 1–10, Aug. 2014.

[83] D. Markl, G. Hannesschläger, S. Sacher, M. Leitner, and J. G. Khinast, “Optical coherence tomography as a novel tool for in-line monitoring of a pharmaceutical film-coating process.,” *Eur. J. Pharm. Sci.*, vol. 55, pp. 58–67, May 2014.

[84] F. Folttmann, K. Knop, P. Kleinebudde, and M. Pein, “In-line spatial filtering velocimetry for particle size and film thickness determination in fluidized-bed pellet coating processes.,” *Eur. J. Pharm. Biopharm.*, vol. 88, no. 3, pp. 931–938, 2014.

[85] E. W. Ciurczak and B. Igne, *Pharmaceutical and Medical Applications of Near-Infrared Spectroscopy*, 2nd ed. Boca Raton: CRC Press, 2015.

[86] P. Frake, D. Greenhalgh, S. M. Grierson, J. M. Hempenstall, and D. R. Rudd, “Process control and end-point determination of a fluid bed granulation by application of near infra-red spectroscopy,” *Int. J. Pharm.*, vol. 151, pp. 75–80, 1997.

[87] K. R. Goode, K. Asteriadou, P. T. Robbins, and P. J. Fryer, “Fouling and Cleaning Studies in the Food and Beverage Industry Classified by Cleaning Type,” *Compr. Rev. Food Sci. Food Saf.*, vol. 12, no. 2, pp. 121–143, Mar. 2013.

[88] H. Martens, J. P. Nielsen, and S. B. Engelsen, “Light scattering and light absorbance separated by extended multiplicative signal correction. application to near-infrared transmission analysis of powder mixtures.,” *Anal. Chem.*, vol. 75, no. 3, pp. 394–404, Feb. 2003.

[89] O. Scheibelhofer, R. Hohl, S. Salar-behzadi, D. Haack, K. Koch, P. Kerschhaggl, S. Sacher, J. C. Menezes, and J. G. Khinast, “A mathematical correction method for window fouling of NIR- probes,” *J. near infrared Spectrosc.*, p. submitted.

[90] J. G. M. Faustino, “Off-line Dynamic Image Analysis vs PAT Monitoring Tool on a Lab-Scale Hot Melt Coating Process,” Técnico Lisboa, 2013.

[91] L. H. Chiang, R. Leardi, R. J. Pell, and M. B. Seasholtz, “Industrial experiences with multivariate statistical analysis of batch process data,” *Chemom. Intell. Lab. Syst.*, vol. 81, pp. 109–119, 2006.

[92] R. Kona, H. Qu, R. Mattes, B. Jancsik, R. M. Fahmy, and S. W. Hoag, “Application of in-line near infrared spectroscopy and multivariate batch modeling for process monitoring in fluid bed granulation,” *Int. J. Pharm.*, vol. 452, no. 1–2, pp. 63–72, 2013.

[93] A. Kulcke and P. Kerschhaggl, “High Speed NIR Spectral Imaging in Recycling Applications,” in *Proceedings of the 3rd International Spectral Imaging Workshop*, 2006, pp. 40–47.

[94] S. Wold, N. Kettaneh, H. Fridén, and A. Holmberg, “Modelling and diagnostics of batch processes and analogous kinetic experiments,” *Chemom. Intell. Lab. Syst.*, vol. 44, no. 1–2, pp. 331–340, 1998.

[95] S. D. Schaber, D. I. Gerogiorgis, R. Ramachandran, J. M. B. Evans, P. I. Barton, and B. L. Trout, “Economic Analysis of Integrated Continuous and Batch Pharmaceutical Manufacturing: A Case Study,” *Ind. Eng. Chem. Res.*, vol. 50, no. 17, pp. 10083–10092, Sep. 2011.

[96] J. S. Srai, C. Badman, M. Futran, M. Krumme, and C. Johnston, “Future supply chains enabled by continuous processing – opportunities and challenges,” in

International Symposium on Continuous Manufacturing of Pharmaceuticals, 2014, p. White Paper 7.

[97] K. Nepveux, J. Sherlock, M. Futran, M. Thien, and M. Krumme, “How Development and Manufacturing will need to be structured – Heads of Development / Manufacturing,” in *International Symposium on Continuous Manufacturing of Pharmaceuticals*, 2014, p. White paper 8.

[98] H. Leuenberger, “New trends in the production of pharmaceutical granules: Batch versus continuous processing,” *Eur. J. Pharm. Biopharm.*, vol. 52, no. 3, pp. 289–296, Nov. 2001.

[99] D. Sarkar, D. Datta, D. Sen, and C. Bhattacharjee, “Simulation of continuous stirred rotating disk-membrane module: An approach based on surface renewal theory,” *Chem. Eng. Sci.*, vol. 66, no. 12, pp. 2554–2567, Jun. 2011.

[100] “Homepage Bokela - Crossflow Filtration.” .

[101] K. Luckert, Ed., *Handbuch der mechanischen Fest-Fluessig-Trennung*. Essen: Vulkan-Verlag GmbH, 2004.

[102] V. D. Ingenieure, *VDI 2762 Part 2 Mechanical solid-liquid separation by cake filtration Determination of filter cake resistance*, no. 2762. 2010.

[103] U. Peuker, “Filtrationseigenschaften in Abhaengigkeit von der fluessigen Phase der Suspension.” Institut für Chemische VT - TU Clausthal, 2008.

[104] R. Wakeman, “The influence of particle properties on filtration,” *Sep. Purif. Technol.*, vol. 58, no. 2, pp. 234–241, Dec. 2007.

[105] R. Bouzerar, M. Y. Jaffrin, A. Lefevre, and P. Paullier, “Concentration of ferric hydroxide suspensions in saline medium by dynamic cross-flow filtration,” *J. Memb. Sci.*, vol. 165, no. 1, pp. 111–123, Jan. 2000.

[106] R. Bouzerar, L. Ding, and M. Y. Jaffrin, “Local permeate flux-shear-pressure relationships in a rotating disk microfiltration module: Implications for global performance,” *J. Memb. Sci.*, vol. 170, pp. 127–141, 2000.

[107] Z. Wang, J. Chu, and X. Zhang, “Study of a cake model during stirred dead-end microfiltration,” *Desalination*, vol. 217, no. 1–3, pp. 127–138, Nov. 2007.

[108] J. Vaxelaire, J. M. Bongiovanni, and J. R. Puiggali, “Mechanical Dewatering and Thermal Drying of Residual Sludge,” *Environ. Technol.*, vol. 20, no. 1, pp. 29–36, Jan. 1999.

[109] K. Sattler, *Thermische Trennverfahren; Grundlagen, Auslegung, Apparate*, 3rd Editio. Weinheim: WILEY-VCH Verlag, 2012, p. 433.

[110] Bokela GmbH, “Cross Flow Filtration - Dyno Filter Prospekt.” .

[111] J. Gursch, R. Hohl, G. Toschkoff, D. Dujmovic, J. Brozio, M. Krumme, N. Rasenack, and J. Khinast, “Continuous Processing of Active Pharmaceutical Ingredients Suspensions via Dynamic Cross-Flow Filtration,” *J. Pharm. Sci.*, Jul. 2015.

[112] E. Tomba, M. De Martin, P. Facco, J. Robertson, S. Zomer, F. Bezzo, and M. Barolo, “General procedure to aid the development of continuous pharmaceutical processes using multivariate statistical modeling - an industrial case study.,” *Int. J. Pharm.*, vol. 444, no. 1–2, pp. 25–39, Feb. 2013.

[113] R. Lakerveld, B. Benyahia, P. L. Heider, H. Zhang, A. Wolfe, C. J. Testa, S. Ogden, D. R. Hersey, S. Mascia, J. M. B. Evans, R. D. Braatz, and P. I. Barton, “The Application of an Automated Control Strategy for an Integrated Continuous Pharmaceutical Pilot Plant,” *Org. Process Res. Dev.*, p. 140812135856003, Aug. 2014.

[114] S. Mascia, P. L. Heider, H. Zhang, R. Lakerveld, B. Benyahia, P. I. Barton, R. D. Braatz, C. L. Cooney, J. M. B. Evans, T. F. Jamison, K. F. Jensen, A. S. Myerson, and B. L. Trout, “End-to-end continuous manufacturing of pharmaceuticals: integrated synthesis, purification, and final dosage formation.,” *Angew. Chem. Int. Ed. Engl.*, vol. 52, no. 47, pp. 12359–63, Nov. 2013.

[115] E. Piacentini, E. Drioli, and L. Giorno, “Pulsed back-and-forward cross-flow batch membrane emulsification with high productivity to obtain highly uniform and concentrate emulsions,” *J. Memb. Sci.*, vol. 453, pp. 119–125, Mar. 2014.

[116] J. Bendick, B. Reed, P. Morrow, and T. Carole, “Using a high shear rotary membrane system to treat shipboard wastewaters: Experimental disc diameter, rotation and flux relationships,” *J. Memb. Sci.*, vol. 462, pp. 178–184, Jul. 2014.

7 List of figures

8 List of tables

9 Publications

9.1 Peer-Reviewed Journals

Roland Hohl, Nicolas Heigl, Daniel Koller, Charles A. Radeke
Comparison of NIR Spectroscopy with DEM Simulations for Tracing the Spatial Dispersion of Water during Mixing
Accepted 11.07.2017 in Particuology

Roland Hohl, Otto Scheibelhofer, Elena Stocker, Sharareh Salar Behzadi, Detlev Haack, Kai Koch, P. Kerschhaggl, Dirk Lochmann, Stephan Sacher, Andreas Zimmer
Monitoring of a Hot-Melt Coating Process via a Novel Multipoint Near-Infrared Spectrometer
AAPS PharmSciTech 2017 Jan 1;18(1):182-193. doi: 10.1208/s12249-016-0504-4. Epub 2016 Mar 2.

Johannes Gursch, **Roland Hohl**, Gregor Toschkoff, Diana Dujmovic, Jörg Brozio, Markus Krumme, Norbert Rasenack and Johannes Khinast
Continuous Processing of Active Pharmaceutical Ingredients Suspensions via Dynamic Cross-Flow Filtration
Journal of Pharmaceutical Sciences Volume 104, Issue 10, Pages 3481–3489, October 2015

Johannes Gursch, **Roland Hohl**, Marco E. Armenante, Diana Dujmovic, Peter van der Wel, Jörg Brozio, Markus Krumme, Norbert Rasenack, and Johannes Khinast
Continuous Drying of Small Particles for Pharmaceutical Applications—An Evaluation of Selected Lab-Scale Systems
American Chemical Society 2015, 19 (12), Pages 2055–2066

Johannes Gursch, **Roland Hohl**, Diana Dujmovic, Jörg Brozio, Markus Krumme, Norbert Rasenack and Johannes Khinast
Dynamic cross-flow filtration: enhanced continuous small-scale solid-liquid separation
Drug Development and Industrial Pharmacy 2016; 42(6):977-984

Scheibelhofer, O.; **Hohl, R.**; Salar-Behzadi, S.; Haack, D.; Koch, K.; Kerschhaggl, P.; Sacher, S.; Menezes, J. C.; Khinast, J.:
Automatic correction for window fouling of near infrared probes in fluidised systems. Journal of near infrared spectroscopy 22 (2014) 3, Pages 229 - 238

M.O. Besenhard, A. Thurnberger, **R. Hohl**, E. Faulhammer, J. Rattenberger, J.G. Khinast
Continuous API-crystal coating via coacervation in a tubular reactor
International Journal of Pharmaceutics Volume 475, Issues 1–2, 20 November 2014, Pages 198–207

Besenhard M.; **Hohl, R.**; Hodzic, A.; Eder, R.; Khinast, J.:
Modeling a seeded continuous crystallizer for the production of active pharmaceutical ingredients. - in: Crystal research and technology [ElektronischeRessource] 49 (2014) 2-3, Pages 92 - 108

9.2 Talks

R. Hohl, O. Scheibelhofer, P. Wahl, S. Sacher, J. G. Khinast
Always the same? Location of Segregation via SpectroscopyAIChE Annual Meeting 2014, Atlanta 19.11.2014

Kren, H.; **Hohl, R**.; Sternad, M.; Cifrain, M.; Koller, S.:
Ex-Situ Method for the Determination of Lithium and Fluoride trapped in the SEI of Lithium Ion Cells during prolonged cycling. - in: Graz Battery Days . Graz am: 01.10.2013

Scheibelhofer, O.; **Hohl, R**.; Salar-Behzadi, S.; Haack, D.; Koch, K.; Kerschhaggl, P.; Lochmann, D.; Sacher, S.; Khinast, J.:
Collecting, condensing, comprehending and culling spectral data: A pharmaceutical process monitored with SIMCA online. - in: Umetrics User Meeting 2013. Castelldefels am: 24.09.2013

Hohl, R.; Khinast, J.:
Strategy of Assessing Continuous Manufacturing Feasibility Based on Process and Materials Knowledge. - in: 48th AAPS Arden Conference. Rockville, Maryland am: 04.03.2013

Scheibelhofer, O.; **Hohl, R**.; Salar-Behzadi, S.; Haack, D.; Koch, K.; Sacher, S.; Menezes, J. C.; Khinast, J.:
Fluid Bed in a Flash. - in: AIChE 2012 Annual Meeting. Pittsburgh am: 28.10.2012

Scheibelhofer, O.; **Hohl, R.**; Sacher, S.; Menezes, J. C.; Khinast, J.:
(Multiawesome) Multispectral Multiprobe Monitoring. - in: 62nd Annual Meeting of the Austrian Physical Society. Graz am: 18.09.2012

9.3 Posters

Gursch, J.; **Hohl, R.**; Dujmovic, D.; Brozio, J.; Krumme, M.; Rasenack, N.; Khinast, J.:
Lösungsmitteleinfluss auf das Filtrationsverhalten organischer Feststoffpartikel. - in: Minisymposium Verfahrenstechnik JKU. Linz am: 02.05.2012

Hohl, R.; Heigl, N.; Radeke, C.; Scheibelhofer, O.; Balak, N.; Koller, D. M.; Khinast, J.:
Multipoint Near-infrared Monitoring and Discrete Element Method Simulation of Fluid Dispensation in Catalysts. - in: 5th International Congress on Pharmaceutical Engineering. Graz am: 29.09.2011

Hohl, R.; Heigl, N.; Radeke, C.; Scheibelhofer, O.; Koller, D. M.; Khinast, J.:
Multipoint NIR Spectroscopy vs. DEM Simulation for the Moisture Quantification During Mixing . - in: 7. KolloquiumProzessanalytik. Linz am: 14.11.2011

Gursch, J.; Dujmovic, D.; **Hohl, R.**; Redlinger-Pohn, J. D.; Brozio, J.; Krumme, M.; Rasenack, N.; Khinast, J.: spin flash dryer - characterization for pharmaceutical application. - in: PharmaSci. Edinburgh am: 02.09.2013